



NTNU – Trondheim
Norwegian University of
Science and Technology

Analysis methods for thin concrete shells of revolution

Andreas Hauso

Civil and Environmental Engineering

Submission date: June 2014

Supervisor: Svein Ivar Sørensen, KT

Norwegian University of Science and Technology
Department of Structural Engineering

Master's thesis

for

Andreas Hauso

Analysis methods for thin concrete shells of revolution

Analysemetoder for tynne aksesymmetriske betongskall

The assignment can be briefly summarised as follows:

- Study the classical theory on thin shells of revolutions, including cylindrical and spherical shells, circular plates and ring beams.
- Calculations of connected thin shells using the classical theory.
- Use the finite element software DIANA for numerical assessments of the same examples. Evaluate how the finite element models capture the thin shell behaviour, especially the effects from the edge disturbances.
- Design of one of the structures, including reinforcement design.
- Nonlinear analysis of the designed structure.

The answer should be organised according to the current guidelines.

Supervisor: *Professor Svein Ivar Sørensen*

The assignment must be submitted to the Department of Structural Engineering within June 10, 2014.

Preface

This MSc thesis was written for the Department of Structural Engineering at the Norwegian University of Science and Technology (NTNU) during 20 weeks in the spring of 2014.

The thesis encompasses the theory on thin concrete shells of revolution. I chose this subject on the basis of both personal interest and my lack of knowledge. Shell structures are not lectured at the NTNU, and i saw the last semester of my study as a possibility for venturing into an interesting field of structural engineering.

I want to thank my supervisor Professor Svein Ivar Sørensen for his support throughout the process. His knowledge and guidance has been of great help.

In addition i would like to thank PhD Candidate Morten Engen for his generous help with the finite element software Diana.

Andreas Hauso

Trondheim, June 2014

Abstract

This paper aims to give an objective comparison of analytical and numerical solutions to thin concrete shells of revolution. The numerical simulations are performed using the finite element software Diana. The main focus is on cylindrical and spherical shells, as they are typical geometries for constructing shells in concrete. Some assessment of the necessary theory on circular plates and ring beams is also presented since these are structural components frequently related to the shells in question.

In order to attain a fundamental understanding of the load carrying behaviour of shells, the classical background material on thin shells of revolution is thoroughly investigated. Detailed deductions of the governing equations in membrane- and bending theory constitute the first part of the paper. This theory is then applied to cases involving typical connected shell structures which highlights different aspects of the analytical theory. Further assessments of these structures are done using finite element software, which provides a basis for comparing the analytical and numerical solutions. Finally, one of the structures are designed in accordance with the Eurocodes, accompanied by a nonlinear analysis. For this purpose a comparative study of line and solid elements is conducted.

In the context of linear static analysis, two- and three-node axisymmetric shell of revolution elements show superb accuracy when compared to the analytical solutions. Intrinsic shell properties, such as the damping of forces and moments from the shell boundaries, are accurately represented.

Element comparison shows a lower degree of accuracy from solid element solutions compared to the line alternative. This is especially true for shear stresses, which show oscillating behaviour near the edge zones of the shells. These oscillations are considered one of the main uncertainties in the solid model used for the nonlinear analysis.

From the nonlinear analysis, the design of the structure was found to be adequate. The results show that the forces have been correctly redistributed to the reinforcement, and that the total load the structure can endure is approximately 1.08 times of the design load.

Finite element analysis provides a powerful tool for evaluating the load response from connected concrete shell structures. Analytical solutions, although bringing valuable insight in the leading principals governing the shell behaviour, are highly exposed to human errors. As a consequence they are less attractive in practice. Finite element simulations coupled with a general understanding of the classical theory is therefore recommended for the executing engineer.

Sammendrag

Denne oppgaven har som formål å gi et objektivt sammenlikningsgrunnlag for numeriske og analytiske løsninger av tynne aksesymmetriske betongskall. De numeriske simuleringene er gjort i elementmetodeprogrammet Diana. Hovedfokuset i oppgaven er satt til sylindriske og sfæriske skall, siden disse er typiske geometrier som benyttes for skallkonstruksjoner i betong. Relevant teori angående sirkulære plater og ringbjelker diskuteres også, siden disse er komponenter som ofte er relatert til skallene i fokus.

For å oppnå en grunnleggende forståelse av aksesymmetriske skall er den analytiske bakgrunnsteorien grundig gjennomgått. I oppgaven gis detaljerte utledninger av de styrende likningene i membran- og bøyningsteori. Teorien benyttes så for å løse valgte sammensatte skallkonstruksjoner. Videre vurdering av konstruksjonene gjøres deretter numerisk for å danne et sammenlikningsgrunnlag mellom løsningene. Til slutt prosjekteres en av konstruksjonene i henhold til Eurokodene, med en tilhørende ikke-lineær analyse. For dette formålet gjennomføres et sammenlikningsstudie av linje- og volumelementer.

Innen lineær elastisk analyse gir to- og tre-node elementer svært gode resultater sammenliknet med de analytiske løsningene. Særegne skall egenskaper, som dempningen av randforstyrrelser, representeres svært nøyaktig.

Sammenlikningen av elementer viser at volum elementer gir en lavere grad av nøyaktighet sammenliknet med linje alternativet. Dette gir spesielt utslag på skjærspenningsfordelingene, som viser oscillerende oppførsel nær skallenes render. Dette er regnet som det største usikkerhetsmomentet i den ikke-lineære analysen.

Den ikke-lineære analysen bekrefter at konstruksjonen er prosjektert på korrekt måte. Analysen viser at skallkreftene er blitt korrekt redistribuert til armeringen, og konstruksjonen kan belastes med en last som tilsvarer rundt 1.08 ganger det prosjekterende lasttilfellet.

Elementanalyse er et kraftig verktøy for vurdering av responsen fra skallkonstruksjoner. De analytiske løsningene gir verdifull innsikt i de styrende prinsippene for skall, men er svært utsatt for menneskelige feil. Element simuleringer kombinert med en generell forståelse av den klassiske teorien er derfor anbefalt for den utøvende ingeniør.

Contents

1	Introduction	1
2	Theory of thin shells	3
2.1	General	3
2.1.1	Classification of shells by the Gaussian curvature	4
2.2	Assumptions	5
3	Membrane theory	7
3.1	Prerequisites	7
3.2	Membrane forces	7
3.3	Deformations	9
3.4	Relative displacements	11
3.5	Geometric shapes	12
3.5.1	Cylinder	12
3.5.2	Sphere	13
3.6	Projection of loads	14
4	Bending theory	15
4.1	Cylindrical shells	15
4.1.1	Differential equation	15
4.1.2	Solution to the differential equation	17
4.1.3	The infinite cylinder	18
4.1.4	Damping length	19
4.2	Spherical shells	21
4.2.1	Differential equation	21
4.2.2	Solution to the differential equation	24
4.3	Ring beams	28
4.4	Circular plates	32
5	Diana	33
5.1	Preprocessing	33
5.2	Analysis	34
5.3	Postprocessing	34
6	Selected shell structures	35
6.1	Analytical solutions	35
6.1.1	Cylinder with circular plate top	35
6.1.1.1	Distributions	38
6.1.2	Cylinder with spherical roof	42
6.1.2.1	Distributions	47
6.1.3	Implementation of ring beam	51
6.1.4	Discussion	56
6.2	Numerical solutions	57
6.2.1	Numerical analysis of the cylinder with circular plate top	58
6.2.1.1	Model	58

6.2.1.2	Results	59
6.2.1.3	Distributions	59
6.2.2	Numerical analysis of cylinder with spherical roof	61
6.2.2.1	Model	61
6.2.2.2	Axisymmetric shell elements	61
6.2.2.3	Results	62
6.2.2.4	Distributions	63
6.2.3	Numerical analysis of the implemented ring beam	65
6.2.3.1	Model	65
6.2.3.2	Results	65
6.2.4	Discussion	67
7	Element comparison	69
7.1	Simple cylinder	69
7.1.1	Model	70
7.1.1.1	Elements	70
7.1.2	Results	71
7.2	Cylinder with circular plate top	72
7.2.1	Models	72
7.2.1.1	Elements	72
7.2.2	Results	73
7.2.2.1	Deformations	73
7.2.2.2	Stresses	74
7.3	Discussion	77
8	Nonlinear analysis	79
8.1	Design in accordance with the Eurocodes	79
8.1.1	Design loads	79
8.1.2	Partial factors for materials	80
8.1.3	Recalculation of moments and forces using design loads . . .	80
8.1.4	Reinforcement	81
8.2	Nonlinear model	83
8.2.1	Material models	83
8.2.2	Finite element model	85
8.2.3	Elements	85
8.3	Solution method	86
8.4	Results	86
8.4.1	Deformations	86
8.4.2	Stresses	89
8.4.2.1	Reinforcement	89
8.4.2.2	Concrete	90
8.4.3	Cracking	94
8.5	Discussion	96
9	Conclusion	97
	References	99

Appendix	100
A Cylinder with circular plate top	101
B Cylinder with spherical roof	105
C Ring beam	111
D Design in accordance with Eurocode 2	117

1 Introduction

Shell structures have played an important role in structural design throughout the centuries. Besides being visually appealing they possess interesting technical properties. From an engineering perspective, shell structures may be called the prima donnas of structures. Their behaviour is difficult to analyse and can be somewhat unpredictable in that apparently small changes of geometry or support conditions may result in totally different responses.

Thin shell structures are beneficial for concrete components requiring high strength without the use of additional support. The inherent curvature of shells allows for decomposition of stress resultants in several directions, enabling a combination of membrane and bending action to obtain an increase in load carrying ability. The high compressive strength and castability properties of concrete make for practical and artistically pleasing structures. In later years the knowledge of the classical shell theory have diminished somewhat among newly educated engineers as finite element technology has become more prominent. Considering the complexity of shell structures this shift in focus can lead to wrong interpretations of finite element solutions.

The purpose of this paper is to investigate the analytical and numerical solutions to thin concrete shells of revolution. Spherical and cylindrical shells are chosen as a basis for theory and calculations, as these they are typical shapes for constructing shells in concrete. Some considerations are also given to the theory on circular plates and ring beams, which are structural components often related to the shells in focus.

In order to achieve a fundamental understanding of the classical theory, the first part of the paper focuses on the theory of thin shells. The characteristics of shells are studied and formulated mathematically as differential equations.

The theory is then applied to selected shell problems with high relevance in civil engineering. This provides a basis for comparing the results to numerical solutions from finite element analysis. Different aspects concerning the finite element modelling and choice of elements will be highlighted.

The paper rounds off by showing how shells can be designed in accordance with the Eurocodes. An accompanying nonlinear finite element analysis is provided for validation of the design. This analysis will also shed light on how the shell structures behave when the linear elastic range of the materials are exceeded.

2 Theory of thin shells

Shells are curved surface structures that combine membrane- and bending action to obtain an increase in stiffness. For this reason they are considered as a combination of the load-carrying behaviour of plates in bending and membrane action. In civil engineering, shells are useful to create large open areas without the need of column support. The first known encounter of shells used for this purpose is the Pantheon in Rome, build in 126 AD (figure 2.1). Although the Romans lacked the engineering knowledge of the modern era, they intuitively understood the load-carrying qualities of shells. To this day the structure is considered a construction marvel. Over the last centuries the theory of shells has been extensively studied, and a comprehensive amount of information are available to engineers in a wide range of engineering fields.

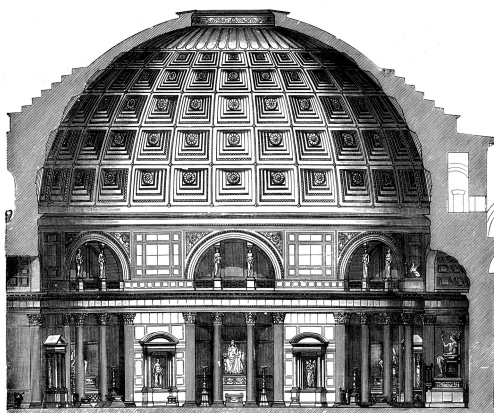


Figure 2.1: The Pantheon in Rome [1]

In the following chapters a detailed study of cylindrical and spherical shells is conducted. These geometrical shapes are chosen as they are considered the most relevant when using concrete as the primary building material. Great focus will be given in developing the governing differential equations and their corresponding solutions. This study can be conducted in several ways, ranging from energy methods to equilibrium of infinitesimal elements. The latter is chosen since it gives the most visual and intuitive understanding of the principals at work.

2.1 General

For technical purposes, *thin* shells are of greatest significance. They are defined as shells with a radius to thickness ratio $\frac{R}{t}$ between 20 and 1000. By comparison, the ratio of an egg is approximately 60 [2]. Modern structures can achieve ratios exceeding 1000, which demonstrates the great load carrying ability of shells. Even

though shells may take several forms, this paper concentrates on shells of revolution. Such shells are generated by rotating a planar curve about an axis lying in the meridian plane. They are mathematically defined by differential geometry, and are therefore ideal for describing several shell structures with relevance for civil engineering.

Thin shells are modelled as 2 dimensional structures, where the geometry is fully defined by the shape of the middle surface and the thickness h [3, ch. 12.4]. The principal radii of curvature, as shown in figure 2.2, are measures of how the shell curves in the hoop and meridian directions. This measure plays a significant role in shell theory since different geometric structures have a distinct configuration of these radii. Analytical solutions can be derived for general shapes and made specific for geometries with intrinsic configurations of the principal radii.

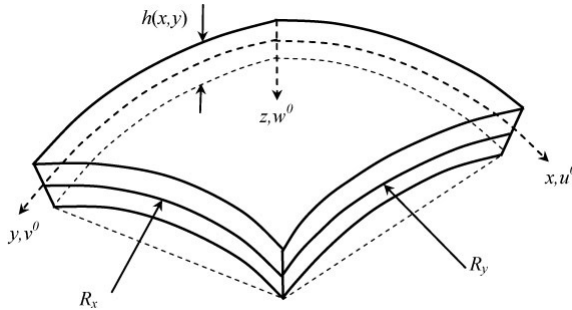


Figure 2.2: Geometry and principal radii of curvature of shell element

The study of shells of revolution is divided into two separate theories; *membrane theory* and *bending theory*. The two theories describe the in plane membrane forces and the effects of edge disturbances, respectively. In certain cases, the stress and deformation states of the shell can be determined solely by the membrane solution. However, membrane theory cannot, in all instances, provide solutions compatible with the actual conditions of deformation. For most practical purposes both theories are required to capture the total load-carrying behaviour of the shells. Hence a total analytical solution consists of a combination of the two theories.

2.1.1 Classification of shells by the Gaussian curvature

More generally, shells may be classified by their Gaussian curvature, defined as

$$K = \frac{1}{r_x r_y},$$

where r_x and r_y are the principal radii of curvature [4]. The Gaussian curvature, and especially its sign, provides useful information about the load-carrying

behaviour of shells. Curved structures make use of the membrane action in the meridian and hoop direction to avoid bending and shear. This is made possible because the curvatures allow for decomposition of the membrane forces in several directions, and is highly related to the Gaussian curvature of the surface.

Figure 2.3 shows three types of curved surfaces defined by their Gaussian curvature. Synclastic surfaces, like domes, have a Gaussian curvature greater than zero. For such shells the edge disturbances tend to damp rapidly, making membrane theory valid for most of the shell surface. They typically show the greatest stiffness. Anticlastic surfaces (saddle surfaces) have a negative Gaussian curvature. The edge disturbances tend to effect a greater part of the shell, making bending theory more prominent. They are less stiff than synclastic structures and require more stiffening. Curves with $K \equiv 0$ are called developable surfaces; a conspicuous feature being that they can be flattened onto a plane without experiencing any strains or stresses. Examples are cylinders and cones. The edge disturbances are damped to a certain degree, but extend further into the shell than for synclastic surfaces. Such shells typically need ring beams to prevent ovalising.

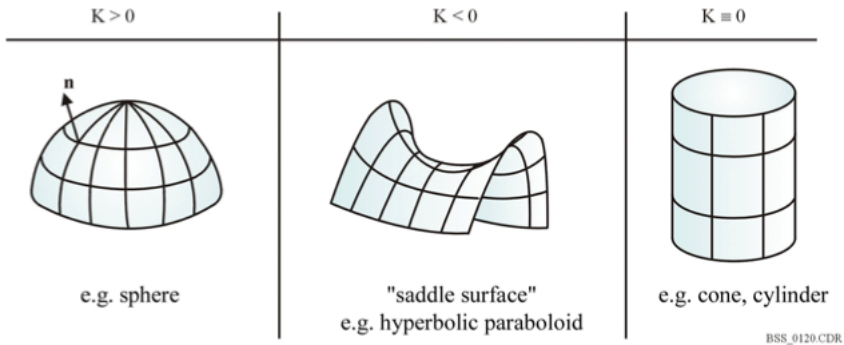


Figure 2.3: Surfaces with different Gaussian curvature [5]

2.2 Assumptions

As for plates, the shell stresses are assumed constant over the thickness and are modelled as two dimensional. The ten resultant forces and moments are found as

$$N_x = \int_{-\frac{h}{2}}^{\frac{h}{2}} \sigma_x \left(1 - \frac{z}{r_y}\right) dz \quad , \quad N_y = \int_{-\frac{h}{2}}^{\frac{h}{2}} \sigma_y \left(1 - \frac{z}{r_x}\right) dz$$

$$N_{xy} = \int_{-\frac{h}{2}}^{\frac{h}{2}} \tau_{xy} \left(1 - \frac{z}{r_x}\right) dz \quad , \quad N_{yx} = \int_{-\frac{h}{2}}^{\frac{h}{2}} \tau_{yx} \left(1 - \frac{z}{r_y}\right) dz$$

$$Q_x = \int_{-\frac{h}{2}}^{\frac{h}{2}} \tau_{zx} \left(1 - \frac{z}{r_y}\right) dz, \quad Q_y = \int_{-\frac{h}{2}}^{\frac{h}{2}} \tau_{zy} \left(1 - \frac{z}{r_x}\right) dz$$

$$M_x = \int_{-\frac{h}{2}}^{\frac{h}{2}} \sigma_x z \left(1 - \frac{z}{r_y}\right) dz, \quad M_y = \int_{-\frac{h}{2}}^{\frac{h}{2}} \sigma_y z \left(1 - \frac{z}{r_x}\right) dz$$

$$M_{xy} = \int_{-\frac{h}{2}}^{\frac{h}{2}} \tau_{xy} z \left(1 - \frac{z}{r_x}\right) dz, \quad M_{yx} = \int_{-\frac{h}{2}}^{\frac{h}{2}} \tau_{yx} z \left(1 - \frac{z}{r_y}\right) dz,$$

where N_x, N_y, N_{xy} , and N_{yx} are the membrane forces, Q_x and Q_y the transverse shear forces and M_x, M_y, M_{xy} and M_{yx} are the bending and twisting moments per unit length [4, c. 26.1]. The addition of the terms $\frac{z}{r_x}$ and $\frac{z}{r_y}$ distinguish the stress resultants in shells from its plate counterpart. These terms stem from the curvature of the surfaces and the fact that the cross sections are trapezoidal. The two principal radii of curvature differ for most shells meaning that the shear forces and moments are no longer equal in the xy and yx planes. However, for thin shells these terms are generally very small and may therefore be neglected. For symmetrically loaded shells of revolution, the amount of stress resultants are further simplified by symmetry. Left are three membrane forces, N_x, N_y and $N_{xy} = N_{yx}$, and two bending moments, M_x, M_y .

Further assumptions are based on the *Kirchhoff-Love* assumptions: [3, ch. 12.2]

- **Geometrically linear:** The strains and displacements are assumed small. Equilibrium is considered for the undeformed structure.
- **Physically linear:** Hooks law apply, and the material is elastic isotropic and homogeneous.
- **Thin shell:** The shell is thin, which means that the factors $\frac{R}{h} > 20$ and $\frac{z}{R} \rightarrow 0$. As a result, an initially plane cross section remain plain during deformation. A direction initially normal to the middle surface will remain normal after deformation.

Additionally, higher order terms are small and are neglected in the equilibrium considerations presented in the following chapters. This will not be pointed out any further in the text.

3 Membrane theory

3.1 Prerequisites

As previously mentioned, the theory of shells are divided into two theories. Membrane theory suggests that arbitrary loads can be resisted solely by membrane forces. This is only true when certain prefixes are made in addition to the general ones previously mentioned:

- Bending and shear stiffness are negligible
- The surface is C_2 continuous
- No abrupt changes in shell thickness
- Only distributed loads (no point loads)
- Edge forces are tangential to the surface. This must also be true for the support conditions.

Simply stated; features which induce bending moments and shear forces in shells must be avoided for membrane theory to fully capture the stress- and displacement state of the shell.

3.2 Membrane forces

A general shell of revolution is considered, as shown in figure 3.1 [3, ch. 12.5]. The element $ABCD$ is positioned on the shell surface by the angles ϕ and θ and the radius r_0 . It is restricted by two meridian and two parallel sections, with principal radii r_1 and r_2 . The arc lengths of the sides AC and CD in the figure are expressed as $L_{AC} = r_0 d\theta$ and $L_{CD} = r_1 d\phi$.

The forces acting on the element are shown in figure 3.2. They are the external forces in z and y direction, and the membrane forces N_ϕ and N_θ . With the absence of shear forces and bending moments the problem becomes statically determinate, and we are left with two rather simple equilibrium equations; equilibrium in the tangent to the meridian and thickness directions. Equilibrium of forces in meridian direction is redundant in membrane theory since it deals with pure shear forces, which is neglected.

Equilibrium in the thickness direction yields [3]:

$$\frac{N_\phi}{r_1} + \frac{N_\theta}{r_2} = -p_z \quad (3.1)$$

where p_z is the external loading in the z direction. Equilibrium of forces in the tangent to the meridian, shown in figure 3.2b, yields [3]:

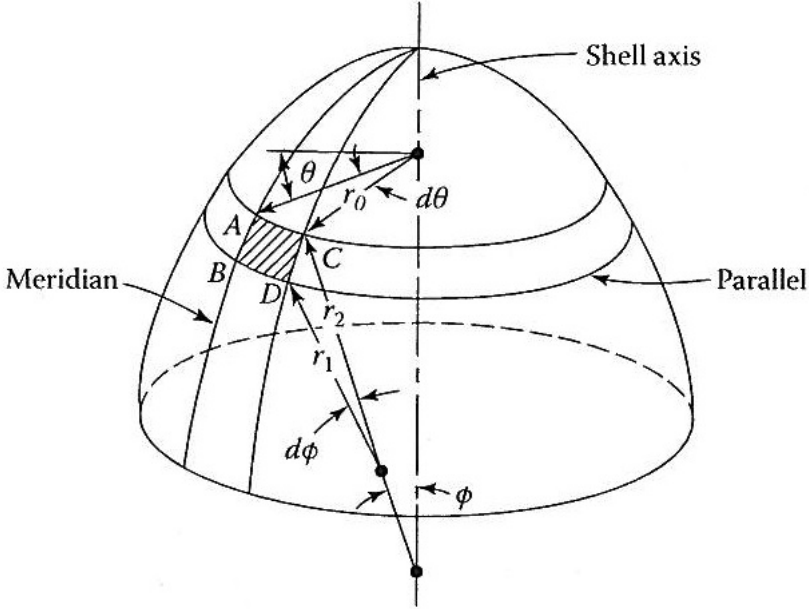


Figure 3.1: Shell of revolution with highlighted parallel sections and principal radii [3, p. 402]

$$\frac{d}{d\phi}(N_\phi r_0) - N_\theta r_1 \cos\phi + p_y r_1 r_0 = 0 \quad (3.2)$$

where p_y is the external loading in y direction.

Thus we are left with one differential and one algebraic equation describing the forces in the shell. The stress resultant in the hoop direction, N_θ , is found by rewriting 3.1 as

$$N_\theta = -\frac{r_2}{r_1} N_\phi + p_z r_2 \quad (3.3)$$

By inserting 3.3 in 3.2, we get the expression for the meridian stress resultant:

$$N_\phi = -\frac{1}{r_2 \sin^2\phi} \int_{\phi_0}^{\phi} r_1 r_2 (p_z \cos\phi + p_y \sin\phi) \sin\phi d\phi + c \quad (3.4)$$

The constant of integration c takes into account different types of loading. For shells of revolution with symmetric load conditions, c is zero. By changing the principal radii of curvature in equations 3.3 and 3.4, expressions for the membrane forces for different types of geometric forms are found.

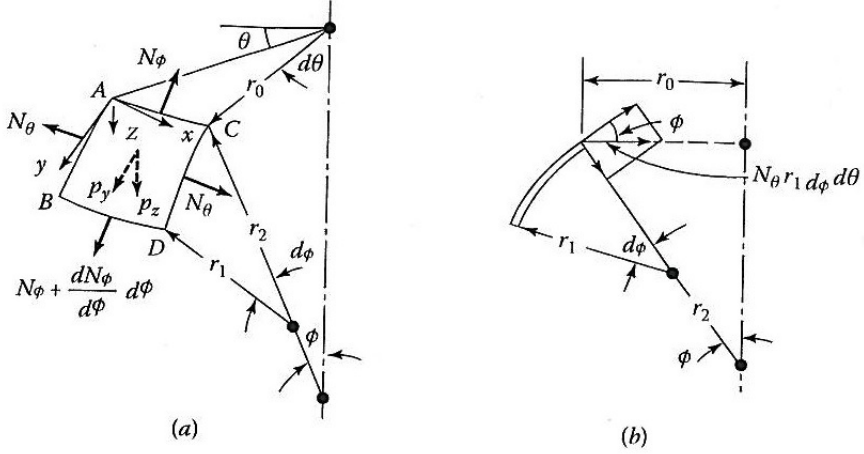


Figure 3.2: Forces acting on infinitesimal element in (a) hoop and (b) meridian direction [3, p 403]

3.3 Deformations

To determine the membrane strains ε_ϕ and ε_θ , an infinitesimal element AB of length $r_1 d\phi$ which curves in the meridian direction is considered, as shown in figure 3.3. AB and A'B' refers to the undeformed and deformed configurations of the element. The two displacement parameters v and w represent the deformation in the tangent to the meridian and thickness directions, respectively.

To express the strains the well known relation $\varepsilon = \frac{A'B' - AB}{AB}$ is used. From figure 3.3 it is apparent that the length A'B' of the deformed element can be written as:

$$A'B' = (r_1 - w)d\phi - v + (v + dv) = (r_1 - w)d\phi + dv.$$

Hence the strain in the tangent to the meridian direction can now be written as

$$\varepsilon_\phi = \frac{(r_1 - w)d\phi + dv - r_1 d\phi}{r_1 d\phi} = \frac{1}{r_1} \frac{dv}{d\phi} - \frac{w}{r_1}. \quad (3.5)$$

The strain in the hoop direction is treated in the same manner by looking at the change in radius r_0 . From figure 3.3 it is clear that the radius in the deformed state can be expressed as $r'_0 = r_0 - w \sin\phi + v \cos\phi$. The strain is now found as:

$$\varepsilon_\theta = \frac{r'_0 d\theta - r_0 d\theta}{r_0 d\theta} = \frac{v}{r_2} \cot\phi - \frac{w}{r_2}, \quad (3.6)$$

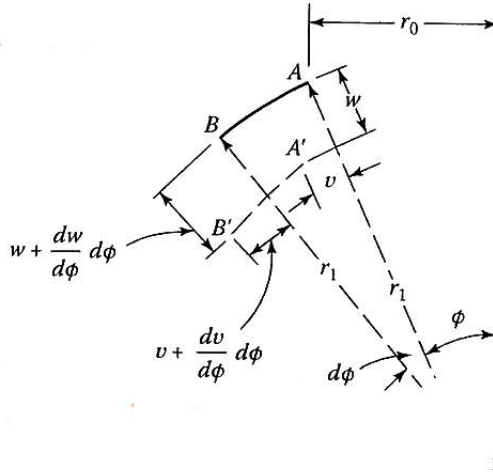


Figure 3.3: Deformation of infinitesimal element in the meridional plane [3, p. 417]

where the relationship $r_0 = r_2 \sin \theta$ is used. By combining 3.5 and 3.6, w is eliminated, and a differential equation for v is obtained:

$$\frac{dv}{d\phi} - v \cot \phi = r_1 \varepsilon_\phi - r_2 \varepsilon_\theta \quad (3.7)$$

Hooke's law in 2 dimensions relate the strains and membrane forces:

$$\varepsilon_\phi = \frac{1}{Eh} (N_\phi - \nu N_\theta) \quad (3.8a)$$

$$\varepsilon_\theta = \frac{1}{Eh} (N_\theta - \nu N_\phi) \quad (3.8b)$$

where E is Young's modulus and ν is the Poisson ratio. By introducing these expressions in 3.7 and solving for v , the final expression for the displacement tangential to the meridian direction is obtained:

$$v = \sin \phi \int_0^\phi \frac{1}{\sin \phi} \frac{1}{Eh} [N_\phi (r_1 + \nu r_2) - N_\theta (r_2 + \nu r_1)] d\phi. + c \quad (3.9)$$

Here the constant c is determined from the boundary conditions. When the displacement v is calculated, w is found from equation 3.6 as

$$w = v \cot \phi - r_2 \varepsilon_\theta. \quad (3.10)$$

Expressions 3.9 and 3.10 gives the membrane deformations for thin shells of general shape.

3.4 Relative displacements

In addition to the displacements v and w , the relative displacements are useful in shell analysis. Figure 3.4 shows a shell displaced in the meridian direction with ring extension δ_m and meridian rotation V_m . Both parameters are useful for compatibility requirements when analysing connected shells, which will become apparent in later sections when example cases are studied.

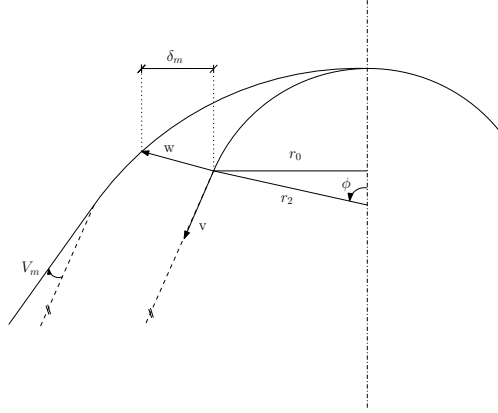


Figure 3.4: Relative displacements in the meridian plane

From equation 3.6, the ring extension δ_m is expressed as:

$$\delta_m = r_0 \varepsilon_\theta = \frac{r_2 \sin \phi}{Et} (N_\theta - \nu N_\phi). \quad (3.11)$$

It can be shown that the meridian rotation can be expressed as $V = \frac{1}{r_1} (\frac{dw}{d\phi} - v)$ [5]. By inserting for the displacements, we end up with the following equation:

$$V_m = \frac{1}{r_1} \left[\frac{\partial}{\partial \phi} \left(\frac{\Delta r}{\sin \phi} \right) - \frac{\cot \phi}{Eh} \left(n_\phi (r_1 + \nu r_2) - n_\theta (\nu r_1 + r_2) \right) \right] \quad (3.12)$$

This concludes the membrane theory for thin shells of revolution. By specifying the principal radii of curvature and the opening angle ϕ_0 of the shell in question, membrane theory for different geometries are determined.

3.5 Geometric shapes

The preceding expressions are general, meaning that they hold for all mathematically defined surfaces. What distinguishes different geometries are the principal radii of curvature and the meridian angle ϕ . As spherical and cylindrical shells are in focus, the expressions for them are investigated further.

3.5.1 Cylinder

Cylinders are examples of developable surfaces with a Gaussian curvature of zero. This stems from the fact that the principal radius of curvature $r_1 = \infty$. Referring to figure 3.1, the surface parameters for cylinders are $r_1 = \infty$, $r_2 = r_0 = a$ and $\phi = \text{const.} = \frac{\pi}{2}$. Since there is no curvature in the meridian direction, we define the parameter s running along the longitudinal axis of the cylindrical shell, as shown in figure 3.5. The resulting expressions for the cylinder is summarised in table 3.1.

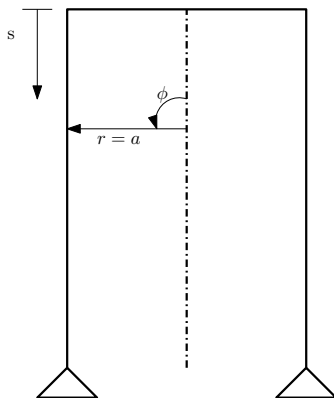


Figure 3.5: Cylinder configuration

Membrane forces	$N_s = - \int_{s_0}^s p_s ds.$
	$N_\theta = ap_z$
Displacements	$v = \frac{1}{Eh} \int_0^s (N_s - \nu N_\theta) ds + c$
	$w = \frac{a}{Eh} (N_\theta - \nu N_s)$
Relative displacements	$\delta = w = \frac{a}{Eh} (N_\theta - \nu N_s)$
	$V = \frac{dw}{ds} = \frac{a}{Eh} \frac{d}{ds} (N_\theta - \nu N_s)$

Table 3.1: Membrane theory for cylindrical shells

3.5.2 Sphere

Spheres have principal radii $r_1 = r_2 = R$. The radius of the hoop circles r_0 are found by the relationship $r_0 = R \sin \phi$, as shown in figure 3.6. Table 3.2 gives a summary of the resulting membrane forces and displacements for spherical shells.

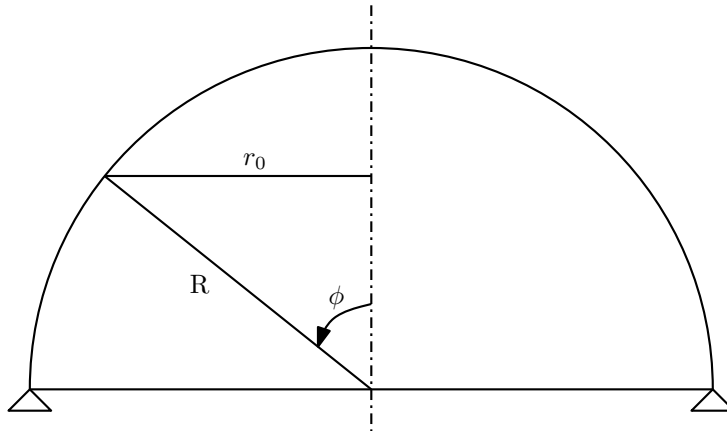


Figure 3.6: Sphere configuration

Membrane forces	$N_\phi = -\frac{R}{\sin^2\phi} \int_{\phi_0}^{\phi} \sin\phi(p_\phi \sin\phi - p_z \cos\phi) d\phi + C$ $N_\theta = Rp_z - N_\phi$
Displacements	$v = \frac{\sin\phi}{Eh}(1 + \nu)R \left[\int_{\phi} \frac{N_\phi - N_\theta}{\sin\phi} d\phi + c \right]$ $w = \frac{R}{Eh}(N_\theta - \nu N_\phi) - v \cot\phi$
Relative displacements	$\delta = \frac{R \sin\phi}{Eh}(N_\theta - \nu N_\phi)$ $V = \frac{1}{Eh} \left[\frac{\partial}{\partial\phi}(N_\theta - \nu N_\phi) - (1 + \nu) \cot\phi(N_\phi - N_\theta) \right]$

Table 3.2: Membrane theory for spherical shells

3.6 Projection of loads

In order for the loads acting on a shell to be of the form implemented in the previously derived formulas, they must be properly decomposed. Table 3.3 gives a summary of load decomposition for some typical load conditions. Note that the thickness of the shell is denoted t in the table.

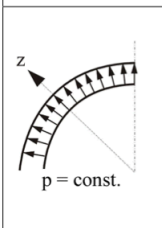
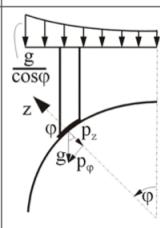
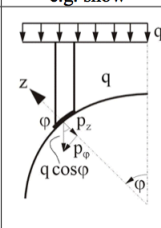
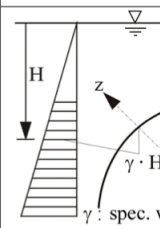
constant interior pressure	self weight $g = \gamma t$; $t = \text{const.}$	const. projected load, e.g. snow	exterior fluid
 <p>$p = \text{const.}$</p>	 <p>$\frac{tg}{\cos\phi}$</p>	 <p>q</p>	 <p>$\gamma : \text{spec. weight}$</p>
$p_\phi = 0$ $p_z = p = \text{const.}$	$p_\phi = g \sin\phi$ $p_z = -g \cos\phi$	$p_\phi = q \cos\phi \sin\phi$ $p_z = -q \cos^2\phi$	$p_\phi = 0$ $p_z = \gamma H(\phi)$

Table 3.3: Projection of various loading on shell surfaces [5]

Tables 3.1, 3.2 and 3.3 conclude the membrane theory for cylindrical and spherical shells. When the geometric and material data are known, they provide all the necessary information for obtaining the membrane solution.

4 Bending theory

Membrane theory fails to provide solutions compatible with the actual conditions of deformation for most practical cases. Bending effects are induced in shells as compatibility of deformation is required at edges and junctions. A theory which takes these aspects into account is developed in the following chapter. Contrary to the membrane theory, the bending theory for thin shells is developed directly for cylindrical and spherical shells. This is done to limit the amount of derivation to a level desired for the scope of this paper.

4.1 Cylindrical shells

4.1.1 Differential equation

Consider the stress resultants on an element of an axisymmetrical loaded cylindrical shell, shown in figure 4.1. Because of symmetry, forces and moments acting in the hoop direction do not vary with θ . The circumferential displacement v thus vanishes in the equilibrium considerations, and only the displacements u and w need to be considered.

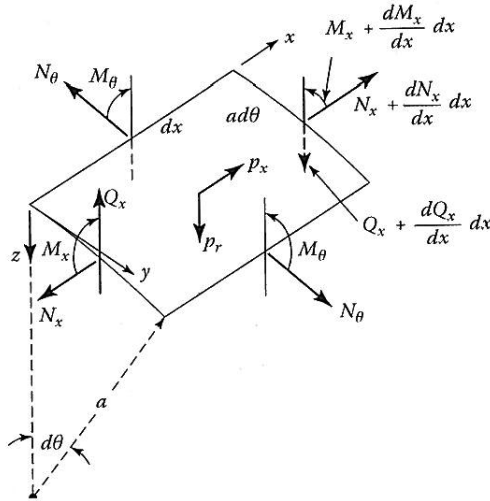


Figure 4.1: Stress resultants on axisymmetrically loaded circular cylindrical shell [3, p. 450]

Equilibrium of forces in the x and z directions, as well as moment equilibrium about the y -axis, require that [3]

$$\frac{dN_x}{dx} + p_x = 0 \quad (4.1a)$$

$$\frac{dQ_x}{dx} + \frac{1}{a}N_\theta + p_r = 0 \quad (4.1b)$$

$$\frac{dM_x}{dx} - Q_x = 0. \quad (4.1c)$$

Since $\frac{dv}{dy} = 0$, The strain-displacement relationships become [6, ch. 15]

$$\varepsilon_x = \frac{du}{dx} \quad (4.2a)$$

$$\varepsilon_\theta = -\frac{w}{a}. \quad (4.2b)$$

It is assumed that the axial force N_x is decoupled from the rest of the system. When $N_x = 0$, the hoop force N_θ can be expressed from the equations 3.8b and 4.2b as

$$N_\theta = -\frac{Eh}{a}w. \quad (4.3)$$

Hooke's law in two dimensions relates the strains and stresses:

$$N_x = \frac{Eh}{1-\nu^2}(\varepsilon_x - \nu\varepsilon_\theta) = \frac{Eh}{1-\nu^2} \left(\frac{w}{a} - \nu \frac{du}{dx} \right) \quad (4.4a)$$

$$N_\theta = \frac{Eh}{1-\nu^2}(\varepsilon_\theta + \nu\varepsilon_x) = -\frac{Eh}{1-\nu^2} \left(\frac{du}{dx} - \nu \frac{w}{a} \right). \quad (4.4b)$$

From 4.4a the strain in the x-direction is expressed in terms of the displacement w and the axial force N_x :

$$\frac{du}{dx} = \frac{1-\nu^2}{Eh}N_x + \nu \frac{w}{a} \quad (4.5)$$

The curvatures in the longitudinal and hoop directions are needed to express the bending moments. The longitudinal curvature κ_x is equal to its plate theory counterpart [6, ch. 15], and the hoop curvature is determined from inspection of figure 4.1. The following equations are obtained:

$$\kappa_x = \frac{d^2w}{dx^2}$$

$$\kappa_\theta = \frac{1}{a+w} - \frac{1}{a} \approx -\frac{w}{a^2} \approx 0.$$

The bending moments are related to the curvatures in the same way as for plates [6, ch. 15]:

$$\begin{aligned} M_x &= -D(\kappa_x - \nu\kappa_\theta) = -D\frac{d^2w}{dx^2} \\ M_\theta &= \nu M_x \end{aligned} \quad (4.6)$$

where D is the flexural rigidity of the shell, expressed as [6, ch. 1]:

$$D = \frac{Eh^3}{12(1-\nu^2)}.$$

Finally, by combining expressions 4.1, 4.5 and 4.6, we arrive at the differential equation for the cylinder:

$$D\frac{d^4w}{dx^4} + \frac{Eh}{a^2}w - \frac{\nu N_x}{aD} = \frac{P_r}{D}. \quad (4.7)$$

A more convenient form of the preceding differential equation is

$$\frac{d^4w}{dx^4} + 4\beta^4w - \frac{\nu N_x}{aD} = \frac{p_r}{D}. \quad (4.8)$$

where

$$\beta^4 = \frac{Eh}{4a^2D} = \frac{3(1-\nu^2)}{a^2h^2}. \quad (4.9)$$

The geometric parameter β is the reciprocal of length and is useful when analysing cylindrical shells. Its inverse is termed the elastic length, and is used to determine the distance from boundaries where the membrane- and bending solutions are sufficiently decoupled.

4.1.2 Solution to the differential equation

Equation 4.8 is an ordinary differential equation with constant coefficients. For a polynomial expression for the loading up to the 3. degree, a particular solution is:

$$w_p = \frac{a^2}{Eh}p_r. \quad (4.10)$$

The homogeneous solution to differential equation 4.8 when $N_x = 0$ is found as

$$w_h = e^{-\beta x}(c_1e^{i\beta x} + c_2e^{-i\beta x}) + e^{\beta x}(c_3e^{i\beta x} + c_4e^{-\beta x}). \quad (4.11)$$

The constants of integration c_1 , c_2 , c_3 and c_4 are determined based on the boundary conditions. Boundary effects which induces bending in the cylinder are added to the membrane solution to arrive at a comprehensive solution for the cylinder. For a practical problem, the solution consists of edge disturbances from both boundaries, as well as the membrane solution.

4.1.3 The infinite cylinder

A cylinder with a high length to diameter ratio is now considered, shown in figure 4.2. Such cylinders are named *infinite*.

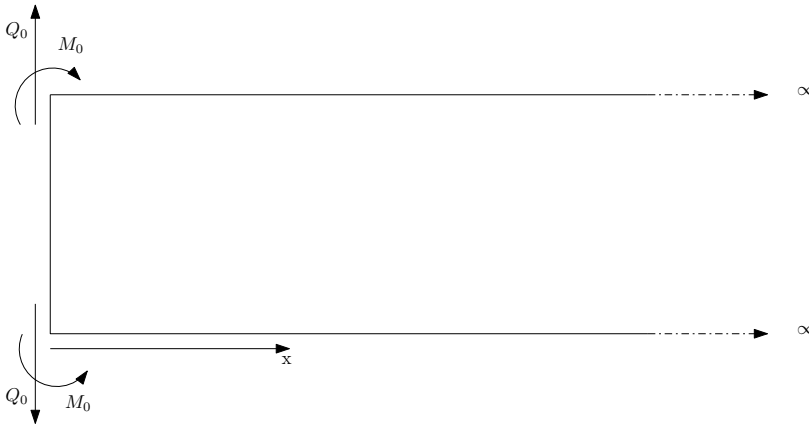


Figure 4.2: Infinite cylinder

The boundary effects in shells diminish when moving away from the edges. Since $e^{-\beta x} \rightarrow 0$ as $x \rightarrow \infty$, the integration constants c_1 and c_2 in equation 4.11 must be different than zero, while c_3 and c_4 vanish. The homogeneous solution now takes the form

$$w_h = e^{-\beta x}(c_1 e^{i\beta x} + c_2 e^{-i\beta x}) = e^{-\beta x}(c_1 \cos \beta x + c_2 \sin \beta x). \quad (4.12)$$

For a more convenient notation, functions describing the distribution of edge forces are defined:

$$\begin{aligned} f_1(\beta x) &= e^{-\beta x} \cos \beta x \\ f_2(\beta x) &= e^{-\beta x} \sin \beta x \\ f_3(\beta x) &= f_1(\beta x) + f_2(\beta x) \\ f_4(\beta x) &= f_1(\beta x) - f_2(\beta x). \end{aligned} \quad (4.13)$$

These functions are defined directly from equation 4.12. By deriving expression 4.12, and inserting it in the expressions for the stresses and displacements, we

arrive at a convenient set of equations describing stress resultants, moments and displacements in the cylindrical shell. The results are summarised in the following matrix [7]:

$$\begin{bmatrix} w \cdot 2D\beta^2 \\ \frac{N_\theta}{2a\beta^2} \\ \frac{dw}{dx} \cdot 2D\beta \\ M_x \\ \frac{Q_x}{\beta} \end{bmatrix} = \begin{bmatrix} f_4(\beta x) & f_1(\beta x) \\ f_4(\beta x) & f_1(\beta x) \\ -2f_1(\beta x) & -f_3(\beta x) \\ f_3(\beta x) & f_2(\beta x) \\ -2f_2(\beta x) & f_4(\beta x) \end{bmatrix} \times \begin{bmatrix} M_0 \\ \frac{Q_0}{\beta} \end{bmatrix} \quad (4.14)$$

M_0 and Q_0 constitute the moment and shear force at the edge $x = 0$. They are simply a reformulation of the integration constants c_1 and c_2 in the solution for the differential equation, but offer a more intuitive understanding of the different shell quantities.

4.1.4 Damping length

The functions defined in 4.13 determine how the moment, shear force and displacements vary away from the edge $x = 0$, shown in figure 4.3. It is apparent from the

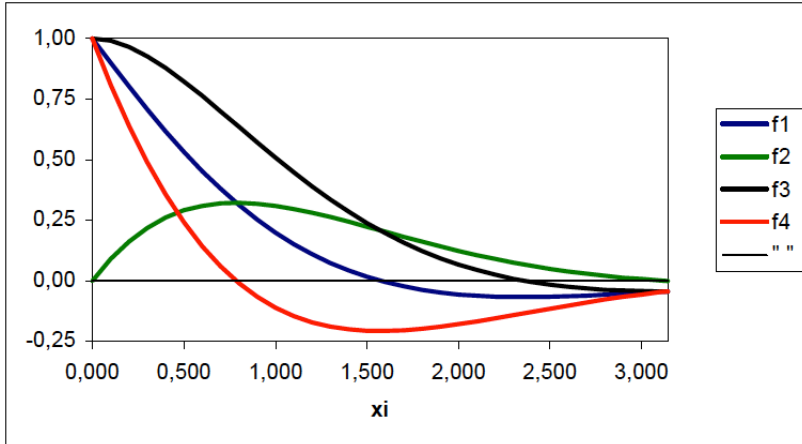


Figure 4.3: Variation of functions [5]

figure that the values of the functions becomes very small when βx has a magnitude of about 3-4. Thus the *damping length* is defined to be the value of x which corresponds to $\beta x = \pi$.

Accordingly, the damping may be defined as

$$L_c = \frac{\pi}{\beta}. \quad (4.15)$$

It is applied as a measure for evaluating whether or not edge disturbances from two edges effect one another. When the latter is the case, the bending effects may be treated separately for the two edges of the cylinder.

4.2 Spherical shells

Bending theory for spherical shells is treated similarly as for cylinders, the main difference being how the loads are carried. Spheres have an extra principal radius of curvature compared to cylinders. Consequently, the resulting differential equations become a bit more tedious.

4.2.1 Differential equation

Again we consider an infinitesimal element ABCD, as shown in figure 4.4. In addition to the membrane forces, the bending moments M_ϕ and M_θ , as well as the shear force Q_ϕ act on the element. The remaining moments and shear forces are zero due to symmetry.

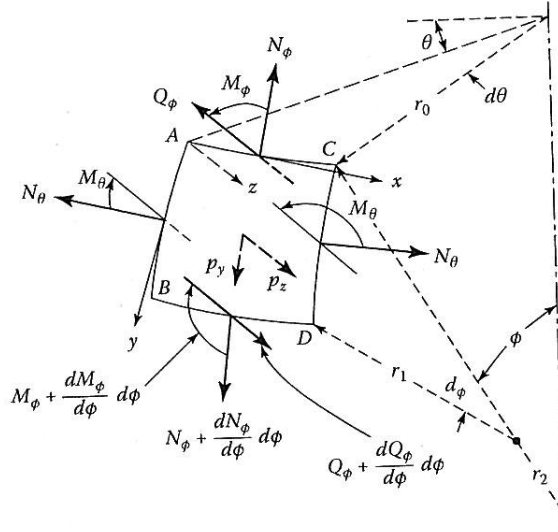


Figure 4.4: Stress resultants on axisymmetrically loaded shell of revolution [3, p. 458]

Equilibrium in the y and z directions, as well as moment equilibrium about the x -axis, yields the following set of differential equations [3]:

$$\begin{aligned}
 \frac{d}{d\phi}(N_\phi r_0) - N_\theta r_1 \cos\phi - r_0 Q_\phi + r_0 r_1 p_y &= 0 \\
 N_\phi r_0 + N_\theta r_1 \sin\phi + \frac{d(Q_\phi r_0)}{d\phi} + p_z r_1 r_0 &= 0 \\
 \frac{d}{d\phi}(M_\phi r_0) - M_\theta r_1 \cos\phi - Q_\phi r_1 r_0 &= 0
 \end{aligned} \tag{4.16}$$

For spherical shells we have $r_1 = r_2 = R$ and $r_0 = R \sin \phi$. Hence equations 4.16 simplify to

$$\frac{d}{d\phi}(N_\phi \sin \phi) - N_\theta \cos \phi - Q_\phi \sin \phi = -p_y R \sin \theta \quad (4.17a)$$

$$N_\phi \sin \phi + N_\theta \sin \phi + \frac{d}{d\phi}(Q_\phi \sin \phi) = -p_z R \sin \phi \quad (4.17b)$$

$$\frac{d}{d\phi}(M_\phi \sin \phi) - M_\theta \cos \phi - R Q_\phi \sin \phi = 0. \quad (4.17c)$$

The strain relations for the spherical shell is the same as for membrane theory, given in expressions 3.5 and 3.6. Consequently, the stress resultants are written as:

$$\begin{aligned} N_\phi &= \frac{Eh}{R(1-\nu^2)} \left[\left(\frac{dv}{d\phi} - w \right) + \nu(v \cos \phi - w) \right] \\ N_\theta &= \frac{Eh}{R(1-\nu^2)} \left[(v \cot \phi - w) + \nu \left(\frac{dv}{d\phi} - w \right) \right]. \end{aligned} \quad (4.18)$$

To express the moments in terms of the displacements v and w , we consider the *total* meridian rotation of the shell, denoted V , shown in figure 4.5.

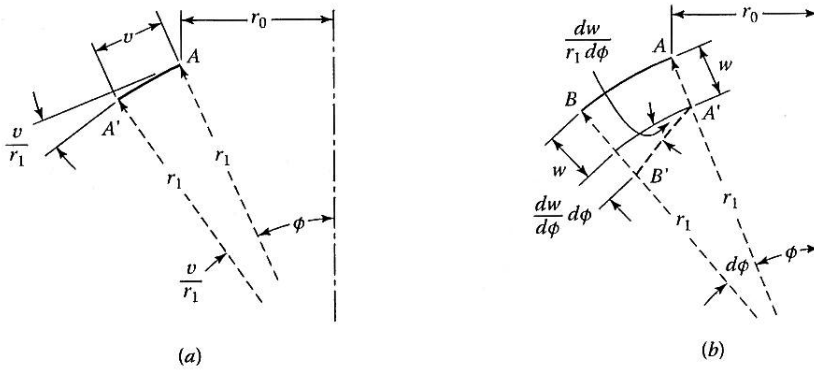


Figure 4.5: Rotation in the meridian direction of axisymmetric shell

It can be shown that the curvatures relate to the total meridian rotation by the following expressions [3, ch. 13]:

$$\begin{aligned} \kappa_\phi &= \frac{1}{R} \frac{dV}{d\phi} \\ \kappa_\theta &= V \frac{\cos \phi}{r_0} \end{aligned}$$

where

$$V = \frac{v}{R} + \frac{1}{R} \frac{dw}{d\phi}. \quad (4.19)$$

From plate theory, we know that the moments and curvatures are related as follows:

$$M_\phi = -D(\kappa_\phi + \nu\kappa_\theta)$$

$$M_\theta = -D(\kappa_\theta + \nu\kappa_\phi)$$

Accordingly, the moments are expressed as:

$$\begin{aligned} M_\phi &= -\frac{D}{R} \left[\frac{dV}{d\phi} + \nu V \cot\phi \right] \\ M_\theta &= -\frac{D}{R} \left[V \cot\phi + \nu \frac{dV}{d\phi} \right] \end{aligned} \quad (4.20)$$

By combining the equations 4.17, 4.18 and 4.20, bending of a spherical shells are reduced to two differential equations for the shear force Q_ϕ and meridian rotation V :

$$\frac{d^2 Q_\phi}{d\phi^2} + \cot\phi \frac{dQ_\phi}{d\phi} - Q_\phi (\cot^2\phi - \nu) = EhV \quad (4.21)$$

$$\frac{d^2 V}{d\phi^2} + \frac{dV}{d\phi} \cot\phi - V (\cot^2\phi + \nu) = -\frac{R^2 Q_\phi}{D} \quad (4.22)$$

A total solution of the two foregoing differential equations can be found by applying hypergeometric series. This results in relatively complex expressions, which are out of the scope of this paper.

An approximate solution, presented by Geckler, is chosen. He showed that the higher order derivatives are the dominant terms in the two differential equations as long as the opening angle ϕ_0 is large enough [6]. This simplifies the mathematics such an extent that the procedure developed for cylindrical shells can be used for spheres. As a consequence equations 4.21 and 4.22 are simplified to

$$\frac{d^2V}{d\phi^2} + \frac{1}{D}Q_\phi R^2 = 0 \quad (4.23)$$

$$\frac{d^2Q_\phi}{d\phi^2} - EhV = 0. \quad (4.24)$$

By eliminating V , the problem of bending of spherical shells are reduced to a fourth order differential equation as a function of the shear force Q_ϕ :

$$\frac{d^4Q_\phi}{d\phi^4} + 4\lambda^4Q_\phi = 0, \quad (4.25)$$

where

$$\lambda^4 = \frac{EhR^2}{4D} = 3(1 - \nu^2) \left(\frac{R}{h}\right)^2. \quad (4.26)$$

4.2.2 Solution to the differential equation

Differential equation 4.25 resembles the equation for cylindrical shells. The general solution is

$$Q_\phi = e^{\lambda\phi}(C_1\cos\lambda\phi + C_2\sin\lambda\phi) + e^{-\lambda\phi}(C_3\cos\lambda\phi + C_4\sin\lambda\phi), \quad (4.27)$$

where C_1 through C_4 are arbitrary constants.

A more convenient way to write the expressions in the following is by replacing the angle ϕ by

$$\psi = \phi_0 - \phi, \quad (4.28)$$

which starts at the edge of the sphere, as shown in figure 4.6. The variable t is introduced as

$$t = \lambda\psi. \quad (4.29)$$

The differential equation can now be rewritten as

$$Q_\phi = e^{-t}(C_1\cos t + C_2\sin t). \quad (4.30)$$

In order to make the solution to the differential equation as convenient as possible, a set of functions are defined in the same manner as for the cylinder:

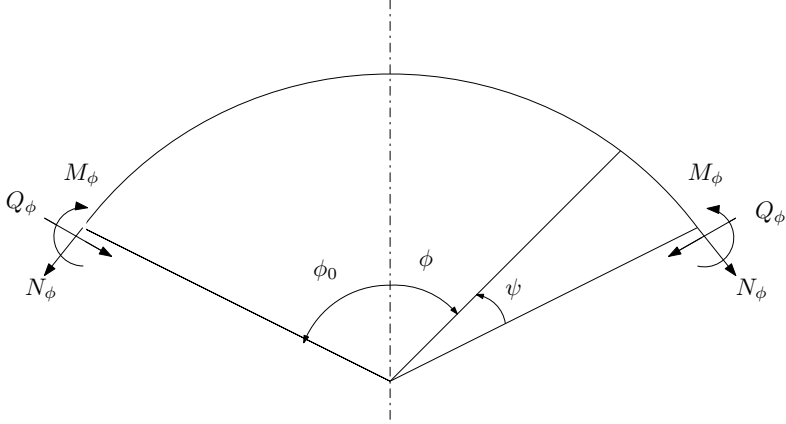


Figure 4.6: Definition of angles and edge forces for spherical shells

$$\begin{aligned}
 f_1(t) &= e^{-t} \cos t \\
 f_2(t) &= e^{-t} \sin t \\
 f_3(t) &= f_1(t) + f_2(t) \\
 f_4(t) &= f_1(t) - f_2(t).
 \end{aligned} \tag{4.31}$$

The different shell parameters contain the first, second and third derivative of Q_ϕ . By deriving 4.30 and applying them in the expressions for the various shell parameters, the shell forces and displacements are found. The results may be summarised in the following matrix [7]:

$$\begin{bmatrix}
 Q_\phi \\
 N_\phi \cdot \tan \phi \\
 N_\theta \frac{1}{\lambda} \\
 M_\phi \frac{EhR}{2\lambda^3 D} \\
 M_\theta \frac{EhR}{2\nu\lambda^3 D} \\
 V \frac{Eh}{2\lambda^2} \\
 \delta \frac{Eh}{\lambda R \sin \phi}
 \end{bmatrix}
 =
 \begin{bmatrix}
 f_1(t) & f_2(t) \\
 -f_1(t) & -f_2(t) \\
 -f_3(t) & f_4(t) \\
 f_4(t) & f_3(t) \\
 f_4(t) & f_3(t) \\
 f_2(t) & -f_1(t) \\
 -f_3(t) & f_4(t)
 \end{bmatrix}
 \times
 \begin{bmatrix}
 C_1 \\
 C_2
 \end{bmatrix} \tag{4.32}$$

δ in the matrix describes the horizontal displacement at the edge of the sphere. This is a useful measure when analysing the junction between connected shells,

and is expressed by the displacements w and v as $\delta = v\cos\phi - w\sin\phi$, shown in figure 4.7(a). Still a more convenient set of equations are desired. As for the cylinder, matrix 4.32 is reformulated by replacing the integration constants C_1 and C_2 with the edge moment and shear force, M_0 and Q_0 . The reformulated expressions become [7]:

$$\begin{bmatrix} R_\phi \cdot \sin\phi \\ M_\phi \cdot \frac{EhR}{2\lambda^2 D} \\ Q_\phi \\ N_\phi \cdot \tan\phi \\ \frac{N_\theta}{\lambda} \\ M_\theta \cdot \frac{EhR}{2\nu\lambda^3 D} \\ V \cdot \frac{Eh}{2\lambda^2} \\ \delta \cdot \frac{Eh}{\lambda R \sin\phi} \end{bmatrix} = \begin{bmatrix} f_4(t) & -f_2(t) \\ 2f_2(t) & f_3(t) \\ -f_4(t) & f_2(t) \\ f_4(t) & -f_2(t) \\ 2f_1(t) & f_4(t) \\ 2f_2(t) & f_3(t) \\ -f_3(t) & -f_1(t) \\ 2f_1(t) & f_4(t) \end{bmatrix} \times \begin{bmatrix} R_0 \cdot \sin\phi \\ M_0 \cdot \frac{EhR}{2\lambda^3 D} \end{bmatrix} \quad (4.33)$$

In addition to the horizontal displacement previously mentioned, the horizontal component of the forces at the boundary of the shell is expressed by R_ϕ . It is a combination of meridian force N_ϕ and shear force Q_ϕ , shown in figure 4.7(b).

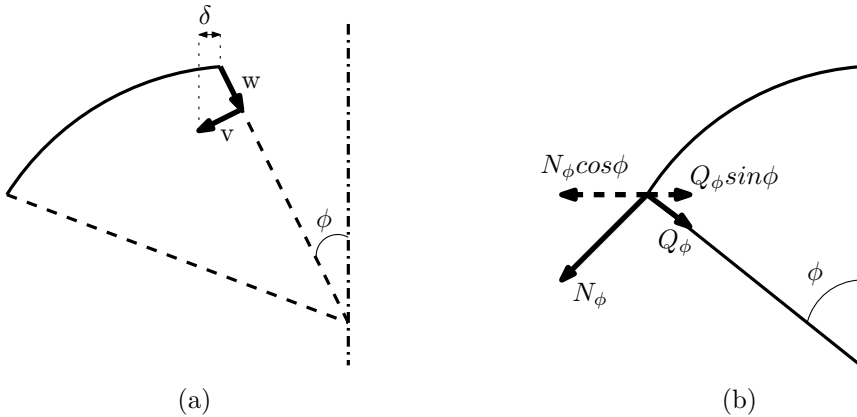


Figure 4.7: (a) Horizontal displacement (b) Horizontal force at edge

The necessary background material for the study of spherical shells of revolution, summarised in matrix 4.33, is hence concluded. When the geometrical and material

data of the structure is known, equations 4.33 gives the necessary expressions for solving the bending theory of the spherical shell.

4.3 Ring beams

Connections between cylinders and spheres have difficulties transferring shear forces because of the small cross sectional area in the connection. Strengthening the connection is often done with a ring beam. The beam ensures an even transfer of shear forces as well as preventing ovalisation of the cylinder. When cylindrical structures are designed using concrete, edge beams can be implemented by either installing a steel beam or by adding extra reinforcement at the cylinder edge. To make room for extra reinforcement, additional concrete is added either by a gradual increase of the cylinder wall thickness or by casting a rectangular concrete cross section. The latter is considered in the following.

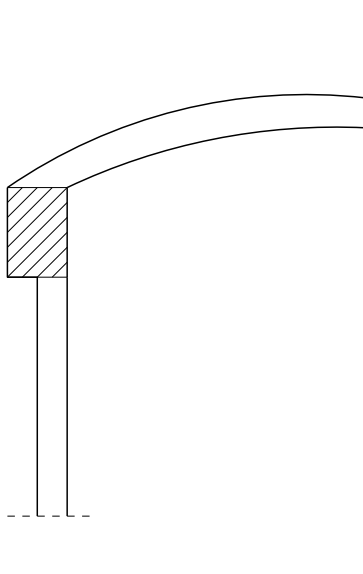


Figure 4.8: Ring beam connecting cylindrical and spherical shell

A typical connection between cylinders and spheres is illustrated in figure 4.8. The connection is considered rigid. The main objective from the following derivations is to express the deformations state of the beam. It is assumed that a vertical deflection of the ring beam is negligible, leaving two degrees of freedom; radial displacement and rotation.

Figure 4.9 shows a force H from the adjacent shells acting on the ring beam. The axial force T in the beam is found from equilibrium of forces:

$$2T = \int_0^\pi H a \cdot \sin\theta d\theta = 2Ha,$$

and rewritten as

$$T = H \cdot a. \quad (4.34)$$

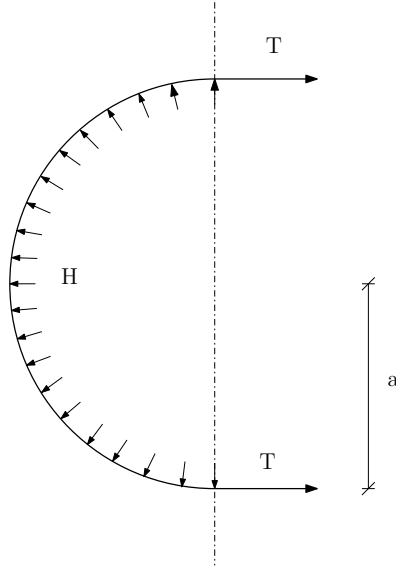


Figure 4.9: Radial force H acting on ring beam

The hoop strains are determined from Hooke's law as

$$\varepsilon_{\theta H} = \frac{T}{EA},$$

and the total change of length becomes

$$\Delta_{\theta} = 2\pi a \varepsilon_{\theta H} = \frac{2\pi a}{EA} T.$$

Finally, the radial expansion can be expressed as [7]:

$$w_h = a \varepsilon_{\theta H} = \frac{a}{EA} T = \frac{a^2}{EA} H. \quad (4.35)$$

Now that the displacement w_h from the force H is determined, the displacement and rotation from bending moments are addressed. The moments acting on the beam are a combination of bending moments transferred directly from the connected shells, as well as shear forces with an eccentricity relative to the beams neutral axis.

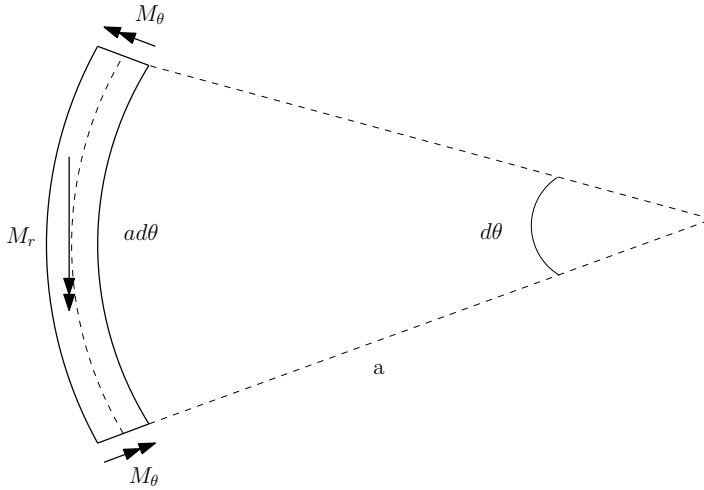


Figure 4.10: Bending moments in ring beam

Moments occur in two directions, shown in figure 4.10 [7]. Moment equilibrium about the tangent axis yields:

$$M_r a d\theta - M_\theta d\theta = 0 \rightarrow M_\theta = a M_r$$

The bending moments results in linearly varying stresses which are expressed as:

$$\sigma = \frac{M_\theta y}{I},$$

where I is the second moment of area about the beams horizontal axis. For a rectangular cross section the second moment of area becomes:

$$I = \frac{bh^3}{12}.$$

The strain in the ring beam from the bending stresses are expresses as:

$$\varepsilon_{\theta M} = \frac{M_\theta y}{EI}.$$

Again the total change of length is determined, now from the bending action. The displacement varies linearly over the beam height:

$$\Delta_{\theta M} = 2\pi a \varepsilon_{\theta M} = \frac{2\pi a y}{EI} M_{\theta M}. \quad (4.36)$$

Finally, the radial displacement as a result of the bending moments acting on the beam is determined as:

$$w_M(y) = a\varepsilon_{\theta M} = \frac{ay}{EI}M_{\theta} = \frac{a^2y}{EI}M_r. \quad (4.37)$$

By deriving 4.37, a constant rotation is obtained:

$$\alpha_r = \frac{w_M(y)}{y} = \frac{a^2}{EI}M_r \quad (4.38)$$

Expressions 4.35, 4.37 and 4.38 constitute the total displacement and rotation of the ring beam, as shown in figure 4.11. From the deformation of the beam the two adjacent shells are coupled through compatibility conditions.

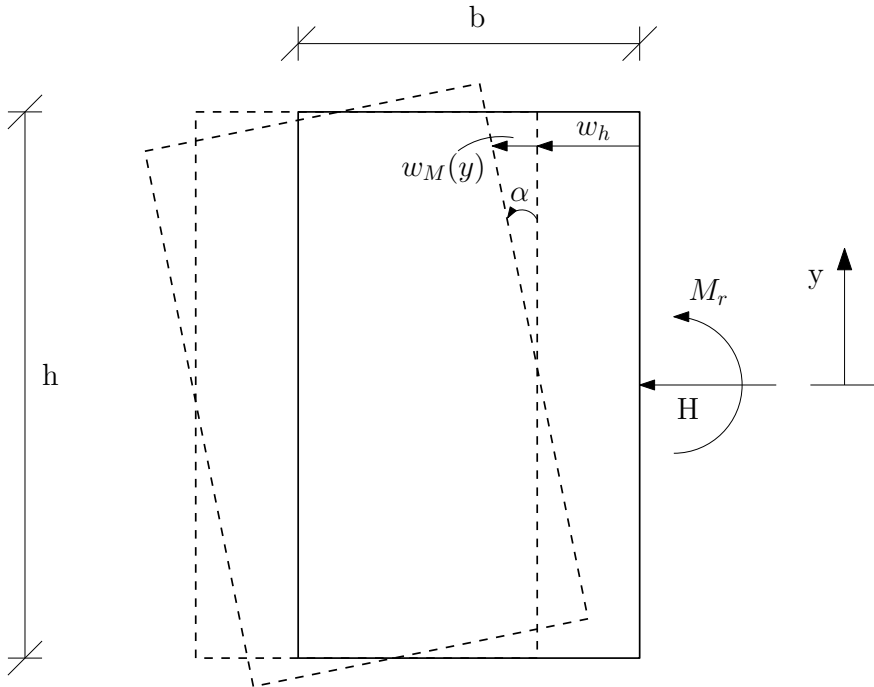


Figure 4.11: Total radial displacement and rotation of ring beam

4.4 Circular plates

A typical way to seal off cylindrical storage tanks is by using circular plates. Plates carry loads mainly by bending and shear action, which in turn induce bending effects onto the cylinder. In order to solve problems involving connection of cylinders and plates, the analytical foundation for circular plates are needed. As this thesis focuses on shells, the analytical foundation for laterally loaded circular plates are summarised in table 4.1. A thorough derivation of the expressions is given in the book *Theory of Plates and Shells* by Timoshenko and Woinowski-Krieger [6].


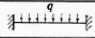
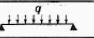
	General formulae			
w	$\frac{qr^4}{64D} + C_1 \frac{r^2}{4} + C_2 \log \frac{r}{a} + C_3$	$\frac{M_a}{2D(1+\nu)}(a^2 - r^2)$	$\frac{q}{64D}(a^2 - r^2)^2$	$\frac{q}{64D}(a^2 - r^2) \left(\frac{5+\nu}{1+\nu} a^2 - r^2 \right)$
$\frac{dw}{dr}$	$\frac{qr^2}{16D} + C_1 \frac{r}{2} + C_2 \frac{1}{r}$	$-\frac{M_a r}{D(1+\nu)}$	$-\frac{qr}{16D}(a^2 - r^2)$	$-\frac{qr}{16D} \left(\frac{3+\nu}{1+\nu} a^2 - r^2 \right)$
$\frac{d^2w}{dr^2}$	$\frac{3qr^2}{16D} + \frac{C_1}{2} - C_2 \frac{1}{r^2}$	$-\frac{M_a}{D(1+\nu)}$	$-\frac{q}{16D}(a^2 - 3r^2)$	$-\frac{q}{16D} \left(\frac{3+\nu}{1+\nu} a^2 - 3r^2 \right)$
C_1		$-\frac{2M_a}{D(1+\nu)}$	$-\frac{qa^2}{8D}$	$-\frac{qa^2(3+\nu)}{8D(1+\nu)}$
C_2		0	0	0
C_3		$\frac{M_a a^2}{2D(1+\nu)}$	$\frac{qa^4}{64D}$	$\frac{qa^4(5+\nu)}{64D(1+\nu)}$
M_r	$-D \left(\frac{d^2w}{dr^2} + \nu \frac{dw}{dr} \right)$	$+M_a$	$\frac{q}{16} [a^2(1+\nu) - r^2(3+\nu)]$	$\frac{q}{16} (3+\nu)(a^2 - r^2)$
M_t	$-D \left(\frac{1}{r} \frac{dw}{dr} + \nu \frac{d^2w}{dr^2} \right)$	$+M_a$	$\frac{q}{16} [a^2(1+\nu) - r^2(1+3\nu)]$	$\frac{q}{16} [a^2(3+\nu) - r^2(1+3\nu)]$
M_a		$+M_a$	$-\frac{qa^2}{8}$	0
M_{ξ}		$+M_a$	$\frac{qa^2}{16}(1+\nu)$	$\frac{qa^2}{16}(3+\nu)$

Table 4.1: Results for circular-slab analysis [2, p. 82]

In the table, a and r refer to the inner and outer radius of the plate, as shown in figure 4.12a. The moments acting on the plate are shown in figure 6.15. This provides the sufficient background material for solving cylindrical shells with circular plate tops.

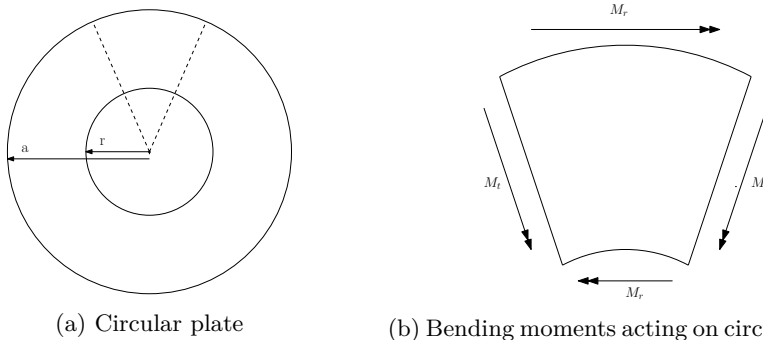


Figure 4.12

5 Diana

The finite element software Diana (displacement analyzer) is used for the numerical simulations in this paper. As the name implies the software is based on the displacement method. It is a multi-purpose finite element program developed by *TNO DIANA BV*, and includes both nonlinear and three dimensional capabilities. The software is developed from a civil engineering perspective, and the most appealing capabilities are therefore in the fields of concrete and soil analysis. Teachers editions version 9.4.4 is used in this paper.

The modelling process can generally be divided into three main parts; preprocessing, analysis and postprocessing. They concern the different phases of the analysis, and a small introduction to each part is presented in the following.

5.1 Preprocessing

In preprocessing the general model is constructed. Shells are modelled in Diana's axisymmetrical environment. Half of the geometry is created and rotated about the y -axis at $x = 0$ to generate a coherent structure. This results in faster processing times and simpler models.

For the linear analyses of thin shells conducted in this paper, the modelling is done in one dimension using straight lines and arches. The models are build up in a layered fashion, from points to lines to attached loads and material properties. Each line and arch are meshed with a predetermined number element per line. The teachers edition restricts element density to 99 elements per line and 1000 elements in total. Staying under this threshold proved sufficient for scope the analyses performed in this paper. Boundary conditions are specified by restricting either points or nodes to displace and/or rotate. Figure 5.1 shows a typical construction of a thin shell model.

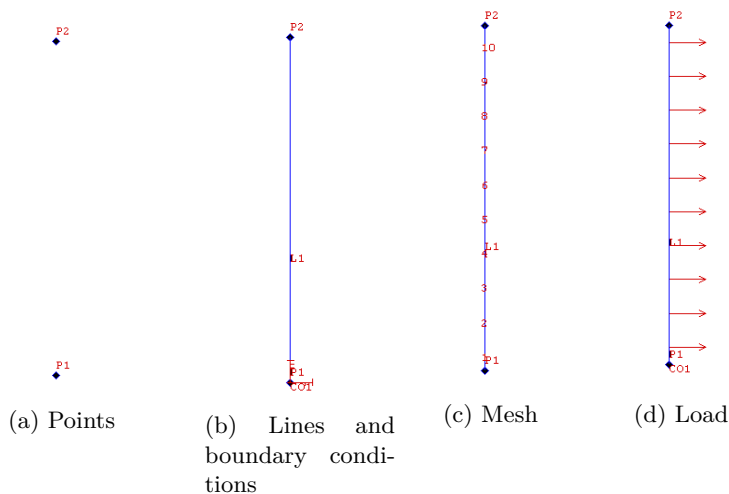


Figure 5.1: Construction of a typical line model

For the purpose of nonlinear analysis, two-dimensional models are necessary. The principals are equal to the previously discussed modelling, but lines now make up surfaces in which reinforcement is placed. Greater consideration of material models must be considered, which is explained in more detail in section 8.2.1.

5.2 Analysis

When the model is completed, a .dat file containing the stiffness matrices and other vital information is generated. After choosing the the desired analysis type, the file is run through the analysis tool in Diana. The dat file is the main text describing the model, and certain parameters, for instance hydrostatic load, can only be specified here.

5.3 Postprocessing

Postprocessing concerns presentation and evaluation of the results. Diana provides several ways of presenting them, ranging from graphs to contour plots.

6 Selected shell structures

In this section a series of shell structures are analysed both analytically and numerically. The examples are chosen such that they highlight all of the previously studied theory. All structures are of connected thin concrete shells with necessary material data chose forehand.

6.1 Analytical solutions

The analytical theory on thin shells is complex and best understood through concrete examples which highlights different aspect of thin shell behaviour. Because of this complexity the upcoming analytical solutions are thoroughly reviewed. This is done to ensure a coherent understanding of the governing principals at work for thin concrete shell structures.

6.1.1 Cylinder with circular plate top

Figure 6.1 shows a cylindrical concrete shell with a circular plate top, loaded with an internal gas pressure of $100 \frac{kN}{m^2}$. The data needed for solving the structure is presented in the figure. A complete integer solution is given in appendix A.

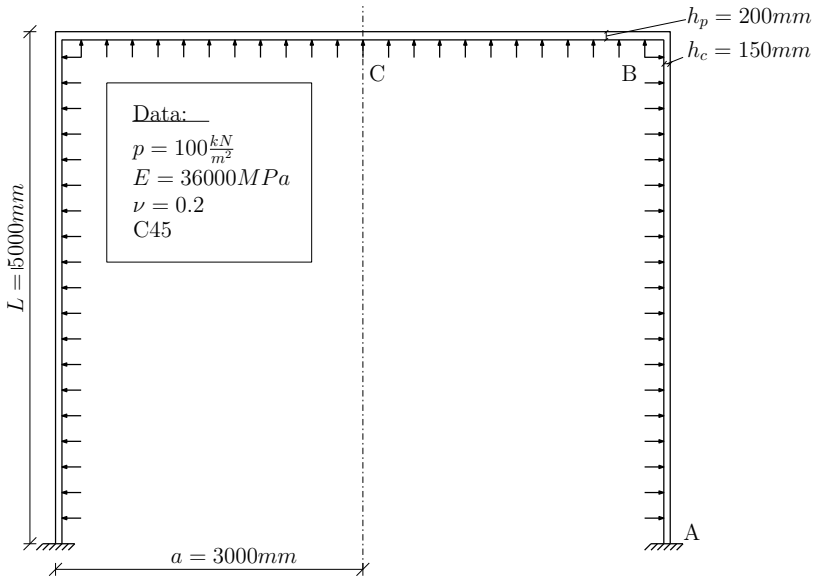


Figure 6.1: Geometry and material data for cylinder with circular plate top

Damping length

As a starting point, the damping length L_c is evaluated in order to check whether or not the cylinder can be simplified as infinite. The elastic length is found from expression 4.9 as:

$$\beta = \sqrt[4]{\frac{3(1-\nu^2)}{a^2 h^2}} = 1.942 \cdot 10^{-3} \frac{1}{mm},$$

and the damping length becomes

$$L_c = \frac{\pi}{\beta} = 1618mm.$$

Since $L_c < 2L$ the two edges of the cylindrical shell can be treated separately.

Edge A

The particular solution w_p from a constant pressure load is constant over the cylinder. From expression 4.10 it is expressed as

$$w_p = \frac{p \cdot a^2}{Eh}.$$

Since w_p is constant there exists no particular solution for the rotation of the cylinder.

The edge disturbances are considered from the homogeneous solution. The initial conditions of the clamped edge are exploited:

$$w(x=0) = 0 \quad , \quad \frac{dw}{dx}(x=0) = 0.$$

From matrix 4.14, the radial displacement w and angle $\frac{dw}{dx}$ are expressed. The homogeneous and particular solutions are combined and written in matrix form:

$$\begin{bmatrix} \frac{1}{2D_c \beta^2} & \frac{1}{2D_c \beta^3} \\ -\frac{1}{2D_c \beta} & \frac{1}{2D_c \beta^2} \end{bmatrix} \times \begin{bmatrix} M_0 \\ Q_0 \end{bmatrix} = \begin{bmatrix} -w_p \\ 0 \end{bmatrix}$$

Solving yields the moment and shear force at edge A:

$$\begin{bmatrix} M_0 \\ Q_0 \end{bmatrix} = \begin{bmatrix} 13.3 \frac{kNm}{m} \\ -51.5 \frac{kN}{m} \end{bmatrix}.$$

This constitutes the necessary information to deduce the total response for the lower face of the cylinder.

Junction B

In order to solve for the moment and shear force acting in the junction of the structure, compatibility and equilibrium conditions are necessary.

For the laterally loaded plate the weight of the concrete must be considered as a downwards distributed load. A reasonable load of $w = 5 \frac{kN}{m^2}$ is therefore subtracted from the internal pressure, leaving a total upward pressure of $95 \frac{kN}{m^2}$ on the plate, denoted q .

At first the plate is considered free to rotate, as shown in figure 6.2a. From table 4.1 the rotation is expressed as as

$$\left(\frac{dw}{dx}\right)_{free} = \theta_q = \frac{qa^3}{16D_p} \left(\frac{3+\nu}{1+\nu} - 1\right),$$

where D_p is the flexural stiffness of the plate. As clockwise rotation is defined as positive, this constitutes a positive rotation. The coupling of the shell and plate creates a joint moment M_a , which causes a counterclockwise rotation in the plate, shown in figure 6.2b. The rotation is expressed as:

$$\left(\frac{dw}{dx}\right)_{moment} = \theta_M = \frac{a}{D_p(1+\nu)} M_a.$$

The total rotation of the plate is the difference between the two foregoing equations:

$$\theta_p = \theta_q - \theta_M.$$

In the case of the cylinder, the rotation is once again expressed from equations 4.14. Since the two edges of the cylinder do not effect one another, $x = 0$ is continually used in the equations. The rotation is found to be

$$\theta_c = \frac{dw}{dx}(0) = -\frac{1}{2D_c\beta} \left(2M_0 + \frac{Q_0}{\beta}\right).$$

From this point on the rotations for the two respective components are combined through compatibility of deformations in the corner.

Compatibility

As the first compatibility condition, an equal rotation of the cylinder and plate in junction B is required, namely that $\theta_c = -\theta_p$. Inserting the respective variables and rearranging yields

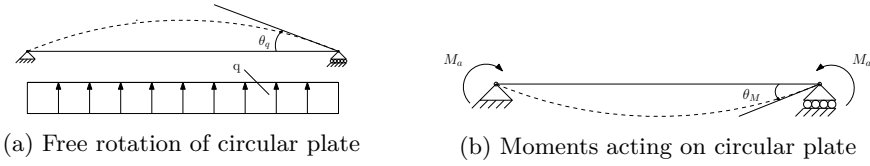


Figure 6.2: Forces and moments acting on circular plate and their corresponding rotations

$$\left(\frac{1}{D_c \beta} + \frac{a}{D_p(1+\nu)} \right) M_a + \frac{1}{2D_c \beta^2} Q_a = \theta_q, \quad (6.1)$$

where M_0 and Q_0 have been replaced by the joint moment and shear force M_a and Q_a .

As a second condition, the plate is considered infinitely stiff in the plane. Hence it is reasonable to consider the radial displacement w at the top of the cylinder to be equal to zero. On this premise, a second condition is obtained from expression 4.14:

$$w_{tot} = w_p + w_h = 0 \rightarrow \frac{1}{2D_c \beta^2} M_a + \frac{1}{2\beta^3 D_c} = -w_p \quad (6.2)$$

By solving equations 6.1 and 6.2, the joint moment and shear force are determined:

$$\begin{bmatrix} M_a \\ Q_a \end{bmatrix} = \begin{bmatrix} 88.5 \frac{kNm}{m} \\ -197.3 \frac{kN}{m} \end{bmatrix}.$$

The edge forces and bending moments obtained in the preceding calculations comprise the necessary information for plotting all the responses in the structure.

6.1.1.1 Distributions

From expressions 4.14 and table 4.1 the distribution of forces and bending moments for increasing values of x are described. The homogeneous and particular solutions are added together to arrive at the total response of the structure. In the plots, $x = 0$ marks the bottom of the cylinder and centre of the plate, respectively.

The bending moments are expressed as follows:

$$M_{xA} = M_0 f_3(\beta x) + \frac{Q_0}{\beta} f_3(\beta x)$$

$$M_{xB} = M_a f_3(\beta x) + \frac{Q_a}{\beta} f_3(\beta x)$$

$$M_r = M_a - \frac{q}{16} (3 + \nu)(a^2 - x^2)$$

$$M_t = M_a - \frac{q}{16} (a^2(3 + \nu) - x^2(1 + 3\nu)).$$

Figure 6.3 shows how the bending moments vary across the length of the cylinder and plate. In the case of the cylindrical shell, it is apparent that the moments damp rapidly from the edges and vanish towards the intermediate part of the shell. As expected the two edges of the shell experience the highest bending moments.

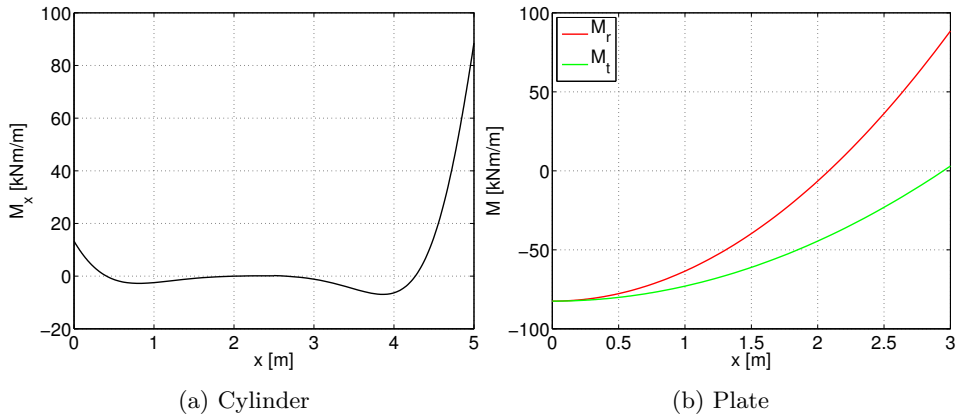


Figure 6.3: Distribution of moments in the structure

The equations describing the distribution of shear forces are:

$$Q_{xA} = -2M_0 f_2(\beta x) + Q_0 f_4(\beta x)$$

$$Q_{xB} = -2M_a f_2(\beta x) + Q_a f_3(\beta x)$$

$$Q_r = -\frac{q}{2} x$$

Figure 6.4 shows the shear force distribution in the structure. As for the moments, the shear force is damped rapidly from the edges of the cylinder.

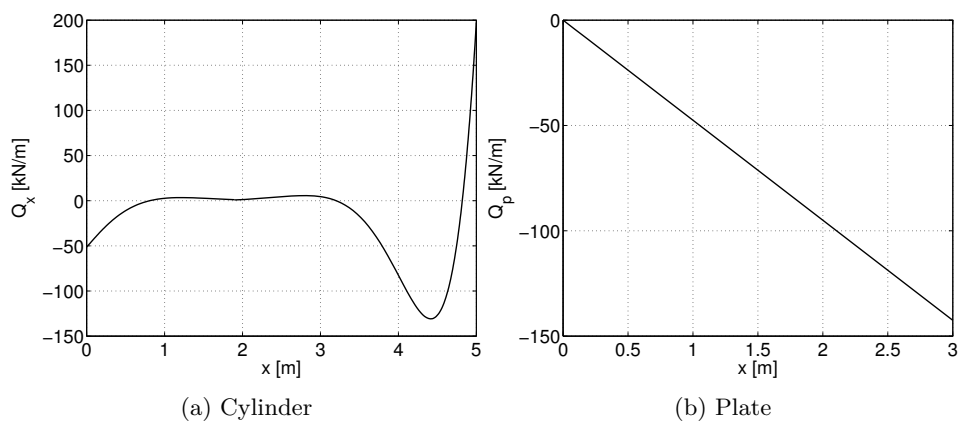


Figure 6.4: Distribution of shear forces in the structure

The hoop force has an additional particular solution to consider. The total solution is expressed as:

$$N_{\theta A} = N_h(\beta x) + N_p = 2a\beta^2(M_0 f_4(\beta x) + \frac{Q_0}{\beta} f_1(\beta x) + pa)$$

$$N_{\theta B} = N_h(\beta x) + N_p = 2a\beta^2(M_a f_4(\beta x) + \frac{Q_a}{\beta} f_1(\beta x) + pa)$$

Figure 6.5 shows how the hoop force is distributed. It has zero magnitude at the edges, while increasing to the particular solution of $300 \frac{kN}{m}$ at the clamped edges.

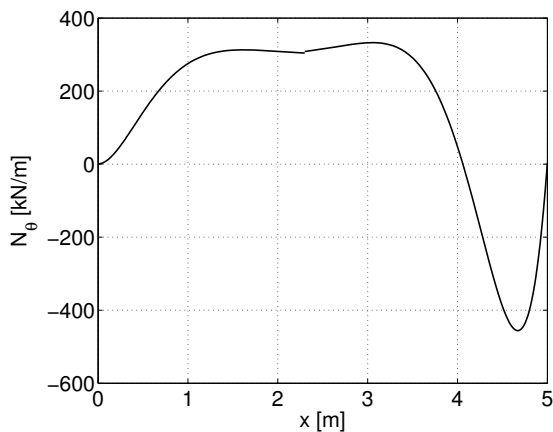


Figure 6.5: Distribution of hoop forces in the cylindrical shell

The preceding distributions emphasise the load carrying behaviour of shells. The moments and shear forces are large at the boundaries and damped out towards the intermediate part of the shell. The dominant load carrying action is the hoop force, which is present in most of the cylindrical shell.

6.1.2 Cylinder with spherical roof

Focus is now shifted to a cylindrical water tank with spherical roofing. The tank is clamped at the bottom edge and has a rigid connection between the shells, as shown in figure 6.6. The system is loaded with a hydrostatic water pressure on the cylinder wall as well as with snow load and self weight on the spherical roof. Relevant material and geometrical data are given in the figure. A total integer solution is given in appendix B.

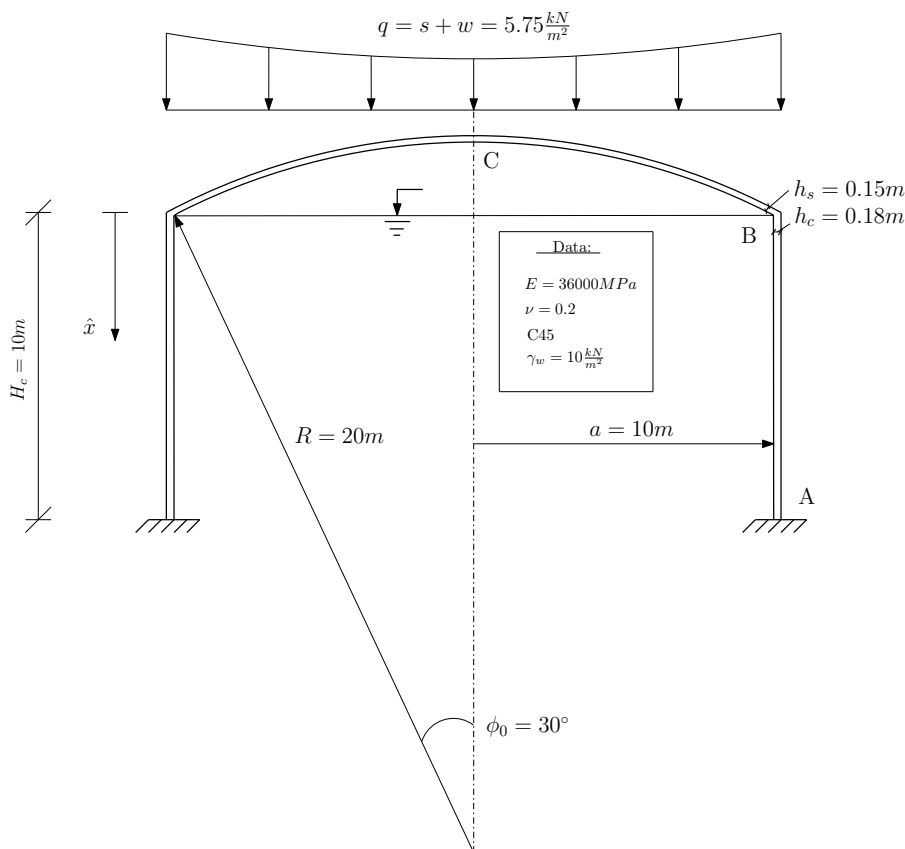


Figure 6.6: Geometry and material data for a cylinder with spherical roof

Loads

It is assumed that the snow load acting on the sphere follows the same distribution as the self-weight. On curved surfaces more material is located where there is greater curvature, resulting in the load distribution shown in figure 6.6. Reasonable magnitudes are chosen for the loads; $s = 2 \frac{kN}{m^2}$ for the snow load and $w = 2.75 \frac{kN}{m^2}$ for the self weight of the concrete. Hence a total load on the roof becomes:

$$q = s + w = 5.75 \frac{kN}{m^2}.$$

From table 3.3, the load q is decomposed into components in the meridian and thickness directions:

$$p_\phi = q \sin\phi, \quad p_z = -q \cos\phi.$$

The decomposed loads are implemented in formulas for the membrane solution of the spherical shell. The hydrostatic water pressure on the cylinder wall varies linearly with depth:

$$p(x) = \gamma_w \hat{x},$$

where γ_w is the specific weight of water. $\hat{x} = 0$ is defined at the upper edge, shown in figure 6.6.

Damping length

The damping length for the cylinder is once again checked to determine whether or not the two edges of the cylinder can be considered decoupled with respect to the edge disturbances. In the same manner as for the previous example, the elastic length is found as

$$\beta = \sqrt[4]{\frac{3(1-\nu^2)}{a^2 h^2}} = 970.1 \cdot 10^{-6} \frac{1}{mm},$$

and the damping length becomes:

$$L_c = \frac{\pi}{\beta} = 3238mm.$$

$H_c < 2L_c$, and the two edges of the cylinder are decoupled. As there are no holes in the sphere it only has one edge, and the damping length does not have to be evaluated.

Edge A

The lower edge of the cylinder experience the full weight of the overhead water. From expression 4.10 the particular solution for the radial displacement is determined as:

$$w_p = \frac{a^2}{Eh_c} p(\hat{x}) = \frac{a^2}{Eh_c} \gamma_w \hat{x}.$$

Deriving w_p with respect to \hat{x} yields a constant particular solution for the angle θ :

$$\theta_p = \frac{a^2}{Eh_c} \gamma_w.$$

By demanding zero displacement and rotation at the edge, two equations with two unknowns are obtained:

$$\begin{bmatrix} \frac{1}{2D_c\beta^2} & \frac{1}{2D_c\beta^3} \\ \frac{1}{2D_c\beta} & \frac{1}{2D_c\beta^2} \end{bmatrix} \times \begin{bmatrix} M_0 \\ Q_0 \end{bmatrix} = \begin{bmatrix} -w_p(10m) \\ -\theta_p \end{bmatrix}$$

Solving the equation system with respect to the edge forces yields:

$$\begin{bmatrix} M_0 \\ Q_0 \end{bmatrix} = \begin{bmatrix} 47.6 \frac{kNm}{m} \\ -97.7 \frac{kN}{m} \end{bmatrix}$$

Junction B

The upper edge of the cylinder experience forces and moments from the roof which propagates downwards the longitudinal axis of the cylindrical shell. In order to determine the moment and shear force in the junction, a set of compatibility requirements are needed. Both the radial displacement and meridian rotation of the two shells must be equal in the junction where they meet, assuming that the connection between them are sufficiently rigid. The expressions for the two shells are therefore addressed separately and united through a set of compatibility conditions at the end.

Cylinder

Since the hydrostatic pressure is zero at the upper edge of the cylinder, the particular solution for the displacement w_p must also be zero. θ_p is constant, as previously shown. From expressions 4.14 the total solution for the upper edge becomes:

$$w(0) = w_h(0) = \frac{1}{2D_c\beta^2} \left(M_{0c} + \frac{Q_{0c}}{\beta} \right) \quad (6.3a)$$

$$\theta(0) = \theta_h(0) + \theta_p(0) = -\frac{1}{2D_c\beta} \left(2M_{0c} + \frac{Q_{0c}}{\beta} \right) + \frac{a^2}{Eh_c} \gamma_w \quad (6.3b)$$

Sphere

Solving for the sphere is more complicated. This is due to the direction of the membrane forces, which are tangential at every point of the surface. As mentioned in the theory, the membrane solution assumes boundary conditions compatible with the prerequisites made in membrane theory. For this reason, a correction of the membrane state is necessary in order to obtain an accurate solution.

Figure 6.7a shows the spherical shell with boundary conditions compatible with membrane theory. The membrane force $N_{\phi m}$ has the angle 30° with the horizontal plane.

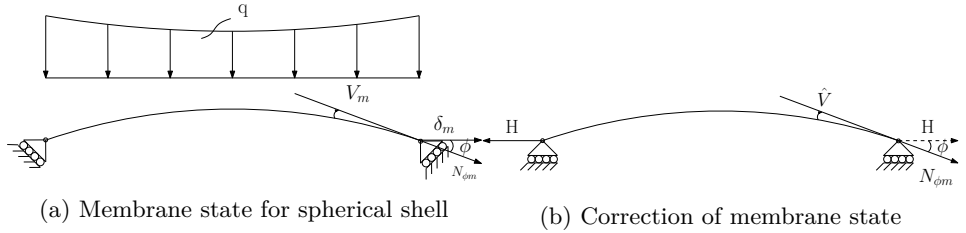


Figure 6.7: Membrane state for spherical roof

Table 3.2 provides the equations describing the membrane forces. The meridian forces at the boundary are expressed as:

$$N_{\phi m} = -\frac{R}{\sin^2 \phi_0} \int_0^{\phi_0} \sin \phi (p_\phi \sin \phi - p_z \cos \phi) d\phi = -\frac{Rq}{\sin^2 \phi_0} (1 - \cos \phi_0) = -61.6 \frac{kN}{m},$$

$$N_{\theta m} = Rp_z - N_{\phi m} = -38.0 \frac{kN}{m}.$$

where $\phi_0 = 30^\circ$ is the opening angle of the shell, shown in figure 6.6.

From the membrane forces, the relative displacement and meridian rotation are determined:

$$\delta_m = \frac{R \sin \phi_0}{E h_s} (N_{\theta m} - \nu N_{\phi m}) = -47.5 \cdot 10^{-6} m$$

$$V_m = \frac{1}{E h} \left[\frac{\partial}{\partial \phi} (N_\theta - \nu N_\phi) - (1 + \nu) \cot \phi_0 (N_\phi - N_\theta) \right] = 23.4 \cdot 10^{-6} rad.$$

These are the membrane quantities which correspond to an ideal sphere, that is, a solution where all loads are resisted solely by membrane forces. The membrane

solution must, however, be corrected to fit the actual boundary conditions, as shown in figure 6.7b. The horizontal component of the meridian force is decomposed as

$$H = -R_{0s} = N_{\phi m} \cos \phi_0 = -53.4 \frac{kN}{m}.$$

The corrected displacement $\hat{\delta}_m$ and rotation \hat{V}_m are found from matrix 4.33, when no moments act on the sphere:

$$\begin{aligned} \hat{\delta}_m &= \frac{2\lambda R \sin \phi}{Eh_s} f_1(0) R_0 = \frac{2\lambda R \sin \phi_0}{Eh_s} (-H) = 1.49 \cdot 10^{-3} m \\ \hat{V}_m &= -\frac{2\lambda^2 \sin \phi}{Eh_s} f_3(0) R_0 = -\frac{2\lambda^2 \sin \phi_0}{Eh_s} (-H) = -2.24 \cdot 10^{-3} \text{ rad} \end{aligned}$$

The total particular solution is found by adding together the membrane states:

$$\begin{aligned} \delta_p &= \delta_m + \hat{\delta}_m = 1.44 \cdot 10^{-3} m \\ V_p &= V_m + \hat{V}_m = -2.26 \cdot 10^{-3} \text{ rad} \end{aligned}$$

Finally, a total solution for the sphere is a combination of the particular and homogeneous solution. The homogeneous solution is found from matrix 4.33, and a complete solution for the sphere is obtained:

$$\delta(0) = \delta_h(0) + \delta_p(0) = \frac{\lambda R \sin \phi}{Eh_s} \left(2R_{0s} \sin \phi + \frac{Eh_s R}{2\lambda^3 D_s} M_{0s} \right) + \delta_p \quad (6.4a)$$

$$V(0) = V_h(0) + V_p(0) = -\frac{2\lambda^2}{Eh_s} \left(R_{0s} \sin \phi + \frac{Eh_s R}{2\lambda^3 D_s} M_{0s} \right) + V_p \quad (6.4b)$$

Compatibility

The compatibility conditions ensure a coherent behaviour in the intersection between the shells. Figure 6.8 provides an overview of forces, moments and deformations for establishing the conditions. They can be summed up as follows:

1. displacement and rotation

- (a) $w(0) = \delta(0)$

- (b) $\theta = -V(0)$

2. Moment and shear force

- (a) $M_{0c} = M_{0s} = M_j$

- (b) $Q_{0c} = -R_{0s} = Q_j$

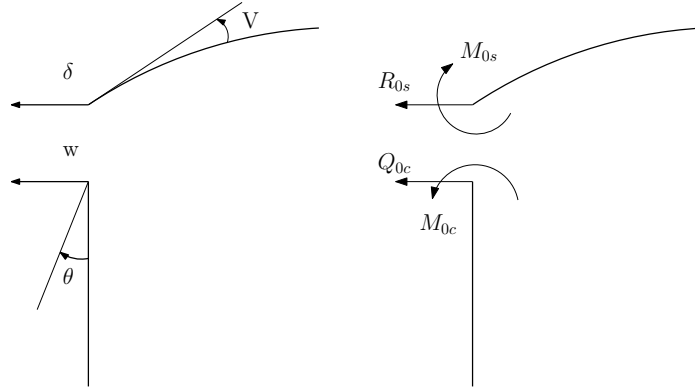


Figure 6.8: Forces and deformations in the connection between the shells

Inserting equations 6.3 and 6.4 in the compatibility conditions described above, two equations representing the displacement and rotation at the intersection are established, as summarised in the following matrix:

$$\begin{bmatrix} \frac{1}{2D_c\beta^2} - \frac{R^2\sin\phi}{2\lambda^2D_s} & \frac{1}{2D_c\beta^3} + \frac{2\lambda R\sin\phi^2}{Eh_s} \\ \frac{1}{D_c\beta} + \frac{R}{\lambda D_s} & \frac{1}{3D_c\beta^2} + \frac{2\lambda^2}{Eh_s}\sin\phi \end{bmatrix} \times \begin{bmatrix} M_j \\ Q_j \end{bmatrix} = \begin{bmatrix} \delta_p \\ V_p - \theta_p \end{bmatrix}$$

Solving the equation system with respect to the integration constants yields:

$$\begin{bmatrix} M_j \\ Q_j \\ R_{0s} \end{bmatrix} = \begin{bmatrix} -9.9 \frac{kNm}{m} \\ 22.7 \frac{kN}{m} \\ -22.7 \frac{kN}{m} \end{bmatrix}$$

Hence the necessary edge forces and moments for determining the response of the structure are found.

6.1.2.1 Distributions

The remaining shell responses are found from matrices 4.14 and 4.33. An important remark is that the horizontal component of the meridian force in the spherical shell, previously denoted H , comes in addition to the shear force Q_j in the junction. Hence the upcoming expressions for the distribution of the shell parameters are corrected to include the effects of the membrane state. Since the edge disturbances

for the cylindrical shell are distributed similarly as in the previous example, only the hoop force are graphed in the following.

In the following plots, $x = 0$ equals the bottom of the cylinder, while $\psi = 0$ represents the edge of the sphere.

The bending moments are expressed as follows:

$$M_{xA} = M_0 f_3(\beta x) + \frac{Q_0}{\beta} f_3(\beta x)$$

$$M_{xB} = M_j f_3(\beta x) + \frac{Q_j}{\beta} f_3(\beta x)$$

$$M_\phi = \frac{4\lambda^3 D_s}{Eh_s R} (R_{os} - H) \sin\phi_0 f_2(t) + M_j f_3(t)$$

$$M_\theta = \nu M_\phi$$

Figure 6.9 shows the distribution of moments in the spherical shell for varying angle ϕ . As expected the bending moments are damped out quickly when moving towards the intermediate parts.

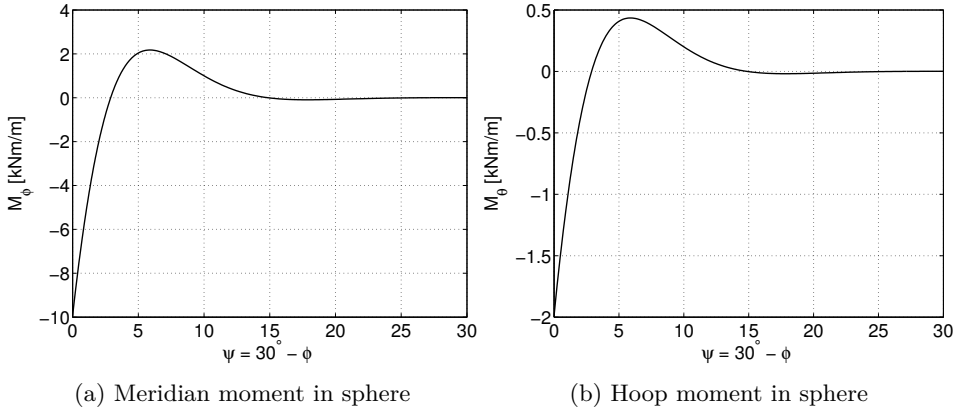


Figure 6.9: Distribution of moments in the sphere

Shear force expressions:

$$Q_{xA} = -2M_0 f_2(\beta x) + Q_0 f_4(\beta x)$$

$$Q_{xB} = -2M_j f_2(\beta x) + Q_j f_4(\beta x)$$

$$Q_\phi = (H - R_{os}) \sin\phi_0 f_4(t) + \frac{Eh_s R}{2\lambda^3 D_s} M_j f_2(t).$$

Figure 6.10 shows the distribution of the shear force in the sphere. It is only significant at the edge of the shell.

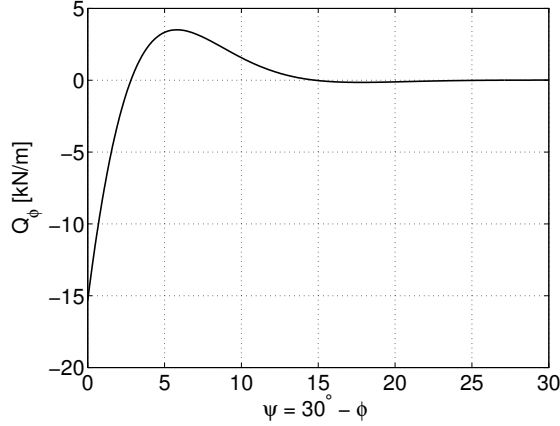


Figure 6.10: Shear force distribution in spherical shell

The hoop force expressions differ from the previous example in that the particular solutions vary with x . They are expressed as:

$$N_{\theta A} = N_h(\beta x) + N_p(x) = 2a\beta^2 \left(M_0 f_4(\beta x) + \frac{Q_0}{\beta} f_1(\beta x) \right) + \gamma_w a(10 - x)$$

$$N_{\theta B} = N_h(\beta x) + N_p(x) = 2a\beta^2 \left(M_j f_4(\beta x) + \frac{Q_j}{\beta} f_1(\beta x) \right) + \gamma_w a x$$

$$N_{\theta s} = N_{\theta h}(t) + N_{\theta m}(\phi) = \lambda \left(2(R_j - H) \sin \phi_0 f_1(t) + \frac{E h_s R}{2\lambda^3 D_s} M_j f_4(t) \right) + N_{\theta m}(\phi)$$

where

$$N_{\theta m}(\phi) = -Rq \cos \phi + \frac{Rq}{\sin^2 \phi} (1 - \cos(\phi))$$

is determined from table 3.1. The hoop forces in the cylinder, shown in figure 6.11a, induce large tension forces in the cylinder. This stems from the applied hydrostatic pressure. The spherical shell on the other hand carries the load in compression for most of the intermediate parts of the shell, shown in figure 6.11b. This makes the curvature of the sphere more ideal for concrete, where compressional forces are desired.

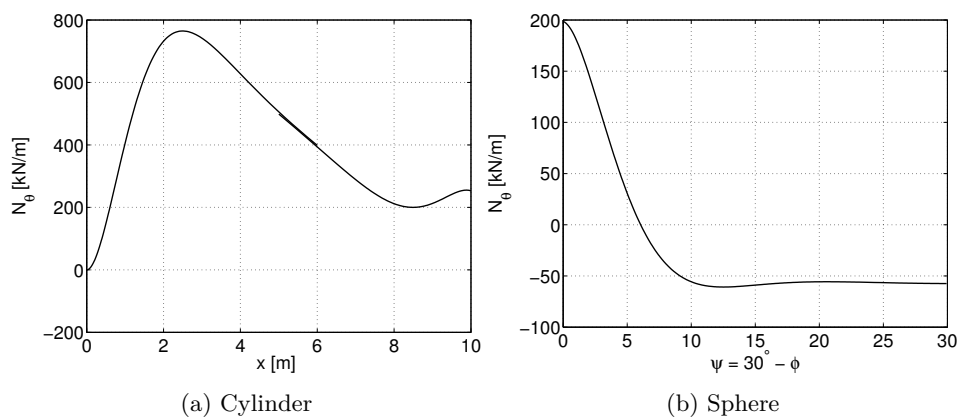


Figure 6.11: Distribution of hoop forces

Distribution of the meridian force:

$$N_\phi = N_{\phi h}(t) + N_{\phi p}(\phi) = \frac{1}{\tan\phi_0} \left((R_j - H)\sin\phi_0 f_4(\beta x) - M_j \frac{Eh_s R}{2\lambda^3 D_s} f_2(\beta x) \right) + N_{\phi m}(\phi)$$

where

$$N_{\phi m}(\phi) = -\frac{Rq}{\sin^2\phi} (1 - \cos(\phi))$$

is determined from membrane theory. Figure 6.12 shows how the meridian force is damped towards the membrane solution. The force is purely in compression which is advantageous for concrete structures.

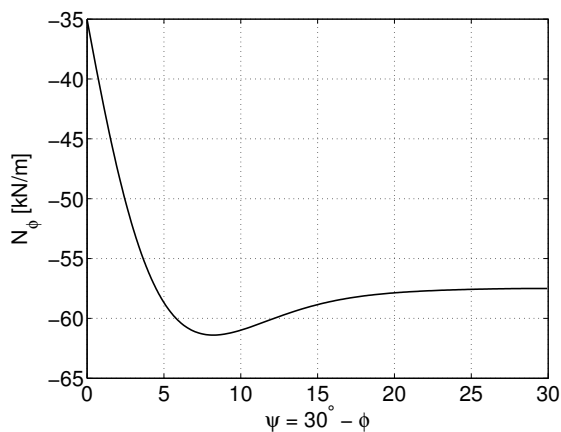


Figure 6.12: Distribution of meridian forces in the sphere

6.1.3 Implementation of ring beam

The cylindrical shell with spherical roof is now further analysed with the introduction of a ring beam in the connection between the shells. The focus is on the shear force and bending moment at the junction of the structure, and how they are altered by the introduction of an edge beam. Material and geometrical data from the previous example remain mostly unchanged so that most results can be reused. A total integer solution is given in appendix C.

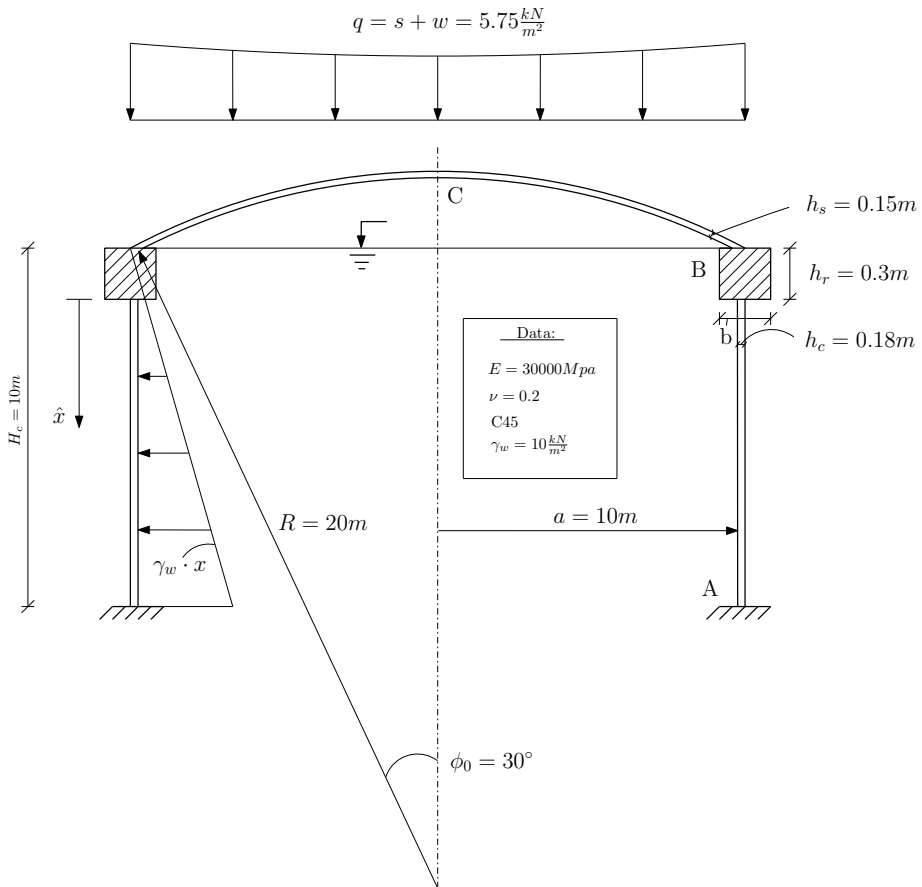


Figure 6.13: Material and geometrical data

Ring beam

As figure 6.13 demonstrates the ring beam has a quadratic cross section with sides of length $0.3m$. The cross sectional area and second moment of area are readily found as:

$$A = bh_r = 90 \cdot 10^3 \text{ mm}^2,$$

$$I = \frac{bh_r^3}{12} = 675 \cdot 10^6 \text{ mm}^4.$$

The coupling of the two shells is achieved through the compatibility of displacements and rotations of the beam. Hence the deformations of the different components must be expressed in the junction.

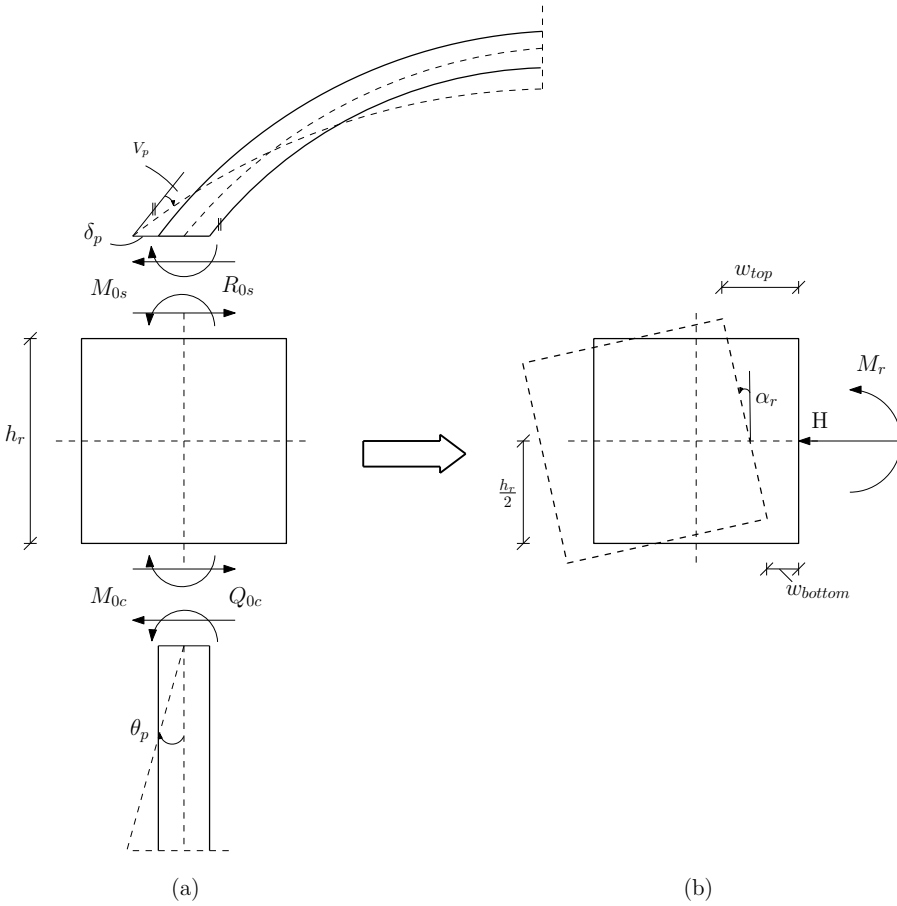


Figure 6.14: (a) Forces and deformations in the connection , (b) Equivalent forces on the ring beam

Figure 6.14 shows the relevant forces and deformations in the junction of the structure, as well as the equivalent forces acting on the ring beam. From the figure it is clear that equivalent moment M_r and hoop force H can be expressed as:

$$\begin{aligned} M_r &= M_{0s} - M_{0c} + \frac{h_r}{2}(Q_{0c} - R_{0s}) \\ H &= -(Q_{0c} + R_{0s}) \end{aligned}$$

We are interested in the displacements in the top and bottom of the ring beam. The displacements are superpositioned from the displacement components of H and M_r . From equations 4.35 and 4.37 the radial displacement at the two edges of the beam are expressed as:

$$\begin{aligned} w_{top} &= w_h + w_M \left(\frac{h_r}{2} \right) = \frac{a^2}{EA} H + \frac{a^2 h_r}{2EI} M_r \\ w_{bottom} &= w_h + w_M \left(-\frac{h_r}{2} \right) = \frac{a^2}{EA} H - \frac{a^2 h_r}{2EI} M_r. \end{aligned}$$

The rotation α_r of the beam is constant and found from 4.38:

$$\alpha_r = \frac{a^2}{EI} M_r.$$

This gives the tools for setting up compatibility conditions describing the deformations of the beam.

Compatibility between cylinder and ring beam

Since the connection between the cylinder and beam is rigid, they have to deform in unity. As the first compatibility condition, equal rotation is demanded, mathematically expressed as:

$$\delta(0) = \delta_h(0) + \delta_p(0) = -\alpha_r$$

By inserting and rewriting, the following equation is obtained:

$$\left(\frac{1}{2D_c\beta^2} + \frac{a^2}{EI} \right) M_{0c} + \left(\frac{1}{2D_c\beta^2} + \frac{a^2 h_r}{2EI} \right) Q_{0c} - \frac{a^2}{EI} M_{0s} + \frac{a^2 h_r}{2EI} R_{0s} = \frac{\gamma_w a^2}{E h_c} \quad (6.5)$$

For the second compatibility condition, equal displacement is demanded:

$$w(0) = w_h(0) = w_{bottom}.$$

A second equation is obtained:

$$\left(\frac{1}{D_c\beta^2} - \frac{a^2h_r}{2EI}\right)M_{0c} + \left(\frac{1}{2D_c\beta^3} + \frac{a^2}{EA} + \frac{a^2h_r^2}{4EI}\right)Q_{0c} + \frac{a^2h_r}{2EI}M_{0s} + \left(\frac{a^2}{EA} - \frac{a^2h_r^2}{4EI}\right)R_{0s} = 0 \quad (6.6)$$

Expressions 6.5 and 6.6 constitute two out of four necessary equations. The remaining two are determined from compatibility between the sphere and beam.

Compatibility between sphere and ring beam

As for the cylinder, compatibility of displacement and rotation is demanded. Unison rotation demands:

$$\delta(0) = \delta_h(0) + \delta_p(30^\circ) = w_{top}$$

Inserting and rewriting:

$$\frac{a^2}{EI}M_{0c} - \frac{a_r^h}{2EI}Q_{0c} - \left(\frac{R}{\lambda D_s} + \frac{a^2}{EI}\right)M_{0s} + \left(\frac{a^2h_r}{2EI} - \frac{2\sin\phi\lambda^2}{Eh_s}\right)R_{0s} = -V_p(30^\circ) \quad (6.7)$$

Unison displacement:

$$\begin{aligned} \frac{a^2h_r}{2EI}M_{0c} - \left(\frac{a^2h_r^2}{4EI} - \frac{a^2}{EA}\right)Q_{0c} + \left(\frac{R^2\sin\phi}{2\lambda^2D_s} - \frac{a^2h_r}{2EI}\right)M_{0s} \\ + \left(\frac{2\lambda R\sin^2\phi}{Eh_s} + \frac{a^2h_r^2}{4EI} + \frac{a^2}{EA}\right)R_{0s} = -\delta_p \end{aligned} \quad (6.8)$$

Equations 6.5, 6.6, 6.7 and 6.8 are arranged in a matrix with four unknowns.

$$\begin{bmatrix}
\frac{1}{2D_c\beta^2} + \frac{a^2}{EI} & \frac{1}{2D_c\beta^2} + \frac{a^2h_r}{2EI} & -\frac{a^2}{EI} & \frac{a^2h_r}{2EI} \\
\frac{1}{D_c\beta^2} - \frac{a^2h_r}{2EI} & \frac{1}{2D_c\beta^3} + \frac{a^2}{EA} + \frac{a^2h_r^2}{4EI} & \frac{a^2h_r}{2EI} & \frac{a^2}{EA} - \frac{a^2h_r^2}{4EI} \\
\frac{a^2}{EI} - \frac{a^h}{2EI} & -\frac{a^h}{2EI} & -\frac{R}{\lambda D_s} - \frac{a^2}{EI} & \frac{a^2h_r}{2EI} - \frac{2\sin\phi\lambda^2}{Eh_s} \\
\frac{a^2h_r}{2EI} & -\frac{a^2h_r^2}{4EI} + \frac{a^2}{EA} & \frac{R^2\sin\phi}{2\lambda^2D_s} - \frac{a^2h_r}{2EI} & \frac{2\lambda R\sin^2\phi}{Eh_s} + \frac{a^2h_r^2}{4EI} + \frac{a^2}{EA}
\end{bmatrix} \times$$

$$\begin{bmatrix}
M_{0c} \\
Q_{0c} \\
M_{0s} \\
R_{0s}
\end{bmatrix} = \begin{bmatrix}
\frac{\gamma_w a^2}{Eh_c} \\
0 \\
-V_p(30^\circ) \\
-\delta_p
\end{bmatrix}$$

Solving the equation system yields:

$$\begin{bmatrix}
M_{0c} \\
Q_{0c} \\
M_{0s} \\
R_{0s}
\end{bmatrix} = \begin{bmatrix}
-4.0 \frac{kNm}{m} \\
14.5 \frac{kN}{m} \\
-10.0 \frac{kNm}{m} \\
-24.9 \frac{kN}{m}
\end{bmatrix}$$

In comparison to the shear forces and bending moment obtained in section 6.1.2, it is clear that the impact from the loads on junction of the structure is drastically reduced. The bending moment acting on the cylinder are is more than halved, which is a significant improvement.

6.1.4 Discussion

Solving thin concrete shells analytically is fairly complicated. Even though the theory on single shells is well defined, the connection of shells and their compatibility conditions give a large margin for human error. From the test cases it is clear that the executing engineer needs a broad range of theoretical knowledge in order to apply it to real life applications.

The test cases increased in complexity from sections 6.1.1 to 6.1.3. The additional principal radius of curvature for spheres compared to cylinders gives additional forces and edge conditions to consider. This is emphasised for the first two examples. The distributions of shear forces and moments are however strictly governed by the functions expressed in 4.13 and 4.31. This inherent property for shell structures solely determines the distributions for the edge disturbances, and the distributions are only distinguished by the size of the edge forces. Thus the shape of the distributions for these responses are similar for the two structures.

The membrane forces are directly linked to the applied loads. Comparing the hoop forces in the cylinders for the two first cases one sees directly how linearly varying hydrostatic pressure differs from a constant pressure load. These membrane forces, shown in figures 6.5 and 6.11a, exert large tensional forces in the cylinders which must be treated in design. The spherical shell transfers membrane forces in a different manner, shown in figures 6.11b and 6.12. Most of the intermediate parts of the shell are in compression, with the exception of the edges. This is highly beneficial when using concrete as building material, and makes large concrete domes possible. The membrane state is generally relatively easy to evaluate. Since the membrane forces dominate load response for the intermediate parts of the shells, they provide a useful tool for quick evaluations of the shell behaviour. This might be used for initial phases of design where swift estimates are needed.

The modification with the ring beam shows a halving of the edge disturbances acting on the cylindrical shell. For this reason it is safe to say that the high forces to be transmitted from the sphere are convincingly equalised. In addition to decreasing the impact on the cylinder, the possibility of ovalisation is reduced. For these reasons the implementation of ring beams may in many situations be desired and/or necessary from a technical standpoint, and gives the engineer greater leeway in design of the structure. The analytical solution concerning ring beams are easily victim of human errors. During the process of calculation, it became apparent that the final solution is sensitive with respect to the particular solutions δ_p and V_m . Enough significant digits are necessary, and calculation by hand is discouraged. In general it is advised to use numerical software for validating the results.

6.2 Numerical solutions

The analytical background material on thin shells of revolution has clear limitations as problems increase in complexity. Needing rigorous, mathematically well defined geometry, it only serve its purpose for relatively simple structures. The advancement of the finite element method gives engineers a valuable tool for analysing complex structures which are out of the scope of the classical theory. The behaviour of shells do, however, have some general features which are useful even when the problems increase in complexity. Failure to recognise them may result in a false interpretation of the results from FEM analyses.

Numerical evaluation of simple examples with associated analytical solutions are rewarding for several reasons. The results validate each other, ensuring both correct calculations and software. The engineer also becomes increasingly aware of possible issues thin shells of revolution pose in numerical analysis. This knowledge can be implemented when analysing more complex problems, giving increased confidence and assurance in the numerical results.

In the following, the preceding structures which were analysed analytically are evaluated numerically in *Diana*. Focus is on the construction of the FEM models, and how the corresponding solutions compare to the result from classical theory.

6.2.1 Numerical analysis of the cylinder with circular plate top

The analytical results from section 6.1.1 showed that the cylinder with circular plate top experience high forces in the plate and junction areas of the structure. This information is used to create a proper model in Diana.

6.2.1.1 Model

The axisymmetric environment in Diana facilitate for a simple one-dimensional model consisting of straight lines. Figure 6.15a shows the model with attached pressure loads. Half of the problem geometry is modelled and rotated about the y -axis at $x = 0$ to create the complete structure. Additional elements are added near the junction and bottom edge to better approximate the solution in the critical sections structure, shown in figure 6.15b.

The clamped bottom edge of the cylinder is constrained against displacement in x and y direction, as well as rotation about the z -axis. In addition the junction between the cylinder and plate are restricted against displacement in the x and y directions. This is done to replicate the compatibility assumptions made for the analytical solution.

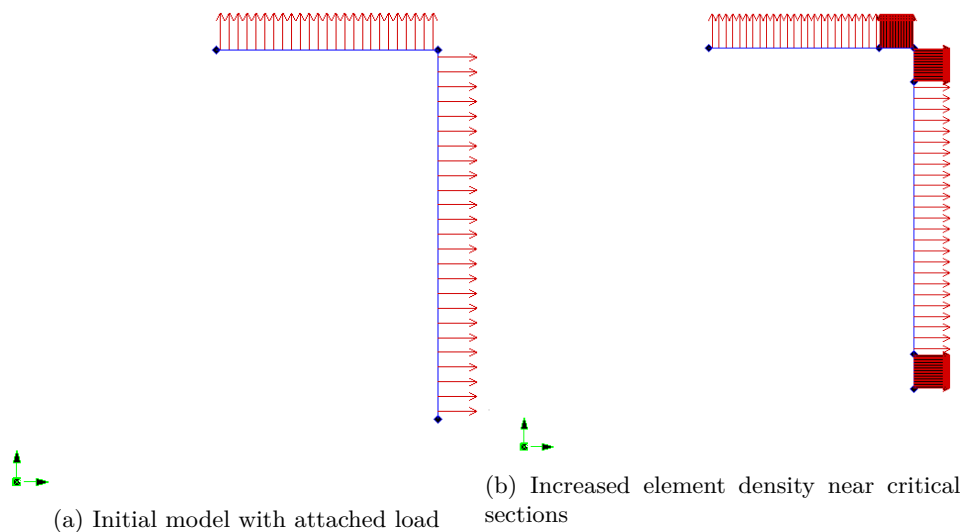


Figure 6.15: Finite element model

The geometry was modelled using L6AXI elements, shown in figure 6.20a. This is a 2 node axisymmetric shell of revolution element with 3 degrees of freedom; two displacements and one rotation.

6.2.1.2 Results

Several rounds of analysis are performed with a gradual increase in number of elements per line. Table 6.1 shows how the edge forces and bending moments converge towards the analytical solution for an increasing number of elements per line. Convergence occurs quickly and a low number of elements is sufficient.

#Elements	$M_a \left[\frac{kNm}{m} \right]$	$Q_a \left[\frac{kN}{m} \right]$	$M_0 \left[\frac{kNm}{m} \right]$	$Q_0 \left[\frac{kN}{m} \right]$
25	86.7	-193	12	- 47.9
50	87.3	-193	12.2	-48.4
75	87.5	-193	12.3	-48.6
99	87.6	-194	12.3	-48.7
Analytical	88.5	-197.3	13.3	-51.5

Table 6.1: Scalar values for moments and shear forces

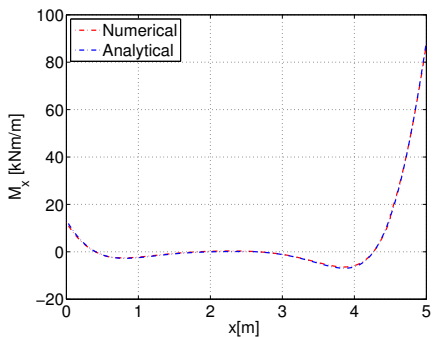
The accuracy of the FEM analysis for the moments and shear forces at the edges suggests that the numerical results are satisfactory.

6.2.1.3 Distributions

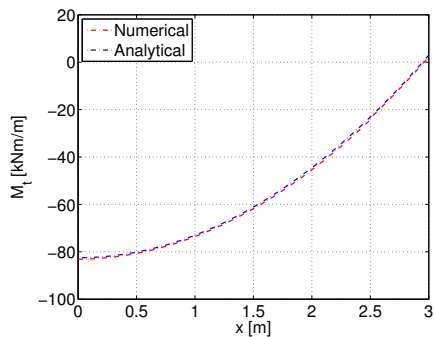
The graphical interface in Diana only gives an illustrative insight in the distribution of forces and moments. To be able to compare the exactness of the distributions, the raw data for each element was extracted as text files using the tabulate capability in Diana. Matlab was used for editing and plotting the data.

Graphing of the numerical results was done for the analysis with 99 elements per line. The plotting was done from each edge of the shells, so that the x-axis represents the height of the cylinder and half the width of the plate. For all the following figures, $x = 0$ represents the bottom of the cylinder and the center of the circular plate.

Figures 6.16, 6.17 and 6.18 shows various responses in the structure graphed both analytically and numerically. They clearly show that the numerical solution matches the analytical in a convincing manner. Both the membrane- and bending state are represented accurately. The fact they demand different attributes from the L6AXI element enhance the confidence in the numerical solution. Also noticeable is the accurate way in which the damping length is represented. All things considered, the finite element shows excellent accuracy.

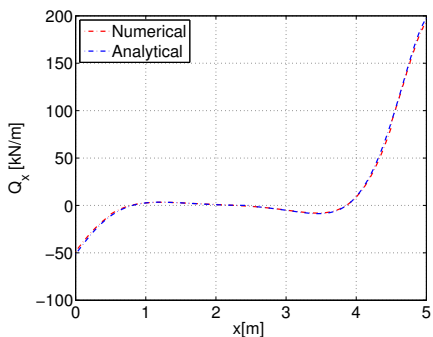


(a) Bending moment M_x in cylinder

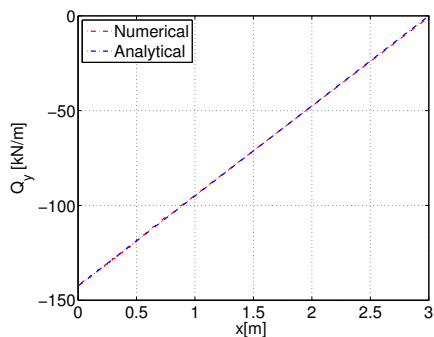


(b) Bending moment M_t in plate

Figure 6.16: Numerical and analytical distributions of bending moments



(a) Shear force in cylinder



(b) Shear force in plate

Figure 6.17: Numerical and analytical distributions of shear forces

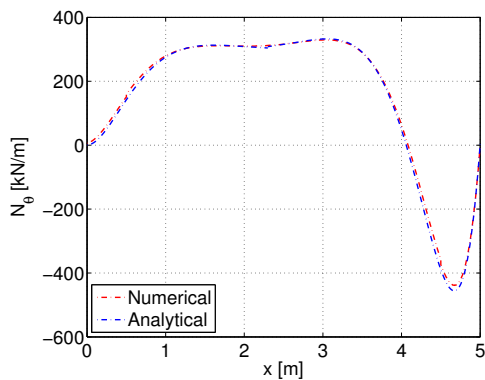


Figure 6.18: Numerical and analytical distribution of the hoop force N_θ in cylinder

6.2.2 Numerical analysis of cylinder with spherical roof

Compared to the previous case, the following requires greater consideration to choice of elements. The curvature of the spherical shell makes the use of three-noded elements more prominent.

6.2.2.1 Model

The structure was modelled using straight lines for the cylinder and arches for the sphere, as shown in figure 6.19. It became clear when running simulations that the sphere needed extra elements to capture the distribution of forces correctly. Additional nodal points was therefore added near the critical sections and in the sphere in order to achieve a better approximations in these areas. The bottom edge of the cylinder is restricted against displacement in the x and y directions, as well as against rotation about the z -axis.

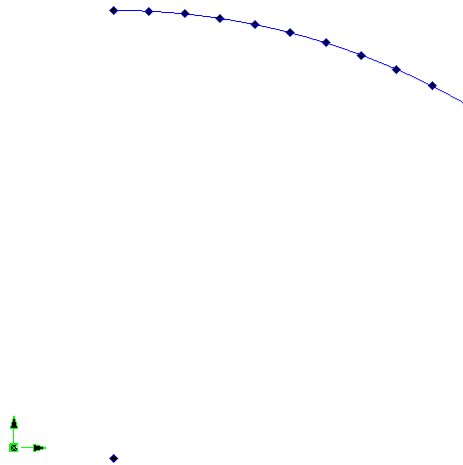


Figure 6.19: Finite element model

6.2.2.2 Axisymmetric shell elements

Diana provides two main shell of revolution elements for one dimensional analysis of axisymmetric shells; the straight two-node *L6AXI* element and the curved three-node *CL9AX* element. Figures 7.3 shows the elements and their local coordinate systems.

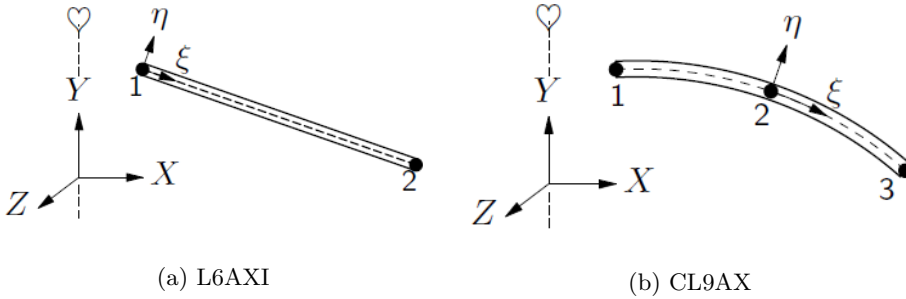


Figure 6.20: Axisymmetric shell of revolution elements [8]

The *CL9AX* element makes use of quadratic shape functions, while linear shape functions are used for the *L6AXI* element. Since the sphere curves in two directions, it is expected that *CL9AX* element converges faster towards the analytical solution.

6.2.2.3 Results

A small comparison of the two elements is conducted to see how they converge towards an analytical solution. As a reference point the junction moment M_a was used. The *CL9AX* elements show promising accuracy even for a low number of elements per line, which is slightly better than the *L6AXI* element. For this reason, further discussion of the numerical results are done for the curved *CL9AX* element.

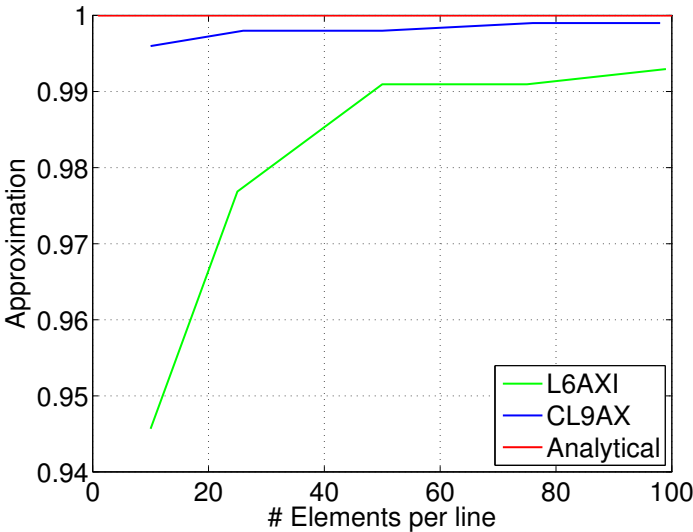


Figure 6.21: Convergence of different element types for increasing element division

6.2.2.4 Distributions

Once again the shell forces and moments are plotted against the analytical solution in order to evaluate the accuracy of the finite element results. This was done for the model having 98 elements per line.

Figures 6.22, 6.23, 6.24 and 6.25 show the distribution of forces and moments in the structure. The overall accuracy of the solutions is convincing. Some minor inaccuracies are introduced from the increased complexity of the problem. The shear force distribution in the spherical shell, given in figure 6.23b, is less smooth compared to the other distributions. This stems from the shape functions for the three-noded elements, which give a linear shear force distribution over the element. This results in the small noise in the figure. Also, the meridian force shown in figure 6.25 has a small deviance between the solutions. The difference is small however, and not considered critical. Again the line elements show great results for linear static analysis.

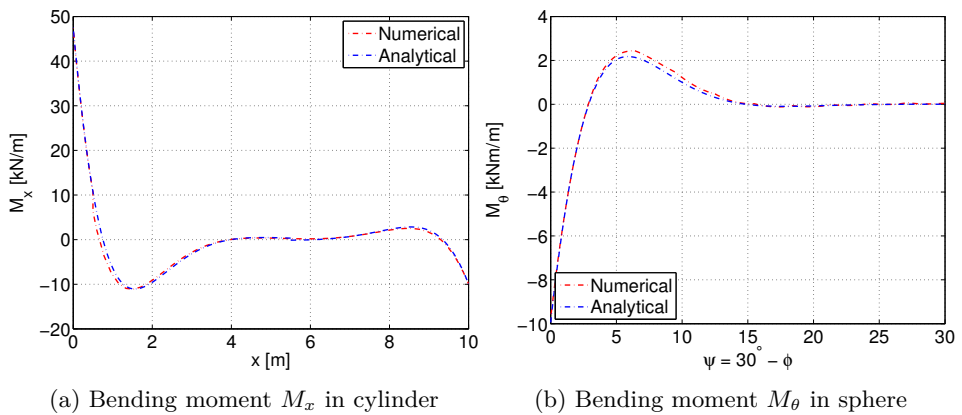
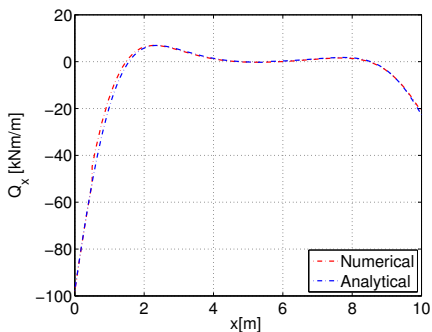
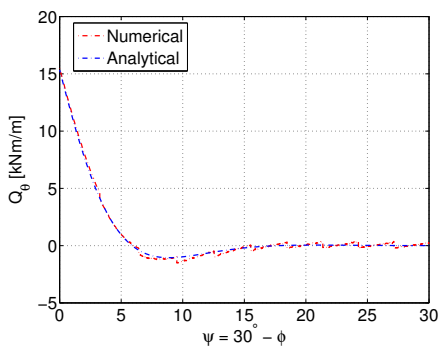


Figure 6.22: Comparison of numerical and analytical distributions of bending moments

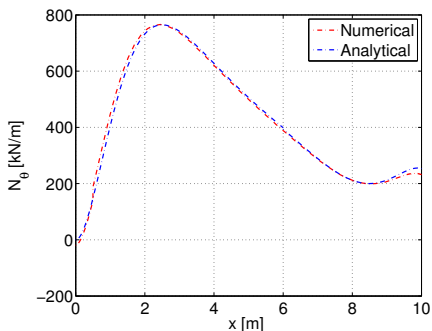


(a) Shear force in cylinder

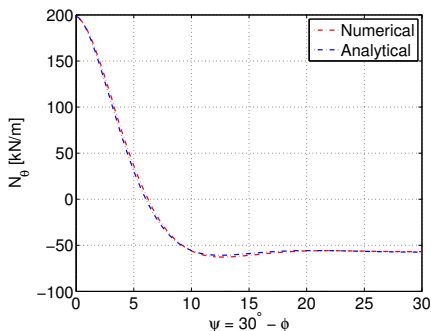


(b) Shear force in sphere

Figure 6.23: Numerical and analytical distributions of shear forces



(a) Hoop force in cylinder



(b) Hoop force in sphere

Figure 6.24: Numerical and analytical distribution of hoop forces

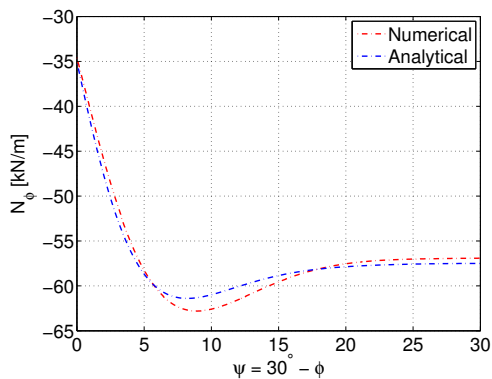


Figure 6.25: Numerical and analytical distributions of the meridian force

6.2.3 Numerical analysis of the implemented ring beam

In the case of the ring beam, it is interesting to see if numerical solutions capture the reduction of bending moments and shear forces in the junction between the two shells.

6.2.3.1 Model

The finite element model used is a modified version of the model in the previous example. Since the focus is on the reduction of forces in the junction of the structure, additional elements are added in this region. The ring beam was modelled by specifying a line with increased thickness, equivalent to the width of the ring beam, at the top face of the cylinder, marked red on figure 6.26. Apart from the mentioned changes the model is identical to the one used in section 6.2.2.

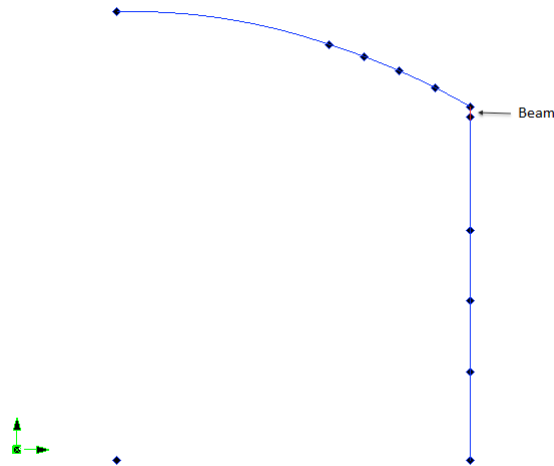


Figure 6.26: Finite element model

6.2.3.2 Results

The analysis was run with 99 elements per line. Table 6.25 gives results from the numerical simulation. The accuracy of the solution is good. Some small differences present which might have been eliminated by modelling the ring beam in a more sophisticated manner. The results are still considered satisfactory for the scope of this paper.

	Analytical	Numerical
$M_{0c}[\frac{kNm}{m}]$	-4.0	-4.2
$Q_{0c}[\frac{kN}{m}]$	14.5	13.4
$M_{0s}[\frac{kNm}{m}]$	-10.0	-9.8
$R_{0s}[\frac{kN}{m}]$	-24.9	-23.8

Table 6.2: Results from numerical simulation

6.2.4 Discussion

Within the context of linear elastic analysis the preceding numerical simulations show satisfactory results. The L6AXI and CL9AX line elements give accurate solutions to both the membrane and bending responses occurring in the structures.

The mesh density of the models have a large influence on the results. This is especially true in regions of the structures where large changes in response occurs. For thin shells these changes are most notable towards the edges. In the intermediate parts the shell the membrane solution dominates. In these regions accurate solutions can be obtained for relatively low mesh densities. At the edges, where the responses undergo large changes over small distances, a greater number of elements should be used to ensure satisfying solutions.

The edge beam was modelled in a rather unrefined fashion. The way of simply increasing the thickness near the top edge of the cylinder did, however, give a representation where the necessary degrees of freedom are accounted for. This is reflected in the results. The simple modification to the model captures the decrease in forces and moments at the upper edge of the cylinder in a satisfactory way.

One appealing aspect of the line models are their simplicity. With rudimentary knowledge of finite element analysis it is easy to create simple models which gives accurate solutions to thin shells of revolution. This gives the engineer a tool for quick and accurate evaluations.

In the preceding chapter the line elements have been established as accurate for linear elastic analysis of thin shells. This provides a comparative basis for understanding how solid elements behave for such structures.

7 Element comparison

Up until this point the numerical analyses have been conducted using line elements. The study of the sample cases establish compelling evidence for the accuracy of these elements for linear analysis of thin shells. In the context of nonlinear analysis, two-dimensional models utilising solid elements are used in order to include reinforcement grids and evaluate stresses.

Before a complete non-linear analysis is carried out the differences between line and solid elements are studied. This provides a basis for understanding how the solid elements capture the shell behaviour, and makes the nonlinear model more reliable in the sense that the element behaviour is studied beforehand.

7.1 Simple cylinder

For the first comparison a well established benchmark test is used. In an article written by *Chapelle* and *Bathe* various benchmark tests for shells are suggested [9]. One of them, the pinched cylinder, is chosen in the following to investigate solutions from different solid elements.

A clamped cylinder loaded with internal pressure is considered. Its simplicity makes it ideal comparing results from different elements. The necessary material and geometrical data for the cylinder are given in figure 7.1.

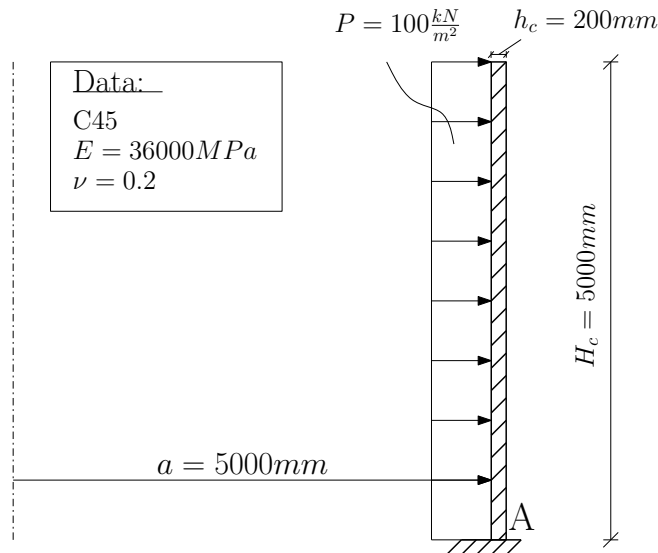


Figure 7.1: Benchmark pinched cylinder

7.1.1 Model

The axisymmetric environment in Diana is recurrently used for making two-dimensional models. Figure 7.2 shows how the cylinder is modelled with axisymmetric solid elements. It consists of a rectangular surface with a predetermined mesh division over the thickness and length. The clamping of the lower edge is done by specifying zero displacement in x and y direction for the bottom line in figure 7.2a. The pressure load is applied at the inner face of the cylinder, shown in figure 7.2b.

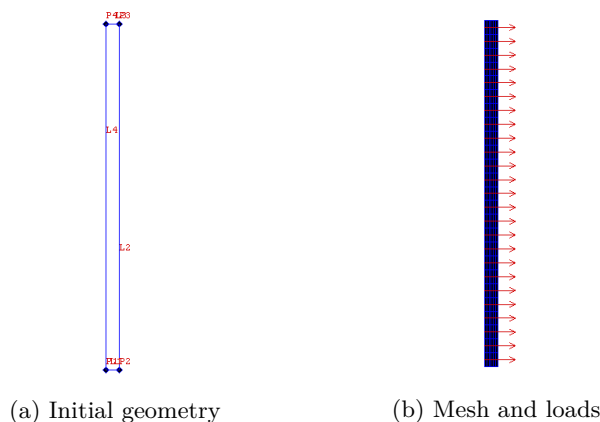


Figure 7.2: Finite element model of cylinder using solid elements

7.1.1.1 Elements

Two promising solid elements are considered; a four-node isoparametric axisymmetric solid ring element and an eight-node isoparametric plane axisymmetric solid ring element with quadrilateral cross section. The Q8AXI element, shown in figure 7.3a, is based on linear interpolation and Gauss integration. The higher order CQ16A element, shown in figure 7.3b, is also based on Gauss integration, but makes use of quadratic interpolation. Both elements have two degrees of freedom at each node, and employ reduced integration.

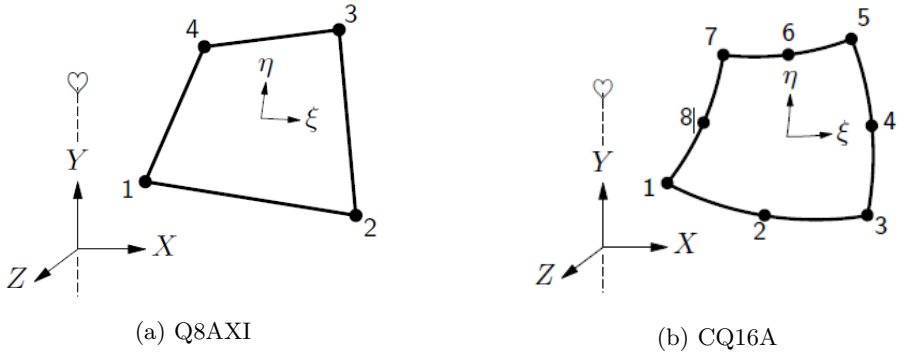


Figure 7.3: Solid ring elements [8]

7.1.2 Results

The edge disturbances present at the clamped edge of the cylinder are in focus. The numerical results from the two-dimensional analysis are given as stresses in the cylinder wall, and are integrated over the thickness to retrieve the shear force and bending moment. Several analyses were run with increasing mesh division to investigate how the results converge.

Longitudinal/Thickness	Q8AXI		CQ16A	
	M_0 [$\frac{kNm}{m}$]	Q_0 [$\frac{kN}{m}$]	M_0 [$\frac{kNm}{m}$]	Q_0 [$\frac{kN}{m}$]
# Elements				
25/6	22.7	-65	28	-73.2
50/8	26.5	-70.6	29.8	-73.7
75/10	28.5	-70.6	31	-73.7
Analytical	29.5	-76.8	29.5	-76.8

Table 7.1: Results from numerical simulation with increasing mesh density

The results are summarized in table 7.1. The CQ16A element shows better convergence toward the analytical solution. This especially true for the shear force, where the Q8AXI element shows a relatively large deviation. Because of the higher order of the CQ16A element these results are expected. For this reason the CQ16A element stands out as the primary candidate for use in a nonlinear analysis.

7.2 Cylinder with circular plate top

To further investigate the accuracy of the CQ16A element, a linear static analysis of the cylinder with plate top is conducted. The nonlinear analysis conducted in section 8 is done for this particular structure. The line model solution to this particular structure was established as accurate in section 6.1.1. This gives an excellent starting point for investigating the linear behaviour of the solid elements.

7.2.1 Models

The models to be compared are showed in figure 7.4. They are similarly constructed but differs in spatial dimensions.

No changes are made to the line model, which remains identical to the one used in section 6.2.1.

Figure 7.5b shows the construction of the solid model. As previously mentioned, this is the same model as the one which is used for nonlinear analysis in section 8. The additional nodal points seen in the figure are there to include reinforcement sections. To make the models comparable, the Young's modulus of the reinforcement steel is set to 1 MPa, which makes the effects of the added reinforcement negligible. Further details of the model are given in section 8.2.

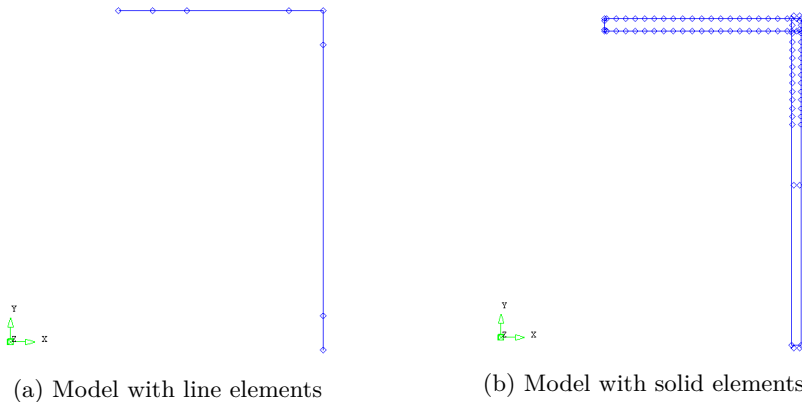


Figure 7.4

7.2.1.1 Elements

As the analysis conducted in section 6.2.1 showed pleasing results, the L6AXI line elements are continually used. The CQ16A element showed the best results in the preceding element comparison, and is therefore chosen for the solid model.

7.2.2 Results

Similar results from the two analyses are expected. A platform for investigation similarities and differences are established by examining the deformations and stresses.

7.2.2.1 Deformations

The two models show similar deformation patterns, shown in figure 7.5. The deformations in the figures are scaled with a factor of 40. The two shapes are identical and as expected given the boundary and load conditions of the structure. The laterally loaded plate shows high deformations, while the cylinder is displaced only a small amount.

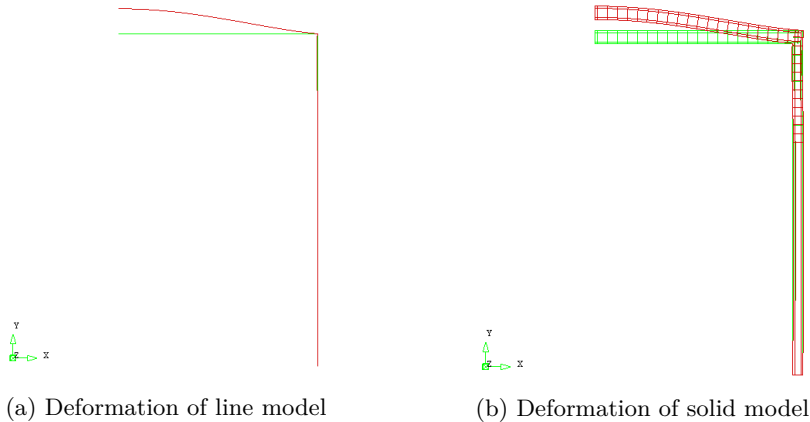


Figure 7.5: Deformation shape for the two models

Table 7.2 gives the magnitudes of the vertical displacement at the centre of the plate and the horizontal displacement of the junction, respectively. The results are close to identical, and the small differences can be attributed to the different approaches used in the modelling.

	Line elements	Solid elements
Vertical displacement	9.75 mm	9.05 mm
Horizontal displacement	0.073 mm	0.283 mm

Table 7.2: Displacements from the two models

7.2.2.2 Stresses

To achieve an objective basis for comparing the stresses, plots over the inner face of the cylinder are produced. Since the two models differ in spatial dimensions, the corner of the structure is an area which is difficult to compare directly. A choice is made to only plot the nodes which are a part of the cylinder, which makes the height of the cylinder in the solid model a bit smaller compared to the line model.

Figure 7.6 shows the the distribution of various stresses over the inner face of the cylinder. They are plotted in the local element coordinate system. The brackets in the figure refers to the meshing of the plate and cylinder surfaces over the thickness and longitudinal directions, respectively.

From the figure it is evident that the solid model gives more crude approximations of stresses compared to the line alternative. This is especially true near the junction of the structure.

The deviation between the solutions are small for the stresses related to the membrane forces and bending moments, shown in figures 7.6a and 7.6c. The differences increase somewhat near the junction of the structure, but they are small and not considered critical.

The shear force distribution gives more reason for concern. The oscillating behaviour near the junctions, seen from figure 7.6b, is clearly a parasitic feature which should not occur in the distributions.

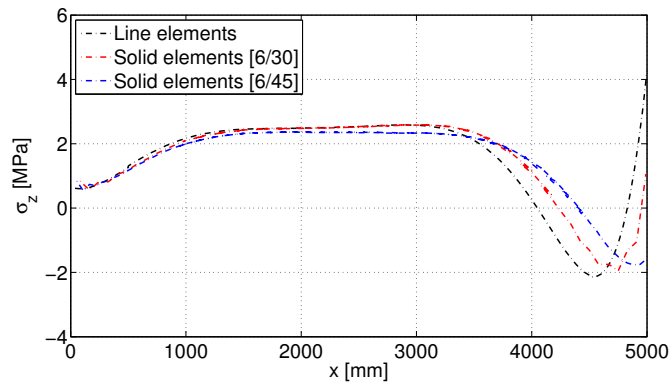
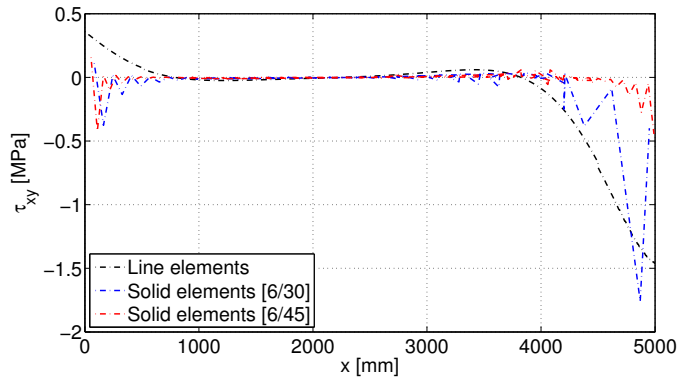
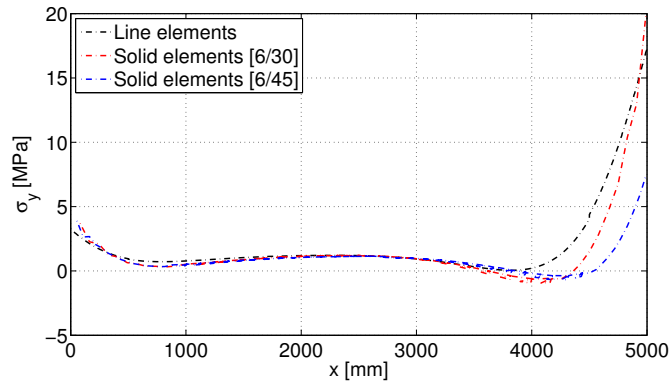


Figure 7.6: Comparison of stresses in cylinder plotted in the local coordinate system

To investigate the oscillating behaviour further, the shear stresses at the neutral axis of the cylinder wall are graphed. This is where they are at their greatest. Figure 7.7 shows the distribution for a mesh density of [6/45]. Compared to the inner face of the cylinder, this distribution contains significantly less noise and generally looks more reasonable. The oscillations are not present, which gives some reassurance in the accuracy of the solid element solutions.

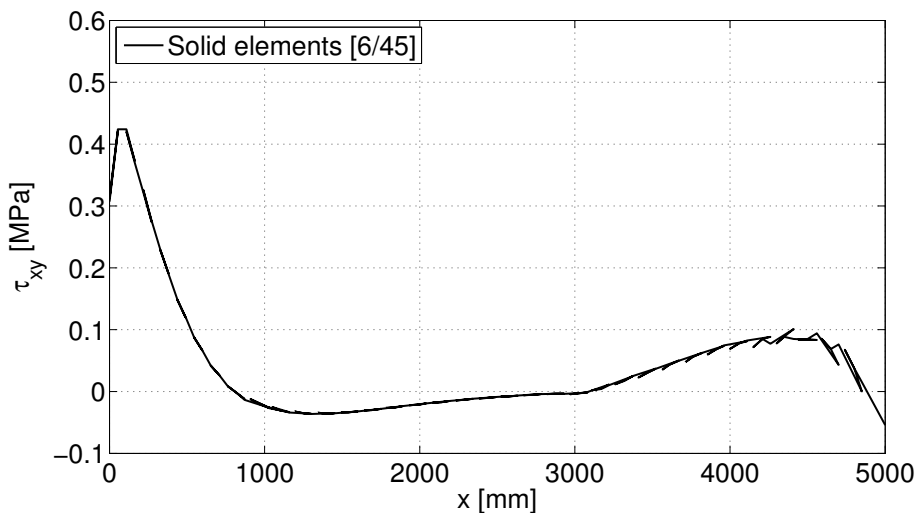


Figure 7.7: Shear force at centre of cylinder wall

7.3 Discussion

The preceding study gives uncertainty in the numeric results from solid shell models. The benchmark test of the pinched cylinder established the CQ16A element as the preferred choice in the following nonlinear analysis. The deviations from the analytical solution are small and within acceptable boundaries.

The second comparison of the line and solid elements show conflicting results. While the stresses from bending and hoop forces are reasonable, the solid model approximate the shear stresses at the edges in a poor manner. The oscillations seen in figure 7.6b might stem from parasitic features which are naturally not desired. The shear stress distribution from the neutral axis of the cylinder gives some assurance in the results, but a great deal of uncertainty in the accuracy of the solid CQ16A element still remains. Further assessment of the element could be done to pinpoint the reasons for this behaviour. This requires a lot of effort which is out of the context of this paper. Even though the accuracy of the results are questionable, the CQ16A solid ring element is used for the following nonlinear analysis. The findings from the preceding section serves as the main possible source of error from the nonlinear solution.

8 Nonlinear analysis

Linear analysis of structures gives limited understanding of the underlying processes at work when the linear range is exceeded. All structures, including the ones studied in this paper, inherit nonlinear characteristics which are technically interesting. Nonlinear response may stem from several sources; geometric, material and boundary nonlinearities are some examples. For most structures, the total response is a combination of such nonlinearities.

In this section the design and nonlinear analysis is done for the example of the cylinder with a plate top. The design is done in accordance with the Eurocodes. For this purpose the partial safety factors are evaluated, and the the structure is reinforced accordingly. The subsequent nonlinear analysis provides the basis for evaluating whether or not the structure is designed in a satisfactory manner.

8.1 Design in accordance with the Eurocodes

The complete design of the structure is done in accordance with the Eurocodes. Load and material factors change the response from the structure, which in turn must be recalculated.

8.1.1 Design loads

The main focus in structural design is to ensure the safety of people and the environment. From an engineering perspective this is done by the use of load and material factors, specified in Eurocode 0 [10]. The partial load factors are determined based on the nature of the loads (self weight, permanente etc.). Table 8.1 shows the factors and how they are combined.

Referring to figure 6.1, there are two loads acting on the plate; the upwards internal pressure and the self weight of the concrete. The partial factor $\gamma_{Gj,inf}$ is used for the self weight since it has a favourable effect on the structure. The pressure load is considered a constant load, which has a partial load factor of 1.2. From the table, two set of expressions giving the design load for the roof are obtained:

$$\text{Case 1 : } q_1 = \gamma_{Gj,inf} \cdot w + \gamma_{Gj,sup} \cdot p = 0.9 \cdot w + 1.2 \cdot p = 115.5 \frac{kN}{m^2}$$

$$\text{Case 2 : } q_2 = \gamma_{Gj,inf} \cdot w + \gamma_{Gj,sup} \cdot p = 1 \cdot w + 1.2 \cdot p = 115 \frac{kN}{m^2}$$

Case 1 results in the largest design load, and is used in further calculations.

The cylinder only experience a constant pressure load

Vedvarende og forbigående dimensjonerende situasjoner	Permanente laster		Dominerende variabel last (*)	Øvrige variable laster (*)
	Ugunstig	Gunstig		
(Ligning 6.10)	$\gamma_{Gj,sup} G_{kj,sup}$	$\gamma_{Gj,inf} G_{kj,inf}$	$\gamma_{Q,1} Q_{k,1}$	$\gamma_{Q,i} \psi_{0,i} Q_{k,i}$
(*) Variable laster er de som er oppført i tabell NA.A1.1 MERKNAD 1 Det brukes følgende sett med γ -verdier: $\gamma_{Gj,sup} = 1,20$; $\gamma_{Gj,inf} = 0,90$; $\gamma_{Q,1} = 1,50$ hvis ugunstig (0 hvis gunstig); $\gamma_{Q,i} = 1,50$ hvis ugunstig (0 hvis gunstig). MERKNAD 2 I tilfeller der påvisning av statisk likevekt også omfatter konstruksjonsdelenes kapasitet, kan det fastsettes en kombinert påvisning basert på tabell NA.A1.2(A) som et alternativ til to separate påvisninger basert på tabell NA.A1.2(A) og NA.A1.2(B), med verdier som angitt nedenfor. $\gamma_{Gj,sup} = 1,35$; $\gamma_{Gj,inf} = 1,0$; $\gamma_{Q,1} = 1,50$ hvis ugunstig (0 hvis gunstig); $\gamma_{Q,i} = 1,50$ hvis ugunstig (0 hvis gunstig).				

Table 8.1: Load combination according to Eurocode 0 [10, Tab. NA.A1.2(B)]

$$p = \gamma_{Gj,sup} \cdot p = 1.2 \cdot 100 \frac{kN}{m^2} = 120 \frac{kN}{m^2},$$

which constitutes the design load acting on the cylinder.

8.1.2 Partial factors for materials

The partial factors for reduction of the material strengths are specified in Eurocode 2 [11, 2.4.2.4]. The calculations are given in appendix D.

8.1.3 Recalculation of moments and forces using design loads

A recalculation of the forces and bending moments based on the design loads are needed before the structure can be reinforced. Table 8.2 shows the results from a finite element analysis conducted in the same manner as in section 6.1.1. Only the edge forces and highest occurring membrane forces are given, since they are used in the reinforcement design.

Cylinder	$M_0 = 15.9 \frac{kNm}{m}$	$M_a = 107.5 \frac{kNm}{m}$
	$Q_0 = -61.8 \frac{kN}{m}$	$Q_a = -240 \frac{kN}{m}$
	$N_{\theta_{bottom}} = 360 \frac{kN}{m}$	$N_{\theta_{top}} = -560 \frac{kN}{m}$
Plate	$M_{r_{edge}} = 107.5 \frac{kNm}{m}$	$M_{t_{edge}} = 31.05 \frac{kNm}{m}$
	$M_{r_{middle}} = -101 \frac{kNm}{m}$	$M_{t_{middle}} = -101 \frac{kNm}{m}$
	$Q_{p_{edge}} = -173.25 \frac{kN}{m}$	

Table 8.2: Recalculated forces and bending moments

As expected, the forces and moments have increased by a sufficient amount.

8.1.4 Reinforcement

Reinforcement steel B500NC is used. It is a typical steel with a characteristic strength of $f_{yk} = 500MPa$.

For shells of revolution with axisymmetric loads the stress states are relatively simple. The absence of twisting moments means that the shells can be designed as one way slabs, and the various shell responses are reinforced separately. The structure was reinforced for the highest occurring forces or moments at each edge of the shell and plate.

The main load carrying function of shells are the membrane forces. For the current example, the hoop force induces tension in most of the structure, but changes sign towards the top of the cylinder where it creates a high compressive force. To minimise the effects of cracking, the hoop reinforcement is placed in two separate layers. Since the hoop force induces tension over most of the cylinder length, it is assumed that the reinforcement carries the complete load.

Flexural and shear reinforcement is only necessary distributed over the damping length near the edge zones of the shell. For practical implementation this would not be appropriate, and most cylinders have flexural reinforcement distributed along their whole length. This is practical because it gives a framework for attaching both shear and hoop reinforcement. This was therefore also done in the finite element model.

The calculation of reinforcement was done in accordance with Eurocode 2 [11]. The details of the calculations are given in appendix D, and summarised in table 8.3.

Moments	Bar cross section	Total reinforcement
M_0	$\phi 12s355$	$320 \frac{mm^2}{m}$
M_a (Tension)	$\phi 16s78$	$2580 \frac{mm^2}{m}$
M_a (Compression)	$\phi 12s650$	$310 \frac{mm^2}{m}$
M_r center	$\phi 16s155$	$1300 \frac{mm^2}{m}$
M_t center	$\phi 16s155$	$1300 \frac{mm^2}{m}$
M_r edge	$\phi 16s120$	$1680 \frac{mm^2}{m}$
M_t edge	$\phi 12s250$	$455 \frac{mm^2}{m}$
Shear forces	Bar cross section	Total reinforcement
Q_0	-	-
Q_a	$\phi 12s65$	$1740 \frac{mm^2}{m}$
Q_p	$\phi 12s148$	$1080 \frac{mm^2}{m}$
Hoop forces (per layer)	Bar cross section	Total reinforcement
N_θ Bottom	$\phi 12s270$	$419 \frac{mm^2}{m}$
N_θ Top	-	-

Table 8.3: Necessary reinforcement for the structure

The plate and top section of the cylinder are heavily reinforced. Figure 8.1 shows how the reinforcement is included in the numerical model. As the figure shows, the reinforcement is placed with practical implementation in mind. Hence several parts of the structure are over-reinforced.

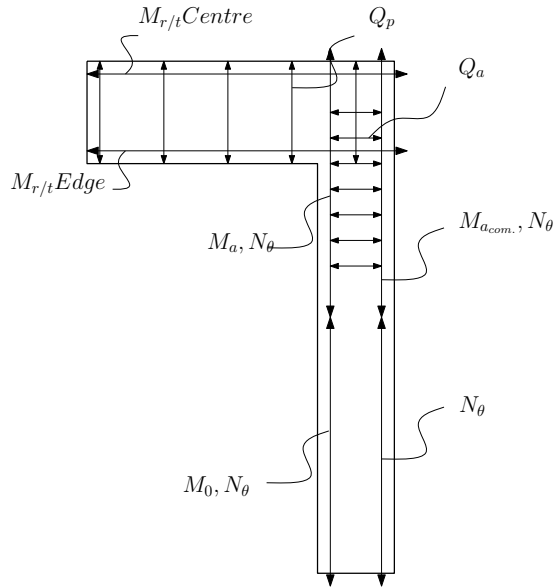


Figure 8.1: Layout of the reinforced structure

8.2 Nonlinear model

The nonlinear model needs greater consideration of aspects concerning the material behaviours and choice of solution method. This is inspected further in the following.

8.2.1 Material models

The choice of material models are important in order to simulate realistic material behaviour. Diana provides a material library with several predefined stress-strain curves, where required input are points on the stress-strain curves. This input is found from Eurocode 2. Since the nonlinear analysis is done for the designed structure, all the following material properties are given as design values.

Concrete

The Thorenfeldt curve, shown in figure 8.2a, was chosen for the concrete in compression. As input it requires the compressive cylinder strength, which in this case is $f_{cd} = 25.5MPa$.

A linear tension softening curve is used for the concrete in tension, shown in figure 8.2b. It is fully defined by the the tensile strength of the concrete ($f_{ctd,0.05}$) and the Mode-I ultimate tensile strain (ε_u). For C45 concrete the design tensile strength

is $f_{ctd,0.05} = 1.53MPa$. The mode-I ultimate tensile strain is more vaguely defined. Sophisticated methods for defining it exist, but they are out of the scope of this paper. The tensional concrete strength is instead defined as zero when the reinforcement yields, which gives a ultimate strain of $\epsilon_u = 2.17 \cdot 10^{-3}$.

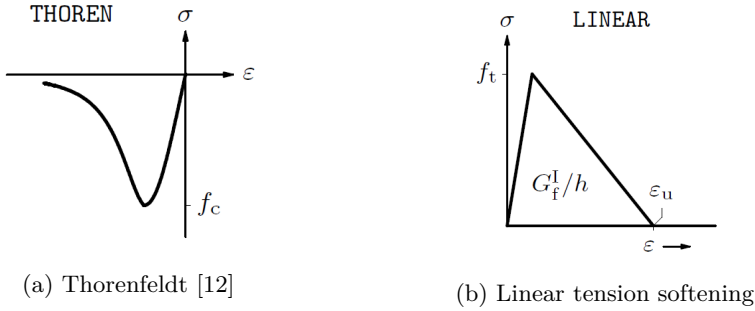


Figure 8.2: Material models for concrete [12]

Reinforcement

The steel material is modelled with linear hardening, shown in figure 8.3. The design yield tensile strength for reinforcement B500NC is $f_{yd} = 434MPa$. The ultimate design tensile strength after hardening is determined from eurocode 2 as $451MPa$ at 3 % strain [11, NA.3.2.7(2)].

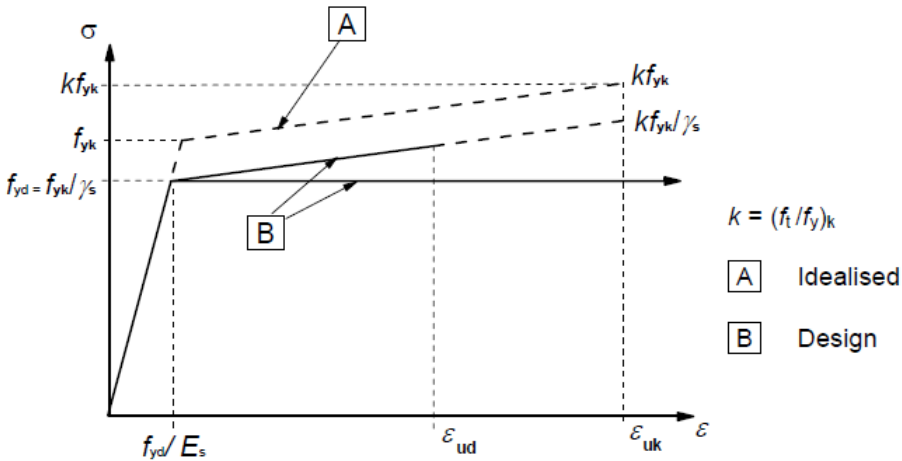


Figure 8.3: Idealised stress-strain curve for reinforcement steel [11, ch. 3.3.6]

8.2.2 Finite element model

The finite element model is constructed as a 2 dimensional structure in the axisymmetric environment in Diana. The geometry consists of three surfaces; the plate, the junction and the cylinder. This is done to ensure satisfactory alignment of the mesh in the junction. The plate and cylinder are meshed with six elements over the thickness and thirty elements along their respective longitudinal axes. Figure 8.4a shows the meshed structure with the applied load.

The reinforcement is implemented by attaching grid sections to lines placed within the surfaces. The layout of the reinforcement is shown in figure 8.4b. For each line in the figure the amount of reinforcement is specified in two directions with units $\frac{mm^2}{mm}$. It is placed with the minimum concrete cover given in Eurocode 2, which is calculated in appendix D.

The bottom edge cylinder is modelled as clamped by restricting displacement in the x and y directions.

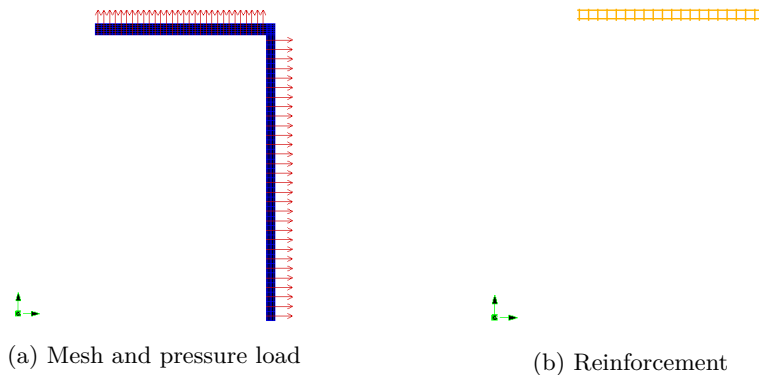


Figure 8.4: Finite element model used in nonlinear analysis

8.2.3 Elements

Linearly interpolated isoparametric elements, like the Q8AXI elements previously studied, are not advisable used in non-linear models. These elements have intrinsic shortcomings, like parasitic shear and volumetric locking, which are not easily dealt with in nonlinear analysis [13, Ch. 11.2]. The Q8AXI element was out of interest tested in the initial phases of the analysis. The results showed clear weaknesses, and inspection of the deformation patterns revealed clear hourglass modes for elements in areas of high stress. The use of higher order elements prevents such behaviour. The CQ16A element, described in section 7.1.1.1 is used, which effectively eliminated the parasitic features.

8.3 Solution method

The analysis was run using purely incremental methods. Both arc-length control and load control was tested with various increments. The model showed some problems finding convergence in certain load steps. To ensure a reliable solution, arc-length control is used with the load applied in two rounds. At first, five load steps with a 5% increase in load was utilised. This is done to ensure that the stiffness used for calculating the initial predictor is reliable. Then 15 load steps with an increase of 10% of the load is used to make sure that the total applied load exceeds the design load. The iterations were done using the modified Newton-Raphson method. To increase the chance of convergence for each load step, a maximum of 100 iterations per step was used.

8.4 Results

Diana provides numerous possible parameters to be studied from the nonlinear analysis. The main focus here will be on the stresses, but some insight into the deformations and crack behaviour is also provided.

8.4.1 Deformations

The deformation of the structure gives useful clues to the accuracy of the numerical solution. Figure 8.5 shows the deformed shape of the structure for a load factor of $\lambda = 1$. The deformations are scaled with a factor of 500. The deformed structure corresponds to the expected shape given the load and boundary conditions. The elements show no sign of parasitic features like hourglass modes, which were highly visible the when linearly interpolated elements were used.

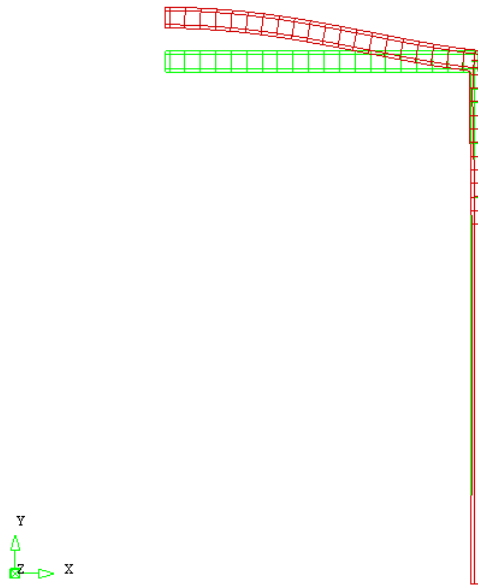


Figure 8.5: Deformed shape for load step $\lambda = 1$

Load-displacement curves are essential tools for understanding the nonlinear behaviour. They are useful for detecting critical points in the in the load history of the structure. Such curves are graphed for increasing load at two of the nodal points; the centre of the plate and corner of the structure.

Figure 8.6 shows the vertical displacement at the centre of the plate. For the load factor λ corresponding to the actual applied load the plate is displaced approximately 53 mm. From a design perspective this displacement is high, and it would not pass the serviceability limit state for displacement control in Eurocode 2 [11, ch. 7.4]. For the scope of a ultimate limit state analysis the displacement is reasonable. It is evident that the structure's load carrying ability is drastically reduced for approximately 1.08 of the applied load. From that point the displacements increase drastically for only small increases in load. This is a critical point in the curve.

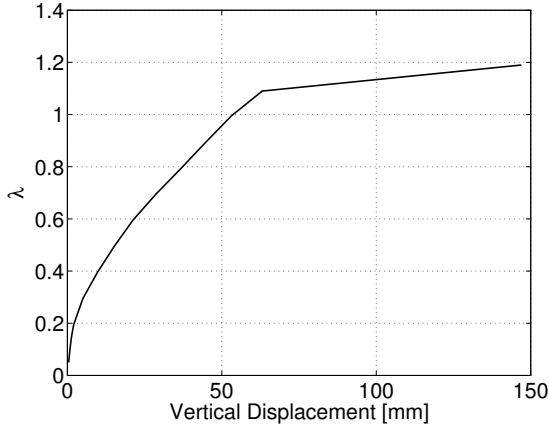


Figure 8.6: Load-displacement curve for the centre of the plate

The analytical solution for this specific structure assumes zero horizontal displacement at the junction between the shell and plate. In practice this assumption is naturally not true. Figure 8.7 shows how the structure is displaced horizontally at the corner. For the actual applied load the structure has a horizontal displacement of about 3.7 mm.

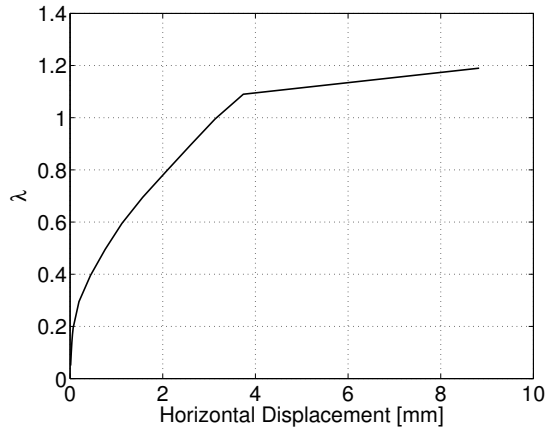


Figure 8.7: Load-displacement curve for the junction of the structure

Overall the structure is able to endure a load approximately 1.08 times the design load, which is clearly visible in both of the load-displacement curves. This gives an indication that the structure is properly designed, and that the applied design load is relatively high.

8.4.2 Stresses

If the structure is designed appropriately, the stresses in the structure should not exceed the strengths of the respective materials. In the following the stresses in the reinforcement and concrete are inspected separately. All stresses are evaluated in the Gauss points for the load case corresponding to the design load.

8.4.2.1 Reinforcement

As was discussed in section 8.1.4, most parts of the structure are conservatively reinforced. This is especially true in the cylinder, where the stresses generally show low values. Figure 8.8 shows that the largest stresses occur at the upper edge where the joint moment is at its largest. The flexural reinforcement is still far from yielding, which stems from the fact that the hoop reinforcement is placed over the whole length of the cylinder.



Figure 8.8: Stresses in cylinder reinforcement for load step $\lambda = 1$ [MPa]

The plate experiences the highest stresses in the structure, which is reflected from the stresses in the reinforcement. Figure 8.9 shows yielding in the middle and edge parts of the plate. The stresses in the shear reinforcement are low. Hence the shear reinforcement may be reduced towards the centre of the plate.

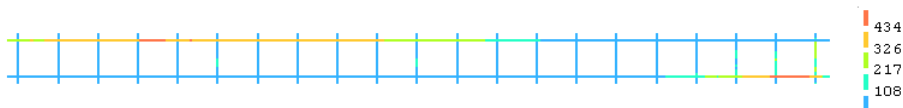


Figure 8.9: Stresses in plate reinforcement for load step $\lambda = 1$ [MPa]

The distribution of stresses in the top and bottom flexural reinforcement in the plate are shown in figure 8.10. Both layers of reinforcement yields where the highest radial moment occurs, and are reduced as the bending moments decrease. The compressive stresses are significantly lower as a consequence of the compressional strength of concrete.

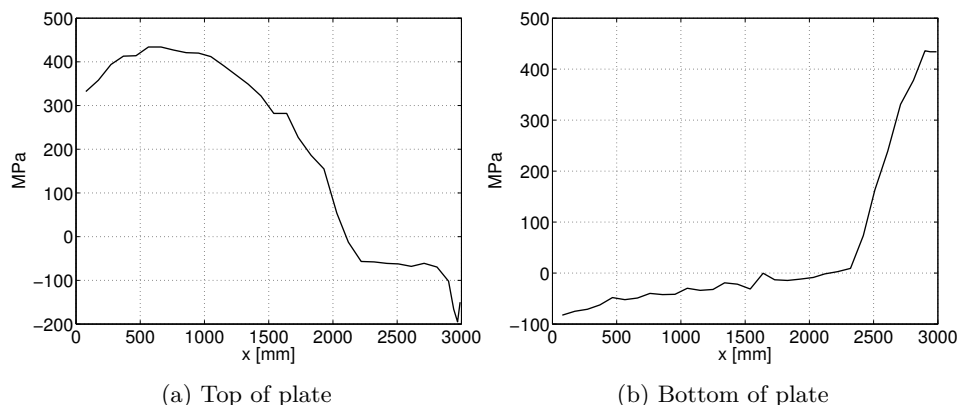


Figure 8.10: Stresses in flexural reinforcement for $\lambda = 1$

8.4.2.2 Concrete

Since the reinforcement yields in certain areas of the structure, it is crucial that the stresses in the concrete does not exceed its design strength.

Figure 8.11 shows contour plots of the stresses occurring in the cylinder. The direction of the stresses are taken from the local coordinate system on element level. As expected, the bending moments give the highest compressional stresses, shown in figure 8.11b. This happens at the upper edge where junction moment is transferred from the plate. The maximum occurring compressive stress is of size -15.4 MPa, which is far from critical. Since the stresses from bending are purely compressional it is evident that the tensional forces are effectively redistributed to the reinforcement.

The analytical assessment of the structure showed that the hoop force imparts tensional forces in most of the cylinder. It is vital that these forces are adequately

redistributed to the reinforcement to avoid fracture. From figure 8.11d it's clear that the stresses have been efficiently reduced. They lie around 1 MPa, which is comfortably below the tensional strength of the concrete.

The shear stresses are small overall, but reach the design tension strength of the concrete at the upper edge, showed in figure 8.11c. This might be attributed to a localisation of stresses at the junction. On the other hand, the study of the solid element behaviour showed oscillating behaviour of shear stresses near the edges zones of the cylinder. The results should therefore be considered as slightly uncertain.

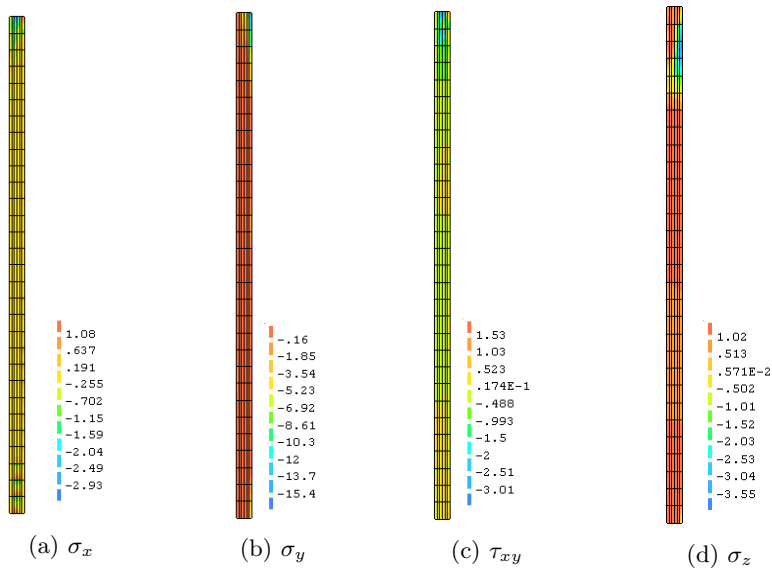


Figure 8.11: Concrete stresses in cylinder plotted in element coordinate system for load step $\lambda = 1$ [MPa]

The plate is less heavily reinforced compared to the cylinder, and as a consequence larger parts of the concrete is utilised. This leads to stresses closer to the concrete compressive strength, as seen from figure 8.12. A maximum stress of -23 MPa is present at the bottom face of the plate, which is close to the design compressive strength of C45 concrete. Stresses in tension are avoided completely by redistribution of tensional forces to the reinforcement.

The shear stresses in the plate are low, as seen from figure 8.12c. This is because the cylinder has a large amount of shear reinforcement.

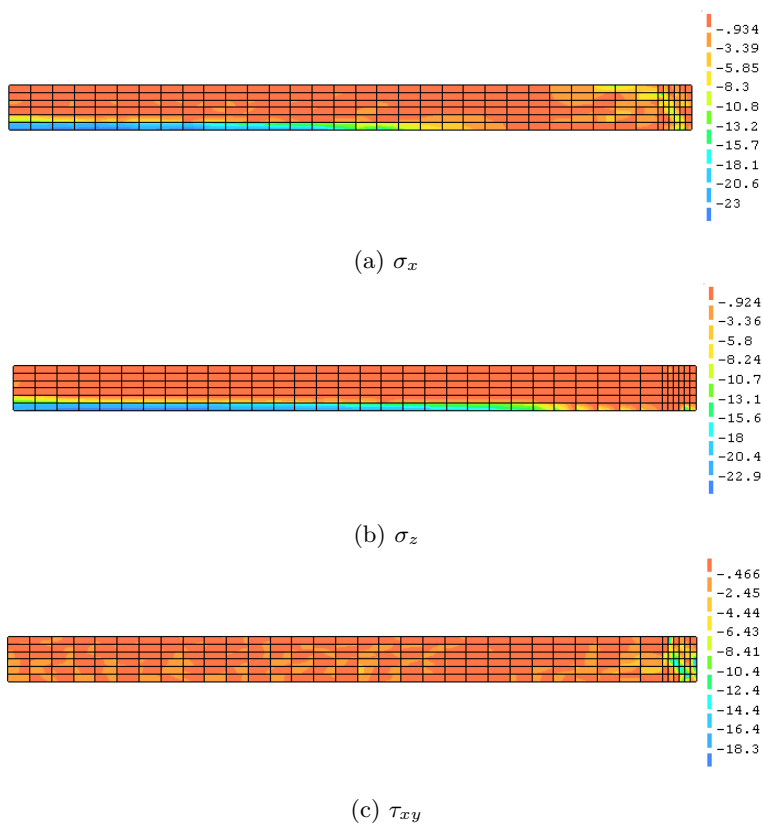


Figure 8.12: Concrete stresses in plate plotted in element coordinate system for load step $\lambda = 1$ [MPa]

An interesting aspect from the nonlinear analysis is to see how the stresses have changed in comparison to the linear analysis which was conducted in section 7.2. Again the stresses are plotted at the inner face of the cylinder.

Figure 8.13 shows the stress responses from both the linear and nonlinear analyses. The stresses from the nonlinear analysis tend to be more constant over the length of the cylinder. This is a result of the redistribution of forces to the reinforcement. As a consequence the stresses are reduced.

The oscillating behaviour that was found for the shear force distribution in section 7.2 is still present for the nonlinear analysis. This is to be expected as the two models are identical with the exception of the added reinforcement.

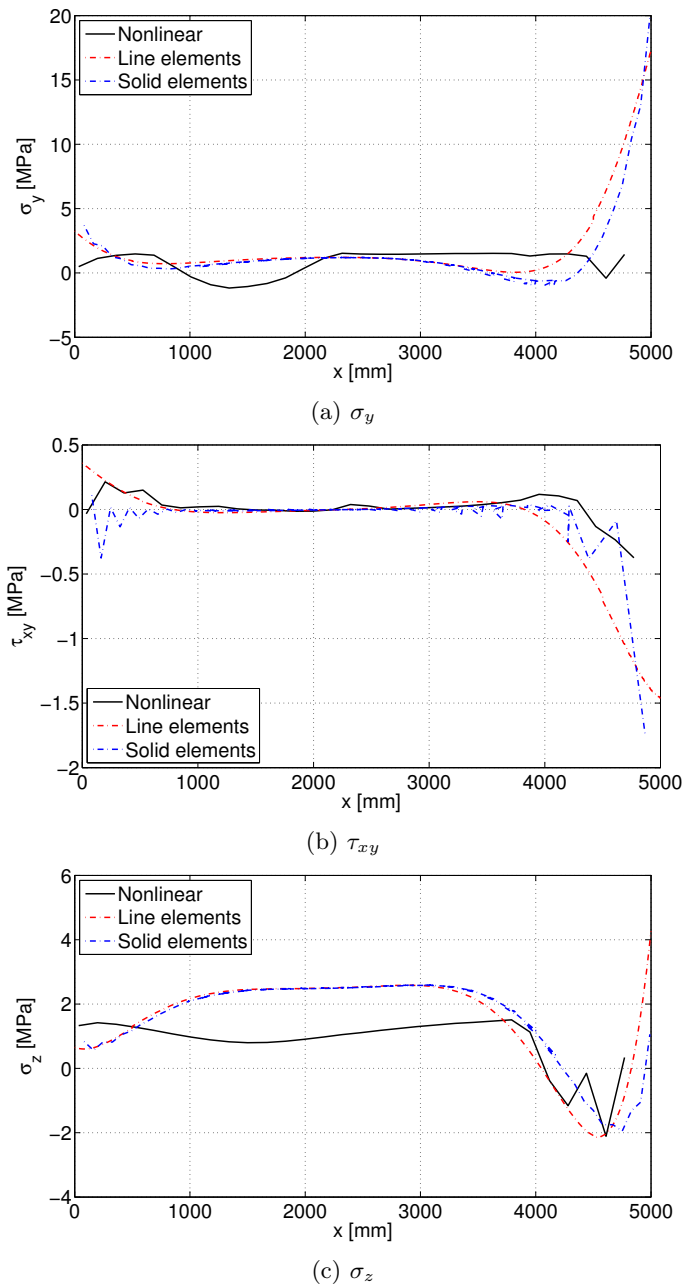


Figure 8.13: Stresses from nonlinear analysis plotted at inner face of cylinder

The nonlinear analysis shows that the structure has a sufficient capacity. This indicates that the structure is adequately designed.

8.4.3 Cracking

Cracks in reinforced concrete have a significant influence on the internal stresses, stiffness and overall behaviour of the structure. Smearred crack models are the most used models for describing crack behaviour in nonlinear analysis of reinforced concrete [14]. It is based on the idea that in concrete, because of its heterogeneity and presence of reinforcement, many small cracks form in central areas which only in later stages of the loading link to form one or more dominate cracks [15]. Compared to discrete crack models, each individual crack is not numerically resolved but rather smeared out over the continuum. A rotating crack analysis was used in the current analysis. The crack evaluation is based on the current load step alone, unlike fixed crack models which take previous crack history into consideration.

The upcoming figures show the crack patterns occurring from the first principal stress σ_1 . As it exceeds the tension strength of the concrete, cracks occurs. Diana gives the strains normal to the cracks as output, from which the crack widths can be calculated. This is not done in the following considerations, and the values of the strains are only meant as an indication of the crack sizes.

The analysis shows that the first cracks are initiated in the junction of the structure and spread quickly to the higher stressed parts of the plate. Figure 8.14 shows the initiation of cracks in the junction of the structure for load of $\lambda = 0.1$. Even for this small load some small cracks are appearing.

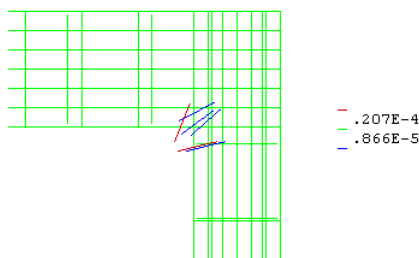


Figure 8.14: Crack initiation at the junction

The cracks evolve further for increasing load. Figure 8.15 visualises how the cracks evolve for increasing load in these regions. The circles seen in the figures indicate the orientation of the crack perpendicular to the x-y plane (the structure is three dimensional). Cracks form in the areas of high stress and gradually evolve along the plate. Load factor $\lambda=1.29$ constitutes a high load on the structure. At this point the bottom face of the plate starts cracking, as seen from figure 8.15c. As most of the bottom face is in compression the occurring cracks indicates compressive fracture of the concrete.

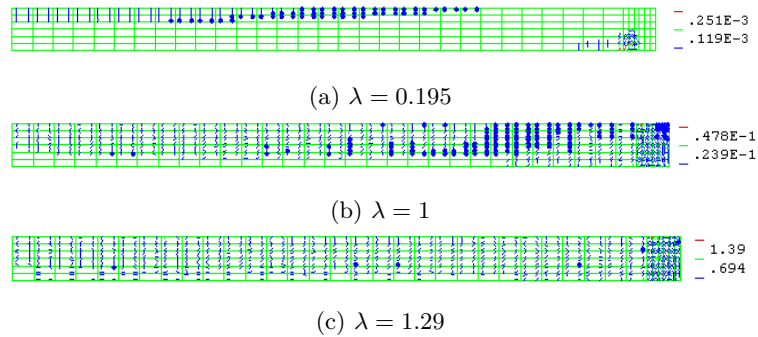


Figure 8.15: Evolution of cracks in plate for increasing load

The cylinder experience less cracking in comparison with the plate. For this reason it is not discussed any further. The amount of cracks appearing in the structure is expected since it has been designed in the ultimate limit state. For a serviceability limit state design these cracks might not pass the requirements from Eurocode 2.

8.5 Discussion

The overall results from the nonlinear analysis appear trustworthy. It is evident that the load for which the structure was designed is high, which is emphasised from the response for increasing loads. The stresses in the structure does, however, lie within the acceptable boundaries defined by the respective material strengths. This indicates that the design of the structure was done appropriately.

Several aspects of the preceding non-linear solution are uncertain. A possible source of uncertainty in the results comes from modelling using partial safety factors (PSFs). In a technical paper written by Vladimir Cervenka it is suggested that nonlinear analysis of reinforced concrete structures where PSFs are applied increase the uncertainty of the solution [16]. Changing the material strengths for the steel and concrete by an uneven amount effectively changes the composite material interaction. This will not be further addressed, but is included as a possible source of error in the results.

A second source of uncertainty lies in the choice of material models. Other, more sophisticated models exist, which might give more accurate results. An optimal stress-strain curve could be obtained from experiments where the different control parameters are more well defined. The results presented above do, however, show pleasing results for the scope of this paper.

A final source of error comes from the oscillating shear stress distribution found in section 7.2. These oscillations are somewhat reduced in the nonlinear analysis, but are still present. It is difficult to analyse how much this effects the stresses in the structure without venturing deeper into the finite element theory on the subject. Since this is not the main focus of this paper it is not considered any further. The shear stresses do not exceed the design strength of the concrete, and the results are therefore considered reasonable.

9 Conclusion

From the analyses conducted in this paper it is evident that shells have intrinsic properties which separate them from other construction components.

The classical theory on shells provides a solid basis for understanding the behaviour of different shells with various load conditions. The analytically resolved sample cases confirm that membrane action is the primary load-carrying response in thin shells. Edge effects have a large impact at the boundaries, but they are rapidly damped out towards the intermediate parts of the shells. It is confirmed that ring beams efficiently reduce the impact on cylinders when they are in connection with spherical shells. For the example of the cylindrical shell with spherical roof, the edge disturbances on the upper edge of the cylinder was nearly halved. It is evident that the analytical solutions to connected thin shells are complex, and as a consequence they are at high risk of human errors. For this reason it is recommended to use finite element software to validate the results.

The results from the linear static analyses using finite element software show exemplary results. Implementation of the *L6AXI* and *CL9AX* line elements give results matching the analytical solutions in a convincing manner. Within the scope of linear elastic analysis, they provide for simple finite element models with a high degree of accuracy.

The study of line and solid elements established a basis for investigating the accuracy of solid elements. The solid model solutions show less accuracy and greater noise in the stress distributions compared to the line alternative. This is especially true for the shear forces, which show oscillating behaviour close to edge zones of the shells. This is considered one of the main uncertainties in the solution from the nonlinear analysis.

The cylinder with circular plate top was designed in the ultimate limit state in accordance with the Eurocodes. The accompanying nonlinear analysis verifies that the design gives sufficient capacity. This confirms that shells of revolution with symmetrical load conditions can be designed similarly to one way slabs. Inspection of the results show large deformations of the plate, which is displaced approximately 53 mm vertically at the centre. From a design perspective, this displacement exceeds the serviceability limit state requirements specified in Eurocode 2. For the scope of an ultimate limit state design however, the displacement is reasonable. The stresses in the structure are shown to be effectively reduced by the added reinforcement. The structure is heavily reinforced, and a reduction of reinforcement area in several regions can safely be done. For increasing loads the analysis shows several small cracks proliferating across the structure. This is expected from the smeared crack model which was used in the analysis. The ultimate load that the structure can endure is found to be 1.08 times the applied design load.

References

- [1] <http://www.arch.mcgill.ca/prof/sijpkcs/abc-structures-2005/lectures-2005/term-work/50-questions/sixth-five.html>, February 2014.
- [2] David P. Billington. *Thin shell concrete structures*. McGraw-Hill book company, 2 edition, 1982.
- [3] Ansel C. Ugural. *Stresses in beams, plates, and shells*. Taylor & Francis Group, third edit edition, 2009.
- [4] Peter Marti. *Theory Of Structures: Fundamentals, Framed Structures, Plates and Shells*. Ernst & Sohn GmBh & Co. KG., 2013.
- [5] Kai-Uwe Bletzinger. Theory of shells. Lecture notes, Lehrstuhl für Statik, Technische Universität München, Summer 2005.
- [6] S. Woinowsky-Krieger S. Timoshenko. *Theory of Plates and Shells*. McGraw-Hill book company, second edition.
- [7] Svein Ivar Sørensen. Beregningsgrunnlaget for betongkonstruksjoner del 2, aksesymmetriske skall.
- [8] TNO DIANA BV. *DIANA User's Manual, Element Library*, 9.4.4 edition.
- [9] D. Chapelle and K.J. Bathe. Fundamental considerations for the finite element analysis of shell structures. *Computers & structures*, 66:19–36, 1998.
- [10] Standard Norge. *Eurocode: Basis for structural design*, ns-en 1990:2002+na:2008 edition.
- [11] Standard Norge. *Eurokode 2: Prosjektering av betongkonstruksjoner del 1-1: Allmenne regler og regler for bygning*, ns-en 1992-1-1:2004+na:2008 edition.
- [12] TNO DIANA BV. *DIANA User's Manual, Material Library*, 9.4.4 edition.
- [13] TNO DIANA BV. *DIANA User's Manual, Analysis Procedures*, 9.4.4 edition.
- [14] Besari Nuroji and I. Imran. Rotated discrete crack model for reinforced concrete and structures. *35th Conference on our world in concrete and structures: 25 - 27 August 2010, Singapore*.
- [15] René de Borst, Joris J.C. Remmers, Alan Needleman, and Marie-Angéle Abellan. Discrete vs. smeared crack models for concrete fracture: bridging the gap. *International journal for numerical and analytical methods in geomechanics*, pages 583–607, 2004.
- [16] Vladimir Cervenka. Reliability-based non-linear analysis according to fib model code 2010. *Structural Concrete*, 14:19/28, 2013.

A Cylinder with circular plate top

Data:

$$\begin{aligned} a &:= 3000 \text{ mm} & h_c &:= 150 \text{ mm} \\ L &:= 5000 \text{ mm} & h_p &:= 200 \text{ mm} \\ E &:= 36000 \text{ MPa} & \nu &:= 0.2 \end{aligned}$$

$$p := 100 \frac{\text{kN}}{\text{m}^2} \quad g := 5 \frac{\text{kN}}{\text{m}^2} \quad q := p - g = (95 \cdot 10^{-3}) \text{ MPa}$$

Flexural stiffnesses:

$$D_c := \frac{E \cdot h_c^3}{12 (1 - \nu^2)} = (10.547 \cdot 10^9) \text{ N} \cdot \text{mm}$$

$$D_p := \frac{E \cdot h_p^3}{12 (1 - \nu^2)} = (25 \cdot 10^9) \text{ N} \cdot \text{mm}$$

Elastic length:

$$\beta := \sqrt[4]{\frac{E \cdot h_c}{4 a^2 D_c}} = (1.941967 \cdot 10^{-3}) \frac{1}{\text{mm}}$$

Damping length:

$$L_c := \frac{\pi}{\beta} = (1.618 \cdot 10^3) \text{ mm}$$

$2 L_c < L$ --> The two edges do not effect one another.

Solution for cylinder:

Particular solution: $w_p := \frac{p \cdot a^2}{E \cdot h_c} = (166.67 \cdot 10^{-3}) \text{ (mm)}$

Homogeneous solution:

$$w(0) = w_p + \frac{1}{2 D_c \cdot \beta^2} \cdot \left(M_0 + \frac{Q_0}{\beta} \right) = 0$$

$$\frac{dw}{dx}(0) = -2 M_0 - \frac{Q_0}{\beta} = 0$$

We solve for the integration constants by setting up an equation system:

$$A := \begin{bmatrix} \frac{1}{2 D_c \cdot \beta^2} & \frac{1}{2 D_c \cdot \beta^3} \\ -\frac{1}{D_c \cdot \beta} & -\frac{1}{2 D_c \beta^2} \end{bmatrix} \quad B := \begin{bmatrix} -w_p \\ 0 \text{ rad} \end{bmatrix}$$

The edge forces become:

$$\begin{bmatrix} M_0 \\ Q_0 \end{bmatrix} := \begin{bmatrix} 13.258 \frac{\text{kN} \cdot \text{m}}{\text{m}} \\ -51.494 \frac{\text{kN}}{\text{m}} \end{bmatrix}$$

Coupling of circular plate and cylinder

Plate free to rotate:

$$\theta_q := \frac{q \cdot a^3}{16 \cdot D_p} \left(\frac{3 + \nu}{1 + \nu} - 1 \right) = (10.6875 \cdot 10^{-3}) \text{ rad}$$

Linking the shell and plate creates an edge moment, which in turn results in an rotation of the plate edge:

$$\theta_M = \frac{M_a \cdot a}{D_p (1 + \nu)} = 1.2 \cdot 10^{-4} M_a$$

M_a is the moment in the junction between the shell and plate.

By requiring equal rotation in the junction, we get the following expression:

$$\frac{dw(0)}{dx} = \frac{1}{2 \cdot D_c \cdot \beta} \left(-2 M_0 - \frac{Q_0}{\beta} \right) = -q = -\theta_q - \theta_M$$

The edge moment and shear force must be the same for both the cylinder and plate, thus

$$M_0 = M_a \quad , \quad Q_0 = Q_a$$

Compatibility condition 1: Equal rotation in junction B: $\theta_c = -\theta_q$

$$1) \quad \left(\frac{1}{D_c \cdot \beta} + \frac{a}{D_p \cdot (1 + \nu)} \right) M_a + \frac{1}{2 D_c \cdot \beta^2} Q_a = \theta_q$$

Compatibility condition 2: It is assumed that the plate has infinite stiffness in the plane. This means that radial displacement is restricted for the shell:

$$w_{tot} = w_p + w_h(0) = 0$$

$$\text{II) } \frac{1}{2 \beta^2 D_c} M_a + \frac{1}{2 \beta^3 D_c} Q_a = -w_p$$

$$K := \begin{bmatrix} \frac{1}{D_c \cdot \beta} + \frac{a}{D_p \cdot (1 + \nu)} & \frac{1}{2 D_c \cdot \beta^2} \\ \frac{1}{2 \beta^2 D_c} & \frac{1}{2 \beta^3 D_c} \end{bmatrix} \quad X := \begin{bmatrix} \theta_q \\ -w_p \end{bmatrix}$$

By solving the equation system, we find the moment and shear force at the junction to be:

$$\begin{bmatrix} M_a \\ Q_a \end{bmatrix} = \begin{bmatrix} 88.5 \frac{kNm}{m} \\ -197.6 \frac{kN}{m} \end{bmatrix}$$

Plotting the distributions of forces and moments is done in matlab.

B Cylinder with spherical roof

Material data:

$$C45 \quad \nu := 0.2 \quad E := 3.6 \cdot 10^7 \frac{\text{kN}}{\text{m}^2} \quad \gamma_w := 10 \frac{\text{kN}}{\text{m}^3} \quad \varphi := 30 \text{ deg}$$

Cylinder: $h_c := 0.18 \text{ m} \quad H_s := 10 \text{ m} \quad a := 10 \text{ m}$

$$D_c := \frac{E \cdot h_c^3}{12 (1 - \nu^2)} = (18.225 \cdot 10^3) \text{ kN} \cdot \text{m}$$

Sphere: $h_s := 0.15 \text{ m} \quad R := 20 \text{ m}$

$$D_s := \frac{E \cdot h_s^3}{12 (1 - \nu^2)} = (10.547 \cdot 10^3) \text{ kN} \cdot \text{m}$$

Cylinder

Elastic length:

$$\beta := \sqrt[4]{\frac{3 (1 - \nu^2)}{a^2 h_c^2}} = (970.984 \cdot 10^{-6}) \frac{1}{\text{mm}}$$

water pressure varies with x as follows:

$$p(x) := \gamma_w x$$

Particular solutions at edges:

$$w_p(x) := \frac{a^2}{E \cdot h_c} \cdot p(x)$$

$$1) \quad w_p(0 \text{ m}) = 0 \text{ mm} \quad , \quad w_p(10 \text{ m}) = 0.002 \text{ m}$$

$$2) \quad \theta_p = \frac{dw}{dx} \quad --> \quad \theta_p := -\frac{\gamma_w a^2}{E \cdot h_c} = -154.321 \cdot 10^{-6} \text{ rad}$$

Lower edge (A)

Total solution (at edge $x=0$):

$$w(0) = w_h(0) + w_p(0) = \frac{1}{2 \cdot D_c \cdot \beta^2} \left(M_0 + \frac{Q_0}{\beta} \right) + w_p(10) = 0$$

$$\theta(0) = \theta_h(0) + \theta_p(0) = -\frac{1}{2 \cdot D_c \cdot \beta} \left(2 \cdot M_0 + \frac{Q_0}{\beta} \right) + \theta_p(0) = 0$$

Solving the equation system with two unknowns:

$$K := \begin{bmatrix} \frac{1}{2 \cdot D_c \cdot \beta^2} & \frac{1}{2 \cdot D_c \cdot \beta^3} \\ \frac{1}{D_c \cdot \beta} & \frac{1}{2 \cdot D_c \cdot \beta^2} \end{bmatrix} \quad X := \begin{bmatrix} -w_p(10 \cdot m) \\ \theta_p \end{bmatrix}$$

The edge moment and shear force are:

$$\begin{bmatrix} M_0 \\ Q_0 \end{bmatrix} = \begin{bmatrix} 47.57 \frac{kN \cdot m}{m} \\ -97.69 \frac{kN}{m} \end{bmatrix}$$

Upper edge (B)

Homogeneous solution (at edge $x=0$):

$$1) \quad w_h = \frac{1}{2 \cdot D_c \cdot \beta^2} \left(M_0 + \frac{Q_0}{\beta} \right)$$

$$2) \quad \theta_h = \frac{1}{2 D_c \beta} \cdot \left(-2 M_0 - \frac{Q_0}{\beta} \right)$$

Total solution:

$$\theta = \theta_p + \theta_h = \frac{1}{2 D_c \beta} \left(-2 M_0 - \frac{Q_0}{\beta} \right) + \frac{\gamma_w a^2}{E \cdot h_c}$$

$$w = w_p + w_h = \frac{1}{2 \cdot D_c \cdot \beta^2} \left(M_0 + \frac{Q_0}{\beta} \right)$$

Spherical shell:

Sphere property:
$$\lambda := \sqrt[4]{\left(\frac{R}{h_s}\right)^2 \cdot 3 (1 - \nu^2)} = 15.042$$

We start of by solving the membrane theory:

It is assumed that the snow load and self-weight are distributed in the same way. The combined load is equal to:

$$g := 5.75 \frac{kN}{m^2}$$

The decomposition of the load is done as shown in the theory part of the paper:

$$p_\varphi := g \cdot \sin(\varphi) \qquad p_z := -g \cdot \cos(\varphi)$$

Meridian force:

$$N_{\varphi,m} = \frac{-R}{\sin^2 \varphi} \int_0^\varphi \sin \varphi (p_\varphi \sin \varphi - p_z \cos \varphi) d\varphi = -\frac{R \cdot g}{\sin^2 \varphi} (1 - \cos \varphi)$$

$$N_{\varphi,m} := -\frac{R \cdot g}{\sin(\varphi)^2} (1 - \cos(\varphi)) = -61.628 \frac{kN}{m}$$

Hoop force:

$$N_{\theta,m} := R \cdot p_z - N_{\varphi,m} = -37.965 \frac{kN}{m}$$

Relative displacement:

$$\delta_{s,m} := \frac{R \cdot \sin(\varphi)}{E \cdot h_s} (N_{\theta,m} - \nu \cdot N_{\varphi,m}) = -47.48 \cdot 10^{-6} \text{ m}$$

Relative rotation:

Derivative part of expression, $\frac{d}{d\varphi} (N_{\theta} - \nu N_{\varphi})$:

$$der := \frac{d}{d\varphi} \left(-R \cdot g \cdot \cos(\varphi) - \frac{R \cdot g}{\sin(\varphi)^2} (\cos(\varphi) - 1) \cdot (1 + \nu) \right) = 77.316 \frac{kN}{m}$$

$$V_{s,m} := \frac{1}{E \cdot h_s} (der - (1 + \nu) \cot(\varphi) (N_{\varphi,m} - N_{\theta,m})) = (23.426 \cdot 10^{-6}) \text{ rad}$$

The sphere does not meet the criterions for a pure membrane solution. Thus the membrane solution must be corrected to correspond to the displacement of the sphere edge:

$$H := N_{\varphi,m} \cdot \cos(\varphi) = -53.372 \frac{kN}{m}$$

The correction of the meridian rotation and displacement are found by applying the formulas for the homogeneous solution for shells when H is the only occurring force:

$$\delta := \frac{2 \lambda \cdot R \cdot \sin(\varphi)^2}{E \cdot h_s} \cdot (-H) = (1.48674 \cdot 10^{-3}) \text{ m}$$

The meridian rotation V is found as:

$$V := -\frac{2 \lambda^2 \cdot \sin(\varphi)}{E \cdot h_s} \cdot -H = -2.236414 \cdot 10^{-3}$$

The total particular solution for the spherical shell with horizontal displacement:

$$\delta_p := \delta_{s.m} + \delta = (1.44 \cdot 10^{-3}) \text{ m}$$

$$V_p := V - V_{s.m} = -2.26 \cdot 10^{-3} \text{ rad}$$

A total solution for the shell now becomes a combination of the particular and homogeneous parts:

$$\delta(0) = \delta_h(0) + \delta_p = \frac{\lambda \cdot R \cdot \sin(\varphi)}{E \cdot h_s} \left(2 R_0 \cdot \sin(\varphi) + M_{0s} \cdot \frac{E h_s \cdot R}{2 \lambda^3 D_s} \right) + \delta_p$$

$$V(0) = V_h(0) + V_p = \frac{-2 \lambda^2}{E \cdot h_s} \left(R_0 \cdot \sin(\varphi) + M_{0s} \cdot \frac{E \cdot h_s \cdot R}{2 \lambda^3 D_s} \right) + V_p$$

We now demand compatibility and equilibrium of forces in the junction between the two shells. This requires that:

- | | | |
|------|---------------------------------------|---------------|
| I) | $w(0) = \delta(0)$ | |
| II) | $\theta(0) = -V(0)$ | Compatibility |
| III) | $M_{0.Cylinder} = M_{0.Sphere} = M_0$ | |
| IV) | $Q_{0.Cylinder} = -R_0 = Q_0$ | Equilibrium |

Intuitively, it must be true that the deformations and forces are equal in the junction.

From I:

$$\left(\frac{1}{2 D_c \cdot \beta^2} - \frac{R^2 \cdot \sin(\varphi)}{2 \lambda^2 D_s} \right) \cdot M_0 + \left(\frac{1}{2 D_c \cdot \beta^3} + \frac{2 \cdot \lambda \cdot R \cdot \sin(\varphi)^2}{E \cdot h_s} \right) Q_0 = \delta_p$$

From II:

$$\left(-\frac{1}{D_c \cdot \beta} + \frac{R}{\lambda \cdot D_s} \right) \cdot M_0 + \left(-\frac{1}{2 \cdot D_c \cdot \beta^2} - \frac{-2 \lambda^2}{E \cdot h_s} \sin(\varphi) \right) Q_0 = V_p - \theta_p$$

We solve the two equations setting up a matrix:

$$K := \begin{bmatrix} \frac{1}{2 D_c \cdot \beta^2} - \frac{R^2 \cdot \sin(\varphi)}{2 \lambda^2 D_s} & \frac{1}{2 D_c \cdot \beta^3} + \frac{2 \cdot \lambda \cdot R \cdot \sin(\varphi)^2}{E \cdot h_s} \\ \frac{1}{D_c \cdot \beta} + \frac{R}{\lambda \cdot D_s} & -\frac{1}{2 \cdot D_c \cdot \beta^2} + \frac{-2 \lambda^2}{E \cdot h_s} \sin(\varphi) \end{bmatrix} \quad Y := \begin{bmatrix} \delta_p \\ V_p - \theta_p \end{bmatrix}$$

The results are summed up in the following matrix:

$$\begin{bmatrix} M_0 \\ Q_0 \\ R_0 \end{bmatrix} := \begin{bmatrix} -9.94 \frac{kN \cdot m}{m} \\ 22.69 \frac{kN}{m} \\ -22.69 \frac{kN}{m} \end{bmatrix}$$

The distributions of forces and bending moments are done in matlab.

C Ring beam

Data:

$$C45 \quad \nu := 0.2 \quad E := 3.6 \cdot 10^7 \frac{\text{kN}}{\text{m}^2} \quad \gamma_w := 10 \frac{\text{kN}}{\text{m}^3} \quad \varphi := 30 \text{ deg}$$

Cylinder: $h_c := 0.18 \text{ m} \quad H_s := 10 \text{ m} \quad a := 10 \text{ m}$

$$D_c := \frac{E \cdot h_c^3}{12 (1 - \nu^2)} = (18.225 \cdot 10^3) \text{ kN} \cdot \text{m} \quad \beta := \sqrt[4]{\frac{3 (1 - \nu^2)}{a^2 h_c^2}} = 0.971 \frac{1}{\text{m}}$$

Sphere: $h_s := 0.15 \text{ m} \quad R := 20 \text{ m}$

$$D_s := \frac{E \cdot h_s^3}{12 (1 - \nu^2)} = (10.547 \cdot 10^3) \text{ kN} \cdot \text{m} \quad \lambda := \sqrt[4]{\left(\frac{R}{h_s}\right)^2 \cdot 3 (1 - \nu^2)} = 15.042$$

Ring beam:

$$b := 0.3 \text{ m} \quad h_r := 0.3 \text{ m}$$

$$I := \frac{b \cdot h_r^3}{12} = (6.75 \cdot 10^8) \text{ mm}^4 \quad A := b \cdot h_r = (9 \cdot 10^4) \text{ mm}^2$$

Particular solutions:

Cylinder:

Hydrostatic load: $p_r = \gamma_w \cdot x$

Displacement: $w_p = \frac{a^2}{E \cdot h_s} p_r = \frac{\gamma_w \cdot a^2}{E \cdot h_c} \cdot x$

Rotation: $\theta_p = \frac{dw_p}{dx} = \frac{\gamma_w \cdot a^2}{E \cdot h_c}$

Sphere:

$$g := 5.75 \frac{kN}{m^2} \quad p_\varphi := g \cdot \sin(\varphi) \quad p_z := -g \cdot \cos(\varphi)$$

Meridian force:

$$N_\varphi = \frac{-R}{\sin^2 \varphi} \int_0^\varphi \sin \varphi (p_\varphi \sin \varphi - p_z \cos \varphi) d\varphi = -\frac{R \cdot g}{\sin^2 \varphi} (1 - \cos \varphi)$$

$$N_{\varphi,m} := -\frac{R \cdot g}{\sin(\varphi)^2} (1 - \cos(\varphi))$$

Hoop force:

$$N_{\theta,m} := R \cdot p_z - N_{\varphi,m} = -37.965 \frac{kN}{m}$$

Relative displacement:

$$\delta_{s,m} := \frac{R \cdot \sin(30 \text{ deg})}{E \cdot h_s} (N_{\theta,m} - \nu \cdot N_{\varphi,m}) = -0.047 \text{ mm}$$

Relative rotation:

Dervative part of expression, $\frac{d}{d\varphi} (N_\theta - \nu N_\varphi)$:

$$der := \frac{d}{d\varphi} \left(-R \cdot g \cdot \cos(\varphi) - \frac{R \cdot g}{\sin(\varphi)^2} (\cos(\varphi) - 1) \cdot (1 + \nu) \right) = 77.316 \frac{kN}{m}$$

$$V_{s,m} := \frac{1}{E \cdot h_s} (der - (1 + \nu) \cot(\varphi) (N_{\varphi,m} - N_{\theta,m})) = (23.426 \cdot 10^{-6}) \text{ rad}$$

Correction of membrane solution:

$$H := N_{\varphi,m} \cdot \cos(\varphi) = -53.372 \frac{kN}{m}$$

$$\delta := \frac{2 \lambda \cdot R \cdot \sin(\varphi)^2}{E \cdot h_s} \cdot (-H) = 1.48674 \text{ mm}$$

$$V := -\frac{2 \lambda^2 \cdot \sin(\varphi)}{E \cdot h_s} \cdot -H = -2.236414 \cdot 10^{-3}$$

The total particular solution for the spherical shell:

$$\delta_p := \delta_{s,m} + \delta = 1.44 \text{ mm}$$

$$V_p := V - V_{s,m} = -2.25984 \cdot 10^{-3}$$

Ring beam:

Rotation:

$$\alpha = \frac{a^2}{E \cdot I} \cdot M_r$$

Displacements:

$$w_{top} = w_h + w_M \left(\frac{h_r}{2} \right) = \frac{H a^2}{EA} + \frac{a^2 \cdot h_r}{2 EI} \cdot M_r$$

$$w_{bottom} = w_h + w_M \left(-\frac{h_r}{2} \right) = \frac{H a^2}{EA} - \frac{a^2 \cdot h_r}{2 EI} \cdot M_r$$

Compatibility cylinder-ring beam

$$1) \quad \theta(0) = \frac{dw_p(0)}{dx} + \frac{dw_h(0)}{dx} = -\alpha$$

$$\frac{\gamma_w \cdot a^2}{E \cdot h_c} - \frac{1}{2 \cdot D_c \cdot \beta} \cdot \left(2 \cdot M_{0s} + \frac{Q_{0s}}{\beta} \right) = -\frac{a^2}{E \cdot I} \cdot M_r = -\frac{a^2}{E \cdot I} \cdot \left(M_{0s} - M_{0c} - (R_{0s} - Q_{0c}) \cdot \frac{h_r}{2} \right)$$

After sorting:

$$\left(\frac{1}{D_c \cdot \beta} + \frac{a^2}{E \cdot I} \right) \cdot M_{0c} + \left(\frac{1}{2 \cdot D_c \cdot \beta^2} - \frac{a^2 \cdot h_r}{2 E \cdot I} \right) \cdot Q_{0c} - \frac{a^2}{E \cdot I} M_{0s} + \frac{a^2 h_r}{2 E \cdot I} R_{0s} = \frac{\gamma_w \cdot a^2}{E \cdot h_s}$$

$$2) \quad w(0) = w_h(0) = w_{bottom}$$

$$\frac{1}{2 D_c \cdot \beta^2} \cdot \left(M_{0c} + \frac{Q_{0c}}{\beta} \right) = \frac{H a^2}{EA} - \frac{a^2 \cdot h_r}{2 EI} \cdot M_r$$

$$\blacksquare = \frac{a^2}{EA} \cdot (-R_{0s} - Q_{0c}) - \frac{a^2 \cdot h_r}{2 EI} \cdot \left(M_{0s} - M_{0c} - (R_{0s} - Q_{0c}) \cdot \frac{h_r}{2} \right)$$

After sorting:

$$\left(\frac{1}{2 D_c \cdot \beta^2} - \frac{a^2 \cdot h_r}{2 EI} \right) \cdot M_{0c} + \left(\frac{1}{2 D_c \cdot \beta^3} + \frac{a^2}{EA} + \frac{a^2 \cdot h_r^2}{4 E \cdot I} \right) \cdot Q_{0c}$$

$$\blacksquare + \frac{a^2 \cdot h_r}{2 E \cdot I} \cdot M_{0s} + \left(\frac{a^2}{EA} - \frac{a^2 \cdot h_r^2}{4 EI} \right) \cdot R_{0s} = 0$$

Compatibility sphere-ring beam

$$3) \quad V_p(30 \text{ deg}) + V_h(0) = \alpha$$

$$-\frac{2 \cdot \lambda^2}{E \cdot h_s} \left(\sin(\varphi) R_{0s} + \frac{E \cdot h_s \cdot R}{2 D_s \cdot \lambda^3} M_{0s} \right) + V_p(30 \text{ deg}) = \frac{a^2}{EI} \cdot \left(M_{0s} - M_{0c} - (R_{0s} - Q_{0c}) \cdot \frac{h_r}{2} \right)$$

After sorting:

$$\frac{a^2}{EI} M_{0c} - \frac{a^2 h_r}{2 EI} Q_{0c} - \left(\frac{R}{\lambda \cdot D_s} + \frac{a^2}{E \cdot I} \right) M_{0s} + \left(\frac{a^2 h_r}{2 EI} - \frac{2 \sin \varphi \cdot \lambda^2}{E \cdot h_s} \right) R_{0s} = -V_p(30 \text{ deg})$$

$$4) \quad \delta_h(0) + \delta_p(30 \text{ deg}) = w_{top}$$

$$\frac{\lambda \cdot R \cdot \sin \varphi}{E \cdot h_s} \left(2 \cdot \sin \varphi \cdot R_{0s} + \frac{E \cdot h_s \cdot R}{2 D_s \cdot \lambda^3} \cdot M_{0s} \right) = \frac{H a^2}{EA} + \frac{a^2 \cdot h_r}{EI} \cdot M_r + \delta_p(30 \text{ deg})$$

$$\equiv -\frac{a^2}{EA} (Q_{0c} + R_{0s}) + \frac{a^2 \cdot h_r}{2 EI} \cdot \left(M_{0s} - M_{0c} - (R_{0s} - Q_{0c}) \cdot \frac{h_r}{2} \right)$$

After sorting:

$$\left(\frac{a^2 h_r}{2 EI} \right) M_{0c} - \left(\frac{a^2 \cdot h_r^2}{4 EI} - \frac{a^2}{EA} \right) Q_{0c} + \left(\frac{R^2 \sin \varphi}{2 \lambda^2 D_s} - \frac{a^2 \cdot h_r}{2 EI} \right) \cdot M_{0s}$$

$$\equiv + \left(\frac{2 \lambda R \cdot \sin \varphi^2}{E \cdot h_s} + \frac{a^2 \cdot h_r^2}{4 E \cdot I} + \frac{a^2}{EA} \right) R_{0s} = -\delta_p(30 \text{ deg})$$

Solving equation system 1-4 yields:

$$\begin{bmatrix} M_{0c} \\ Q_{0c} \\ M_{0s} \\ R_{0s} \end{bmatrix} = \begin{bmatrix} -4.04 \frac{kNm}{m} \\ 14.49 \frac{kN}{m} \\ -9.95 \frac{kNm}{m} \\ -24.93 \frac{kN}{m} \end{bmatrix}$$

Forces and bending moments in the junction are significantly reduced

D Design in accordance with Eurocode 2

- References:* [1] Standard Norge. Eurocode 2: Prosjektering av betongkonstruksjoner del 1-1:Allmenne regler og regler for bygning, ns-en 1992-1-1:2004+na:2008 edition.
- [2] Svein Ivar Sørensen .Betontongkonstruksjoner, Beregning og dimensjonering etter Eurocode 2. Tapir akademiske forlag, 2012

General data

Material factors:

$$\alpha_{cc} := 0.85 \quad \gamma_c := 1.5 \quad \gamma_s := 1.15$$

Cross section:

$$b := 1000 \frac{mm}{m} \quad h_c := 150 \text{ mm} \quad h_p := 200 \text{ mm} \quad \begin{array}{l} \text{EC2 NA.2.4.2.4} \\ \text{EC2 NA.3.1.6(1)P} \end{array}$$

Concrete:

$$f_{ck} := 45 \text{ MPa} \quad f_{cd} := \alpha_{cc} \cdot \frac{f_{ck}}{\gamma_c} = 25.5 \text{ MPa} \quad f_{ctm} := 3.8 \text{ MPa}$$

Reinforcement:

$$f_{yk} := 500 \text{ MPa} \quad f_{yd} := \frac{f_{yk}}{\gamma_s} = 434.783 \text{ MPa}$$

Bar sizes used:

$$\varphi = 12 \text{ mm} \quad A_{\varphi 12} := \frac{\pi}{4} \cdot (12 \text{ mm})^2 = 113.097 \text{ mm}^2$$

$$\varphi = 16 \text{ mm} \quad A_{\varphi 16} := \frac{\pi}{4} \cdot (16 \text{ mm})^2 = 201.062 \text{ mm}^2$$

Concrete cover (EC2 4.4.1.1):

Choose exposure class XC2

$$c_{nom} = c_{min} + \Delta c_{dev}$$

$$c_{min,b} := \varphi$$

$$c_{min,dur} := 25 \text{ mm}$$

$$\Delta c_{dur,st} := 0$$

$$\Delta c_{dur,add} := 0$$

$$\Delta c_{dur,\gamma} := 0$$

$$c_{min} := \max(c_{min,b}, c_{min,dur} + \Delta c_{dur,\gamma} - \Delta c_{dur,st} - \Delta c_{dur,add}, 10 \text{ mm}) = 25 \text{ mm}$$

For reinforcement bars with diameters less than 25 mm, the exposure requirement determines the minimum cover.

Bottom Cylinder:

Effective depth:

$$d := h_c - c_{min} - \frac{\varphi}{2} = 119 \text{ mm}$$

Flexural reinforcement [2]

$$M_{Ed} := 15.9 \frac{\text{kN} \cdot \text{m}}{\text{m}}$$

$$M_{Rd} := 0.275 \cdot b \cdot d^2 \cdot f_{cd} = 99.304 \frac{1}{\text{m}} \cdot \text{kN} \cdot \text{m}$$

$$M_{Ed} < M_{Rd}$$

$$z := \left(1 - 0.17 \cdot \frac{M_{Ed}}{M_{Rd}} \right) \cdot d = 115.761 \text{ mm} \quad \text{condition:} \quad z < 0.95 d$$

$$A_{sm} := \frac{M_{Ed}}{z \cdot f_{yd}} = 315.91 \frac{\text{mm}^2}{\text{m}}$$

$$s := \frac{A_{\varphi 12}}{A_{sm}} = 358.005 \text{ mm}$$

$\varphi 12s355$ Is chosen

Check of minimum reinforcement (*EC2 NA 9.2.1.1*):

$$A_{s,min} := 0.26 \cdot \frac{f_{ctm}}{f_{yk}} \cdot b \cdot d = 235.144 \frac{\text{mm}^2}{\text{m}}$$

$$A_{sm} > A_{s,min}$$

Hence the final reinforcement is:

$$A_{sm} := A_{\varphi 12} \cdot \frac{b}{355 \text{ mm}} = 318.584 \frac{\text{mm}^2}{\text{m}}$$

Shear Reinforcement [2]

$$Q_{Ed} := -61.8 \frac{\text{kN}}{\text{m}}$$

Members not requiring design shear reinforcement (*EC2 6.2.2*):

$$k := 1 + \sqrt{\frac{200 \text{ mm}}{d}} = 2.296 \quad k < 2.0$$

$$C_{Rd,c} := 0.12 \quad \rho_l := \frac{A_{sm}}{b \cdot d} = 0.0027 \quad k := 2$$

$$V_{Rd,c} := \left(C_{Rd,c} \cdot k \cdot \left(100 \rho_l \cdot f_{ck} \right)^{\frac{1}{3}} \cdot \text{MPa}^{\frac{2}{3}} \right) \cdot b \cdot d = 65.472 \frac{\text{kN}}{\text{m}}$$

$V_{Rd,c} > Q_{Ed}$ No need for shear reinforcement.

Top edge Cylinder

Flexural reinforcement [2]

Choose $\varphi := 16 \text{ mm}$ in tension

Cover: $d := h_c - c_{min} - \frac{\varphi}{2} = 117 \text{ mm}$

$$M_{Ed} := 107.5 \frac{\text{kN} \cdot \text{m}}{\text{m}}$$

$$M_{Rd} := 0.275 \cdot b \cdot d^2 \cdot f_{cd} = 95.994 \frac{\text{kN} \cdot \text{m}}{\text{m}}$$

$$M_{Ed} > M_{Rd}$$

Additional compressional reinforcement is necessary.

Choose $\varphi = 12 \text{ mm}$ in compression

$$A_{s1} := \frac{M_{Rd}}{f_{yd} \cdot 0.835 \cdot d} = (2.26 \cdot 10^3) \frac{\text{mm}^2}{\text{m}}$$

$$\Delta M_{Ed} := M_{Ed} - M_{Rd} = 11.506 \text{ kN}$$

Distance between reinforcement layers:

$$h_b := h_c - 2 \cdot c_{min} - \frac{16 \text{ mm}}{2} - \frac{12 \text{ mm}}{2} = 86 \text{ mm}$$

$$A_{s2} := \frac{\Delta M_{Ed}}{f_{yd} \cdot h_b} = 307.716 \frac{\text{mm}^2}{\text{m}}$$

Total tensile reinforcement are:

$$A_{s_{m,t}} := A_{s1} + A_{s2} = (2.568 \cdot 10^3) \frac{\text{mm}^2}{\text{m}}$$

Total compressional reinforcement are:

$$A_{sm.c} := A_{s2}$$

Bars in tension:

$$s := \frac{A_{\varphi 16}}{A_{sm.t}} = 78.305 \text{ mm}$$

Choose $\varphi 16s78$

This gives a final reinforcement of:

$$A_{sm.t} := A_{\varphi 16} \cdot \frac{b}{78 \text{ mm}} = (2.578 \cdot 10^3) \frac{\text{mm}^2}{\text{m}}$$

Bars in compression:

$$s := \frac{A_{\varphi 12}}{A_{sm.c}} = 367.539 \text{ mm}$$

Choose $\varphi 12s365$

This gives a final reinforcement of:

$$A_{sm.c} := A_{\varphi 12} \cdot \frac{b}{365 \text{ mm}} = 309.856 \frac{\text{mm}^2}{\text{m}}$$

Shear Reinforcement

$$Q_{Ed} := -197.3 \frac{\text{kN}}{\text{m}}$$

Members not requiring design shear reinforcement (EC2 6.2.2):

$$k := 1 + \sqrt{\frac{200 \text{ mm}}{d}} = 2.307 \quad k < 2.0$$

$$C_{Rd.c} := 0.12 \quad \rho_l := \frac{A_{sm}}{b \cdot d} = 0.0027 \quad k := 2$$

$$V_{Rd.c} := \left(C_{Rd.c} \cdot k \cdot \left(100 \rho_l \cdot f_{ck} \right)^{\frac{1}{3}} \cdot MPa^{\frac{2}{3}} \right) \cdot b \cdot d = 64.736 \frac{kN}{m}$$

$$Q_{Ed} > V_{Rd.c}$$

Shear reinforcement is necessary.

Members requiring shear reinforcement (EC2 6.2.3):

$$\cot\theta := 2.5 \quad z := 0.9 \cdot d = 105.3 \text{ mm}$$

$$\frac{A_{sw}}{s} = A_{sq} = \frac{Q_{Ed} \cdot 1 \text{ m}}{z \cdot f_{yd} \cdot \cot\theta} \quad A_{sq} := - \frac{Q_{Ed} \cdot 1 \text{ m}}{z \cdot f_{yd} \cdot \cot\theta} = (1.724 \cdot 10^3) \frac{mm^2}{m}$$

$$\text{choose} \quad \varphi := 12 \text{ mm}$$

$$s_q := \frac{A_{\varphi 12}}{A_{sq}} = 65.609 \text{ mm}$$

$$\text{choose} \quad \varphi 12s65$$

This leads to an actual reinforcement area of:

$$A_{sq} := A_{\varphi 12} \cdot \frac{b}{65 \text{ mm}} = (1.74 \cdot 10^3) \frac{mm^2}{m}$$

Hoop force reinforcement lower edge

$$N_{\theta} := 360 \frac{kN}{m}$$

The hoop force causes tension, and we assume that the concrete has no tensile strength. The reinforcement is placed in two layers along the whole length of the cylinder.

$$A_{sn} := \frac{N_{\theta}}{f_{yd}} = 828 \frac{mm^2}{m}$$

Per layer:

$$A_{sn2} := \frac{A_{sn}}{2} = 414 \frac{mm^2}{m}$$

Choose: $\varphi := 12 \text{ mm}$

$$s_n := \frac{A_{\varphi 12}}{A_{sn2}} = 273.182 \text{ mm}$$

Choose $\varphi 12s270$ $A_{sn} := A_{\varphi 12} \cdot \frac{b}{270 \text{ mm}} = 418.879 \frac{mm^2}{m}$

This reinforcement is placed in two layers with the concrete cover previously found from each edge.

Hoop reinforcement at upper edge

The hoop force at the upper edge is in compression. Hence it is necessary to check the concrete stresses occurring.

$$N_{\theta} := -560 \frac{kN}{m}$$

Concrete area per meter:

$$A_c := b \cdot h_c = (1.5 \cdot 10^5) \frac{mm^2}{m}$$

$$N_{Rd} := f_{cd} \cdot A_c = (3.825 \cdot 10^3) \frac{kN}{m}$$

$$N_{Rd} > N_\theta$$

No compressional reinforcement needed.

Reinforcement of circular plate

Flexural reinforcement

The two moments in the plate change sign when moving from the edge towards the center. Hence reinforcement must be laid in two layers. In addition, the two moments work in different directions.

Radial and hoop moments - center [2]

At the center of the plate, the radial and hoop moment have the same value. They need the same amount of reinforcement, only in different directions:

$$M_r := -101 \frac{kN \cdot m}{m} \quad M_t := -101 \frac{kN \cdot m}{m}$$

Choose $\varphi := 16 \text{ mm}$

Effective depth: $d := h_p - c_{min} - \frac{\varphi}{2} = 167 \text{ mm}$

$$M_{Rd} := 0.275 \cdot b \cdot d^2 \cdot f_{cd} = 195.572 \frac{1}{m} \cdot kN \cdot m$$

$$M_r = M_t < M_{Rd}$$

$$z := \left(1 - 0.17 \cdot \frac{M_r}{M_{Rd}} \right) \cdot d = 181.662 \text{ mm} \quad \text{condition: } z < 0.95 d \quad \text{ok}$$

$$A_{sm} := \frac{M_r}{z \cdot f_{yd}} = -1.279 \cdot 10^3 \frac{mm^2}{m}$$

$$s := -\frac{A_{\varphi 16}}{A_{sm}} = 157.233 \text{ mm}$$

Choose $\varphi 16s155$

This gives a final reinforcement for the two moments:

$$A_{sm} := A_{\varphi 16} \cdot \frac{b}{155 \text{ mm}} = (1.297 \cdot 10^3) \frac{mm^2}{m}$$

Radial moments at edge [2]

$$M_r := 107.5 \frac{kN \cdot m}{m}$$

$$M_{Rd} := 0.275 \cdot b \cdot d^2 \cdot f_{cd} = 195.572 \frac{kN \cdot m}{m}$$

$$M_r < M_{Rd}$$

$$z := \left(1 - 0.17 \cdot \frac{M_r}{M_{Rd}} \right) \cdot d = 151.395 \text{ mm} \quad \text{condition: } z < 0.95 d \quad \text{ok}$$

$$A_{sm} := \frac{M_r}{z \cdot f_{yd}} = (1.633 \cdot 10^3) \frac{mm^2}{m}$$

$$A_{\varphi 16} := \frac{\pi}{4} \cdot \varphi^2 = 201.062 \text{ mm}^2$$

$$s := \frac{A_{\varphi 16}}{A_{sm}} = 123.113 \text{ mm}$$

Choose $\varphi 16s120$

This gives a final of:

$$A_{sm} := A_{\varphi 16} \cdot \frac{b}{120 \text{ mm}} = (1.676 \cdot 10^3) \frac{\text{mm}^2}{\text{m}}$$

Hoop moments at edge [2]

Choose $\varphi := 12 \text{ mm}$

Effective depth: $d := h_p - c_{min} - \frac{\varphi}{2} = 169 \text{ mm}$

$$M_t := 31 \frac{\text{kN} \cdot \text{m}}{\text{m}}$$

$$M_{Rd} := 0.275 \cdot b \cdot d^2 \cdot f_{cd} = 200.284 \frac{1}{\text{m}} \cdot \text{kN} \cdot \text{m}$$

$$M_t < M_{Rd}$$

$$z := \left(1 - 0.17 \cdot \frac{M_t}{M_{Rd}} \right) \cdot d = 164.553 \text{ mm} \quad \text{condition: } z < 0.95 d$$

$$z := 0.95 \cdot d$$

$$A_{sm} := \frac{M_t}{z \cdot f_{yd}} = 444.098 \frac{\text{mm}^2}{\text{m}}$$

$$A_{\varphi 12} := \frac{\pi}{4} \cdot \varphi^2 = 113.097 \text{ mm}^2$$

$$s := \frac{A_{\varphi 12}}{A_{sm}} = 254.667 \text{ mm}$$

Choose $\varphi 12s250$

This gives a final reinforcement reinforcement for the two moments:

$$A_{sm} := A_{\varphi 12} \cdot \frac{b}{250 \text{ mm}} = 452.389 \frac{\text{mm}^2}{\text{m}}$$

Shear reinforcement in plate (EC2 6.2.2):

$$Q_{Ed} := 173.25 \frac{\text{kN}}{\text{m}}$$

Members not requiring design shear reinforcement:

$$k := 1 + \sqrt{\frac{200 \text{ mm}}{d}} = 2.088 \quad k < 2.0$$

$$C_{Rd,c} := 0.12 \quad \rho_l := \frac{A_{sm}}{b \cdot d} = 0.0027 \quad k := 2$$

$$V_{Rd,c} := \left(C_{Rd,c} \cdot k \cdot \left(100 \rho_l \cdot f_{ck} \right)^{\frac{1}{3}} \cdot \text{MPa}^{\frac{2}{3}} \right) \cdot b \cdot d = 92.977 \frac{\text{kN}}{\text{m}}$$

$$Q_{Ed} > V_{Rd,c}$$

Shear reinforcement is required.

Members requiring shear reinforcement (EC2 6.2.3)

$$\cot\theta := 2.5 \quad z := 0.9 \cdot d = 152.1 \text{ mm}$$

$$\frac{A_{sw}}{s} = A_{sq} = \frac{Q_{Ed} \cdot 1 \text{ m}}{z \cdot f_{yd} \cdot \cot\theta} \quad A_{sq} := -\frac{Q_{Ed} \cdot 1 \text{ m}}{z \cdot f_{yd} \cdot \cot\theta} = -1.048 \cdot 10^3 \frac{\text{mm}^2}{\text{m}}$$

$$\text{choose} \quad \varphi := 12 \text{ mm}$$

$$s_q := \frac{A_{\varphi 12}}{A_{sq}} = 107.925 \text{ mm}$$

Choose $\varphi 12s148$

This leads to an actual reinforcement area of:

$$A_{sq} := A_{\varphi 12} \cdot \frac{b}{105 \text{ mm}} = (1.077 \cdot 10^3) \frac{\text{mm}^2}{\text{m}}$$